

**STUDY OF CHLORIDE THRESHOLD DETERMINATION FOR  
SYSTEMS WITH CORROSION INHIBITING ADMIXTURES AND  
CORROSION RATES OF VARIOUS STEELS IN CEMENT MORTAR**

*A THESIS*

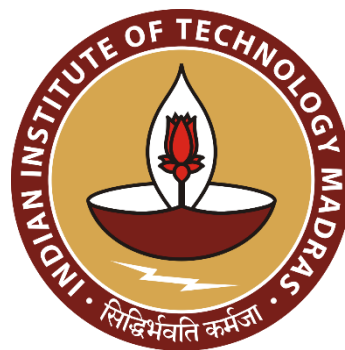
*Submitted by*

**JAYACHANDRAN KARUPPANASAMY**

*for the award of the degree*

*of*

**DOCTOR OF PHILOSOPHY**



**DEPARTMENT OF CIVIL ENGINEERING  
INDIAN INSTITUTE OF TECHNOLOGY MADRAS  
CHENNAI, INDIA**

**May 2017**



## **THESIS CERTIFICATE**

This is to certify that the thesis titled “**STUDY OF CHLORIDE THRESHOLD DETERMINATION FOR SYSTEMS WITH CORROSION INHIBITING ADMIXTURES AND CORROSION RATES OF VARIOUS STEELS IN CEMENT MORTAR**” submitted by **Jayachandran Karuppanasamy**, to the Department of Civil Engineering, Indian Institute of Technology Madras, Chennai, for the award of the degree of Doctor of Philosophy is a bona fide record of research work carried out by him under my supervision. The contents of this thesis, in full or in parts, have not been submitted and will not be submitted to any other Institute or University for the award of any degree or diploma.

**Dr. Radhakrishna G. Pillai**

Research Guide

Assistant Professor

Department of Civil Engineering

Indian Institute of Technology Madras

Chennai - 600 036, India

Chennai, India

May 19, 2017



## ACKNOWLEDGEMENTS

I thank IIT Madras for this delightful opportunity to study with the guidance of Dr. Radhakrishna G. Pillai. I express my deepest sense of gratitude for his valuable guidance, constant support, friendly approach, patience for long discussions, thoughtful feedback, encouragement, and commitment to this research program. Apart from the research, I have learned from him, uncompromising standards for quality, brilliant way of teaching, correcting students with encouraging words and motivation, which would be helpful for my professional career as a teacher as well as researcher.

I am very much grateful to Prof. Ravindra Gettu and Prof. Manu Santhanam for their valuable support, comments, and suggestions during various stages of this research program. Additionally, I express my gratitude for their tireless efforts and help in weekly research group meetings.

I would like to express my gratitude to my Doctoral Committee Members Prof. Amlan Kumar Sengupta, Department of Civil Engineering, and Prof. S. Ganesh Sundara Raman, Department of Metallurgical and Materials Engineering, and Prof. M. S. Sivakumar, Department of Applied Mechanics, IIT Madras for their constant support, refreshing insights and suggestions towards this research program. I express my sincere thanks to the present Head, Department of Civil Engineering, Prof. K. Ramamurthy, and the former heads Prof. A. Meher Prasad and Prof. S.R. Gandhi for facilitating various academic needs during my stay in the department.

I take this opportunity to express my sincere thanks to Prof. M. S. Mathews and Prof. K. Ramamurthy, who inspired and encouraged me throughout this research program. I would like to thank Prof. Surendra P. Shah, Prof. Mark G. Alexander, Prof. Yunus Ballim, Prof. Vellore Gopalaratnam, and Prof. Carmen Andrade for their valuable discussions and inputs during their stay at IIT Madras. I am also extremely thankful to all faculty members of Building Technology and Construction Management (BTCM) division for their intangible support.

I express my sincere thanks to all lab staff, especially Mr. Soundarapandian, Ms. Malarvizhi, Mr. Krishnan, and Mr. Subramanian, for their help in the experimental

work. I thank Mr. R. Murali, Department workshop facility for his inestimable help in fabrication of moulds and test setups.

I am very delightful to acknowledge the support from all beloved intern students, especially Vasugi Jegan, Vandhana Mary Jacob, Kunal Gupta, Arun Kishore, Anubin Joy, Anupama Purani, Anto Vibin Marckson, Nandhini Vasudevan, Meera M. Gopal, Oviya Pugal, Namitha Chacko, Geetha Subramaniam, for their valuable contributions in this research study.

My sincere thanks to all my friends and fellow researchers at IIT Madras, Dr. Bahurudeen A., Srinivasan Nagarajan, Prabha Mohandoss, Dr. Dhanya B. S., Sakthivel Thangavel, Sripriya Rengaraju, Ranjitha R., Rajmohan K. S., Ramachandran E., Dr. Karthikayini M. P., Venkatachalam S., Sooraj A. O. Nair, Sanoop P., Dr. Mohammed Haneefa, Vibha Venkataramu, Aruna Muthumanickam, Saranya Nithiyanandan, Dr. Ganesh A. Devkar, Chinchu Cherian, Hemalatha M. S., Dr. Vijayavengadesh Kumar J., Sujatha Jose, Sheetal Surana, Deepak Kamade, Aswathy Rajendran, Dr. Vasugi V. V. and all others for the suggestions, discussions and help rendered during different stages of my research work.

I am also thankful to Project Associates, especially Anila Mohan, Pushpakaran P., Vigneshwaran Rao, Anto Vibin Marckson, Sindhu Sadasivam, who had helped me in many ways. The support from BTCM office and Civil Engineering office is gratefully acknowledged. I am very much grateful to all my friends and well-wishers, for making my stay at IIT Madras most pleasant and memorable. I express my profound thanks to all of them who have supported to complete the research study.

My heartfelt thanks to my beloved family members Karuppanasamy S., Dhanalakshmi K., Tamizharasi K., Dr. Ravi Kumar Kandasamy, Saravana Kumar K. Ms. Ineya R. and all other relatives, family friends who sacrificed a lot for me with their continuous encouragement, love, patience. There are no words to express my appreciation to them.

**Jayachandran Karuppanasamy**

## ABSTRACT

Service life of reinforced concrete systems can be defined as the sum of corrosion initiation period ( $t_i$ ) and corrosion propagation period ( $t_p$ ). In this thesis,  $t_i$  is defined as the time required to initiate chloride-induced corrosion in concrete structures and  $t_p$  is defined as the time between the initiation of chloride-induced corrosion and the initiation of corrosion-induced cracking of cover concrete. This thesis provides the development of the modified accelerated chloride threshold test (mACT) method. Then, experimental observations on and probabilistic estimates of the chloride threshold ( $Cl_{th}$ ), and corrosion rate ( $i_{corr}$ ), which are the two key parameters required to estimate  $t_i$  and  $t_p$ , respectively are presented.

In general, the larger the  $Cl_{th}$ , the longer will be the  $t_i$ . To increase the  $Cl_{th}$  of new concrete systems, corrosion inhibiting admixtures (CIAs) can be used. Both anodic (AN) and bipolar (BP) type CIAs are available in the market. However, the quantitative assessment of the effect of CIAs on the  $Cl_{th}$  is not well reported. Thus, engineers are not able to reliably estimate the  $t_i$  of steel-cementitious systems with CIAs, especially during the planning and design stages.

During the initial stages of this thesis work, it was found that the existing short-term test methods that uses external potential gradient for accelerating the movement of chlorides are not suitable to reliably assess the  $Cl_{th}$  of steel-cementitious systems with CIAs. This is because of the movement of nitrites and other anions towards the embedded steel working electrode along with the chlorides. This leads to an unwanted change in the nitrite (or anion) concentration at the steel-cementitious interface during the course of testing. Such changes may not occur in real structures. Therefore, the use of external potential gradient can give erroneous results and must be avoided while determining the  $Cl_{th}$  of steel-cementitious systems with CIAs.

This thesis, then focuses on the development of a Modified Accelerated Chloride Threshold (MACT) test procedure to determine the  $Cl_{th}$  for steel-cementitious systems with CIAs. The mACT test specimens consisted of a mortar cylinder (100 mm diameter and 150 mm length) in which a 20 mm long steel working electrode, Nickel-Chromium counter electrode, and a Haber-luggin probe (for placing the Saturated Calomel reference electrode) were embedded to form a 3-electrode corrosion cell. For this study, the Quenched and Self-Tempered (QST) steel rebar pieces that are widely used in India were used. Note that

QST steel is known as Thermo-Mechanically Treated (TMT) steel in the Indian subcontinent. The test specimens were exposed to 15% NaCl solution and Linear Polarization Resistance (LPR) tests were conducted once in every  $\approx 3.5$  days. A statistical procedure was developed to identify stable polarization resistance ( $R_p$ ) data and then to detect the corrosion initiation based on statistically significant variations in the measured  $R_p$  as a function of the exposure period. Once corrosion initiation is detected, the specimens were autopsied and the chloride content in mortar powder collected from adjacent to the steel piece was determined and defined as  $Cl_{th}$ . The typical duration required to complete the mACT test is about 120 days – better the CIA, more will be the test duration.

The mACT test method was validated by comparing the  $Cl_{th}$  values obtained for QST steel embedded in Ordinary Portland Cement (OPC) mortar with no inhibitors with those reported in the literature. Both were found to exhibit similar means and range of values. Also, the  $Cl_{th}$  of QST steel embedded in cementitious systems with the following two widely used CIAs were evaluated: (i) AN inhibitor [consisting of calcium nitrite] and (ii) BP inhibitor [consisting of both calcium nitrite and amino alcohol]. Ten mACT specimens each with (1) Without inhibitor (W/O), (2) AN inhibitor, and (3) BP inhibitor were tested – leading to a total of 30 specimens. Both AN and BP type specimens exhibited enhanced  $Cl_{th}$ . The  $Cl_{th}$  of QST steel embedded in cementitious system without inhibitors and with AN, and BP inhibitors can be expressed as normal (N) distributions as follows:  $\sim N(1.12, 0.5)$ ,  $\sim N(1.4, 0.33)$ , and  $\sim N(2, 0.6)$  percent by weight of cement (%bwoc), respectively. In short, it was found that the BP inhibitor performed better than AN inhibitor. Then, the probability density functions of  $t_i$  for systems with QST steel embedded in cementitious systems without inhibitors and with AN, and BP inhibitors were obtained using the  $Cl_{th}$  determined using mACT test method, other assumptions on chloride ingress, and Life-365™ software program. It was concluded that the use of CIAs could significantly delay the initiation of chloride-induced corrosion, especially when the moisture levels are high, as in marine environments.

Another parameter affecting the total service life is  $i_{corr}$ , which greatly influences the  $t_p$ . Many existing concrete structures are built using Plain Mild (PM), and Cold Twisted Deformed (CTD) steel bars. Also, QST/TMT and Prestressing (PS) steel reinforcement are extensively used in today's construction. For estimating the  $t_p$  of concrete structures, the current practice, in general, is to assume that the  $i_{corr}$  of different steel reinforcement are

equal to that of PM steel. This is because  $i_{\text{corr}}$  of PM steel is widely available and that of other steels (CTD, QST, PS, etc.) are not widely available in the literature. However, such assumptions might result in erroneous estimations of  $t_p$ . This thesis provides  $i_{\text{corr}}$  data obtained from a 33-month long laboratory test on corrosion of PM, CTD, QST, and PS steels embedded in chloride-contaminated mortar. Twenty-five specimens of each steel type – leading a total of 100 specimens - were tested. Linear polarization resistance (LPR) tests were conducted to obtain the  $i_{\text{corr}}$ . The statistical distributions of  $i_{\text{corr, wet}}$  and  $i_{\text{corr, dry}}$ , for each steel, are developed. For PM, CTD, QST, and PS steel embedded in mortar, and exposed for wet conditions ( $i_{\text{corr, wet}}$ ) found to be  $\sim$ Weibull (2.5, 20.7, 0),  $\sim$ Lognormal (0.45, 3.2, 0),  $\sim$ Gamma (6.8, 3.5, 0), and  $\sim$ Weibull 3P (1.3, 6.5, -0.02), respectively. Similarly, distribution for dry condition ( $i_{\text{corr, dry}}$ ) is also represented.

It was also found that, in general, the CTD and QST steel reinforcement exhibit higher  $i_{\text{corr}}$  than the PM and PS steel reinforcement. This thesis also provides a parametric study on the probabilistic estimations of  $t_p$  using (1) the model developed by Wang and Zhao (1993) and (2) the developed statistical distributions of  $i_{\text{corr}}$  for both wet and dry conditions and (3) considering the possible effect of the annual rainfall period of 3 months. The reinforced concrete system considered for the estimation has 50 mm thick cover and 30 MPa of concrete. The outcome shows that the median of  $t_p$  for a system with CTD and QST steel reinforcement are less than 10 years, whereas it is less than 20 years for the systems with PM and PS steel rebar. This thesis also provides statistical charts for the estimation of  $t_p$  for systems with various steels. Moreover, the probabilistic estimations on  $t_p$  and the time required for 5, 10, and 15 % reduction in tensile strength of PM, CTD, QST, and PS steel rebar embedded in mortar exposed to cyclic wet-dry exposure are provided.

In short, this thesis provides experimental methods and statistical tools to obtain quantitative information on  $Cl_{\text{th}}$  and  $i_{\text{corr}}$  for various steel-cementitious systems, which can serve as the input parameters to estimate the  $t_i$  and  $t_p$  of such systems exposed to chloride environments. However, it should be noted that there are other environmental and material parameters that affect the  $Cl_{\text{th}}$ ,  $i_{\text{corr}}$ , chloride ingress rate, etc. and their effects should be taken into account while estimating service life. Such quantitative information can help engineers in selecting durable materials during the planning and design stages itself -thereby enhancing the overall service life of concrete structures exposed to chloride environments.



# TABLE OF CONTENTS

<b>ACKNOWLEDGEMENTS.....</b>	<b>v</b>
<b>ABSTRACT .....</b>	<b>vii</b>
<b>LIST OF FIGURES .....</b>	<b>xv</b>
<b>LIST OF TABLES .....</b>	<b>xix</b>
<b>LIST OF ABBREVIATIONS .....</b>	<b>xxi</b>
<b>1 INTRODUCTION .....</b>	<b>1</b>
1.1 PROBLEM STATEMENT .....	1
1.2 DEFINITIONS .....	3
1.3 RESEARCH HYPOTHESES AND ASSUMPTIONS .....	3
1.4 OBJECTIVES AND SCOPE .....	4
1.5 RESEARCH METHODOLOGY .....	5
1.6 ORGANIZATION OF THESIS .....	6
<b>2 LITERATURE REVIEW .....</b>	<b>7</b>
2.1 INTRODUCTION .....	7
2.2 BASIC MECHANISMS OF CORROSION.....	7
2.2.1 Anodic reactions.....	7
2.2.2 Cathodic reactions .....	8
2.3 SERVICE LIFE OF CONCRETE STRUCTURES .....	9
2.3.1 Corrosion initiation period ( $t_i$ ).....	10
2.3.2 Corrosion propagation period ( $t_p$ ).....	10
2.4 MODELING OF CORROSION INITIATION PERIOD.....	10
2.4.1 Chloride diffusion coefficient of concrete ( $D_{cl}$ ) .....	11
2.4.2 Chloride threshold ( $Cl_{th}$ ) of steel in cementitious systems.....	15
2.4.3 Recommended upper limit of chloride concentration in new concrete...	19
2.5 MODELING CORROSION PROPAGATION PERIOD .....	19
2.5.1 Existing models to predict the corrosion propagation period.....	21
2.5.2 Influence of cracking on corrosion of rebar .....	24
2.6 CORROSION RATES OF STEEL REINFORCEMENT .....	25
2.7 TYPES OF REINFORCEMENT USED IN REINFORCED CONCRETE.....	27
2.7.1 Plain mild (PM) steel.....	27

2.7.2 Cold-twisted deformed (CTD) steel .....	27
2.7.3 Quenched and self-tempered (QST) or Thermo-mechanically-treated (TMT) steel.....	28
2.7.4 Prestressing (PS) steel .....	28
2.8 TYPES OF CORROSION INHIBITORS.....	29
2.8.1 Types of corrosion inhibiting admixtures (CIAs) .....	29
2.8.2 Migrating corrosion inhibitors (MCIs).....	31
2.9 CORROSION MEASUREMENT TECHNIQUES .....	31
2.9.1 Hall-cell potential test.....	32
2.9.2 Linear polarization resistance (LPR) technique .....	33
2.9.3 Electrical impedance spectroscopy (EIS).....	36
2.10 EXISTING TEST METHODS TO DETERMINE $CL_{TH}$ OF STEEL IN SYSTEM WITH CIAs	39
2.11 ISSUES WITH THE APPLICATION OF POTENTIAL GRADIENT IN EVALUATING THE PERFORMANCE OF CIAs IN STEEL-CEMENTITIOUS SYSTEMS .....	40
2.12 RESEARCH NEEDS .....	41
2.13 SUMMARY .....	41
<b>3 RESEARCH SIGNIFICANCE .....</b>	<b>43</b>
<b>4 MATERIALS AND METHODS.....</b>	<b>45</b>
4.1 INTRODUCTION .....	45
4.2 OBJECTIVE 1: DETERMINATION OF THE EFFECT OF EXTERNAL POTENTIAL ON ANION TRANSPORT THROUGH MORTAR .....	45
4.2.1 Introduction .....	45
4.2.2 Specimen design and preparation.....	45
4.2.3 Test setup to apply external potential.....	47
4.2.4 Determination of chloride and nitrite concentration .....	49
4.3 OBJECTIVE 2: DEVELOPMENT OF MODIFIED ACT (MACT) TEST METHOD .....	51
4.3.1 Specimen configuration and materials used.....	51
4.3.2 Casting, curing, and chloride exposure .....	56
4.3.3 Corrosion measurements .....	56
4.3.4 Statistical approach to detect corrosion initiation .....	59
4.3.5 Method to determine the chloride and nitrite concentration .....	62
4.4 OBJECTIVE 3: DETERMINATION OF CHLORIDE THRESHOLD OF QST STEEL EMBEDDED IN SYSTEMS WITH CIAs .....	63

4.5	OBJECTIVE 4: DETERMINATION OF CORROSION RATES OF DIFFERENT STEELS ....	64
4.5.1	Introduction .....	64
4.5.2	Specimen design and preparation.....	65
4.5.3	Curing and exposure conditions .....	66
4.5.4	Corrosion test setup and corrosion rate measurements .....	67
4.6	SUMMARY.....	70
<b>5</b>	<b>RESULTS AND DISCUSSIONS.....</b>	<b>71</b>
5.1	INTRODUCTION .....	71
5.2	OBJECTIVE 1: DETERMINATION OF THE EFFECT OF EXTERNAL POTENTIAL ON THE MIGRATION OF ANIONS THROUGH MORTAR.....	71
5.2.1	Migration of chloride ions .....	71
5.2.2	Migration of nitrite ions (anions) .....	72
5.2.3	Variation in the chloride-nitrite ratio.....	74
5.2.4	Summary of test results (Objective 1).....	75
5.3	OBJECTIVE 2: DEVELOPMENT OF mACT TEST METHOD .....	76
5.3.1	Inverse polarization resistance data for specimens without inhibitors....	77
5.3.2	$Cl_{th}$ for specimens without inhibitor and validation of mACT test method	78
5.3.3	Summary of test results (Objective 2).....	80
5.4	OBJECTIVE 3: DETERMINATION OF CHLORIDE THRESHOLD OF QST STEEL EMBEDDED IN SYSTEMS WITH CIAS.....	80
5.4.1	Inverse polarization resistance data for specimens with AN and BP inhibitors.....	80
5.4.2	$Cl_{th}$ of QST steel embedded in systems with CIAs .....	83
5.4.3	Duration of mACT testing for systems with and without CIAs.....	84
5.4.4	Practical application of the mACT .....	85
5.4.5	Limitations of the mACT test method.....	89
5.4.6	Summary of test results (Objective 3).....	90
5.5	OBJECTIVE 4: DETERMINATION OF CORROSION RATES OF DIFFERENT STEELS ...	91
5.5.1	Corrosion rate of different steels in laboratory.....	91
5.5.2	Average annual corrosion rate in the field .....	96
5.5.3	Statistical distributions of corrosion rate of different steels.....	96
5.5.4	Probabilistic estimation of $t_p$ to initiate crack in cover concrete .....	99

5.5.5 Probabilistic estimation of $t_p$ for varying reduction in cross-sectional area ( $t_p, \Delta\%$ ).....	101
5.5.6 Summary .....	105
<b>6 CONCLUSIONS AND FUTURE RECOMMENDATIONS.....</b>	<b>107</b>
6.1 INTRODUCTION .....	107
6.2 CONCLUSIONS.....	108
6.2.1 Effect of external potential on the migration of anions through mortar	108
6.2.2 Development of mACT test method.....	109
6.2.3 Chloride threshold of QST steel embedded in systems with CIAs .....	109
6.2.4 Corrosion rates of different steels.....	110
6.3 RECOMMENDATIONS FOR FUTURE WORK.....	111
<b>REFERENCES.....</b>	<b>113</b>
<b>APPENDIX A – mACT PROCEDURE TO DETERMINE THE CHLORIDE THRESHOLD OF STEEL EMBEDDED IN CEMENTITIOUS SYSTEMS .....</b>	<b>127</b>
<b>APPENDIX B - STANDARD TEST METHOD TO DETERMINE TOTAL CHLORIDE CONTENT IN MORTAR OR CONCRETE USING THE SPECIFIC ION PROBE .....</b>	<b>141</b>
<b>APPENDIX C - PROCEDURE TO DETERMINE THE NITRITE CONCENTRATION FROM HARDENED CEMENTITIOUS SYSTEM USING UV SPECTROMETER .....</b>	<b>151</b>
<b>APPENDIX D - CORROSION PROPAGATION MODELS FROM LITERATURE.....</b>	<b>155</b>
<b>APPENDIX E – CHLORIDE DIFFUSION MODELS FROM LITERATURE...</b>	<b>165</b>
<b>LIST OF PUBLICATIONS BASED ON THIS THESIS .....</b>	<b>169</b>
<b>DOCTORAL COMMITTEE.....</b>	<b>171</b>
<b>CURRICULUM VITAE.....</b>	<b>173</b>

## LIST OF FIGURES

Figure 1.1 Research methodology .....	5
Figure 2.1 Corrosion process on the surface of steel (Bentur et al., 1998) .....	8
Figure 2.2 Service life of a reinforced concrete structure exposed to chlorides (modified from Tutti, 1982) .....	9
Figure 2.3 Schematic of chloride-induced corrosion mechanisms (Silva et al., 2012)....	16
Figure 2.4 $Cl_{th}$ reported in literature (reproduced from Pillai and Annapareddy, 2013)..	17
Figure 2.5 Relative volume of various corrosion products (Gaidis and Rosenberg, 1987) .....	20
Figure 2.6 Effect of corrosion propagation on structural performance. ....	20
Figure 2.7 Schematic half-cell potential test setup.....	32
Figure 2.8 Typical linear polarization resistance test setup (Jaime et al., 2013).....	33
Figure 2.9 A typical LPR plot .....	35
Figure 2.10 Nyquist and Bode plots for a typical steel-cementitious system .....	37
Figure 2.11 Equivalent electrical circuit for a typical steel-cementitious system.....	38
Figure 4.1 Comparison of ACT specimens with modified RCPT test .....	47
Figure 4.2 Test setup to study the effect of anion migration due to external potential ....	48
Figure 4.3 DC potential source used for this study (Agilent E3611A) .....	49
Figure 4.4 Mortar powder ground at the steel-mortar interface .....	49
Figure 4.5 Chloride ion specific electrode connected to conductivity meter .....	50
Figure 4.6 UV-Visible spectrometer .....	50
Figure 4.7 Schematic of the mACT test setup.....	52
Figure 4.8 Photograph of the mACT test setup in the laboratory .....	52
Figure 4.9 Cross section of the mACT mould.....	53
Figure 4.10 Nichrome mesh connected with copper rod.....	53
Figure 4.11 Saturated calomel reference electrode .....	54
Figure 4.12 Haber-Luggin probe .....	54
Figure 4.13 A typical working electrode used for mACT testing .....	55
Figure 4.14 A typical linear polarization resistance (LPR) curve .....	57
Figure 4.15 Equipotential and equicurrent lines between WE and CE .....	57
Figure 4.16 Plot showing $R_{cm}$ with respect to time for a specimen .....	58
Figure 4.17 Flowchart to conduct mACT test .....	60
Figure 4.18 Statistical approach used in mACT method to detect corrosion initiation ...	61

Figure 4.19 Specimen autopsied across the steel mortar interface.....	62
Figure 4.20 Concrete profile grinder (Germann Inc. Model No. PF-1100) .....	63
Figure 4.21 Representation of probabilistic corrosion propagation period.....	64
Figure 4.22 Corrosion test specimen with a steel bar embedded in mortar .....	66
Figure 4.23 Schematic of the 3-electrode corrosion cell setup .....	68
Figure 4.24 Corrosion test setup with corrosion cell, potentiostat, and computer .....	69
Figure 5.1 Variation in chloride due to application of external potential .....	71
Figure 5.2 Variation in chloride at different depth w.r.t potential applied.....	72
Figure 5.3 Variation in nitrite due to application of external potential .....	73
Figure 5.4 Variation in nitrite at different depth w.r.t potential applied .....	73
Figure 5.5 Variation in chloride-to-nitrite ratio due to application of external potential.	74
Figure 5.6 Variation in chloride-nitrite ratio at different depth w.r.t potential applied ...	75
Figure 5.7 Inverse polarization resistance Vs chloride exposure time for systems without inhibitor (W/O) .....	78
Figure 5.8 $Cl_{th}$ of QST steel in systems without CIAs (plain mortar).....	79
Figure 5.9 Inverse polarization resistance Vs chloride exposure time for systems with anodic inhibitor (AN).....	81
Figure 5.10 Inverse polarization resistance Vs chloride exposure time for systems with bipolar inhibitor (BP).....	82
Figure 5.11 $Cl_{th}$ of QST steel in systems with and without CIAs .....	83
Figure 5.12 Exposure period required to initiate corrosion in QST steel.....	85
Figure 5.13 Effect of CIAs on $t_i$ of concrete with $D_{cl} = 3 \times 10^{-12} \text{ m}^2/\text{s}$ and located at (a) marine splash zone, (b) within 800 m from the ocean, and (c) within 1.5 km from the ocean.....	86
Figure 5.14 Effect of CIAs on $t_i$ of concrete with $D_{cl} = 2 \times 10^{-12} \text{ m}^2/\text{s}$ and located at (a) marine splash zone, (b) within 800 m from the ocean, and (c) within 1.5 km from the ocean.....	88
Figure 5.15 Average corrosion potential of PM, CTD, QST, and PS steel.....	93
Figure 5.16 Average corrosion current density of PM, CTD, QST, and PS steel.....	93
Figure 5.17 Average $i_{corr, wet}$ of various steels measured .....	94
Figure 5.18 Average $i_{corr, dry}$ of various steels measured .....	95
Figure 5.19 Distributions for $i_{corr, wet}$ and $i_{corr, dry}$ of various steel reinforcement.....	98
Figure 5.20 Estimated crack initiation period based on $i_{corr, annual}$ .....	101
Figure 5.21 $t_{p, 5\%}$ , $t_{p, 10\%}$ , and $t_{p, 15\%}$ loss in PM steel rebar w.r.t. exposure period.....	102

Figure 5.22.  $t_{p, 5\%}$ ,  $t_{p, 10\%}$ , and  $t_{p, 15\%}$  loss in CTD steel rebar w.r.t. exposure period..... 103

Figure 5.23  $t_{p, 5\%}$ ,  $t_{p, 10\%}$ , and  $t_{p, 15\%}$  loss in QST steel rebar w.r.t. exposure period ..... 103

Figure 5.24.  $t_{p, 5\%}$ ,  $t_{p, 10\%}$ , and  $t_{p, 15\%}$  loss in PS steel rebar w.r.t. exposure period ..... 104



## LIST OF TABLES

Table 2.1 Diffusion equations for different boundary conditions [Carslaw and Jaeger 1947] .....	12
Table 2.2 Different variables considered and the variation in the approaches adopted by various service life prediction models. ....	14
Table 2.3 Recommendations in international standards on upper limit of chloride content in concrete.....	19
Table 2.4 Input parameters required for different propagation models.....	22
Table 2.5 Corrosion rate of steel specimen represented in literature .....	26
Table 2.6 Interpretation of corrosion potential readings [ASTM C 876 (2015)] .....	32
Table 4.1 Chemical composition of Ordinary Portland Cement (OPC).....	46
Table 4.2 Physical Properties of Ordinary Portland Cement (OPC).....	46
Table 4.3 Particle size distribution of sand used for cement mortar .....	46
Table 4.4 Typical properties of AN and BP corrosion inhibitor .....	47
Table 4.5 Chemical composition of Simulated Pore Solution (SPS) .....	48
Table 4.6 Chemical composition (% by weight) of different steel rebars.....	55
Table 4.7 Experimental design for the mACT tests .....	55
Table 5.1 Chloride threshold of QST steel embedded in cementitious systems with and without CIAs.....	84
Table 5.2 $t_i$ (years) for systems with CIAs Chloride threshold of QST steel embedded in cementitious systems with and without CIAs.....	89
Table 5.3 Goodness of fit for $i_{\text{corr}}$ of PM, CTD, QST, and PS steel reinforcement exposed from 19 to 24 month of wet data and 27 <sup>th</sup> and 33 <sup>rd</sup> month dry data.....	97
Table 5.4 Summary of $i_{\text{corr, wet}}$ distributions based on the corrosion rate of different steel reinforcement .....	99
Table 5.5. Summary of $i_{\text{corr, dry}}$ distributions based on the corrosion rate of different steel reinforcement .....	99
Table 5.6 Parameters considered for estimating $t_i$ using Wang and Zhao (1993) .....	100



## LIST OF ABBREVIATIONS

%bwoc	: % by weight of cement
$\varnothing_t$	: Diameter of corroded rebar at time, t
$\Delta$	: Thickness of corrosion product
$\gamma$	: Crack expansion coefficient
$\mu_5$	: Sum of $R_p$ data set considered for analysis
$\mu_{st}$	: Sum of stable $R_p$ data set
$\rho_{st}$	: Density of steel
$\sigma_5$	: Standard deviation of $R_p$ data set considered for analysis
$\sigma_{st}$	: Standard deviation of stable $R_p$ data set
ACT	: Accelerated threshold test
AN	: Anodic
B	: Stern-Geary coefficient
BP	: Bipolar
$C_i$	: Initial chloride concentration of concrete
CIA	: Corrosion Inhibiting Admixtures
$Cl_{th}$	: Chloride threshold value
COV	: Coefficient of variation
$C_s$	: Surface chloride concentration
CTD	: Cold Twisted Deformed
D	: Initial diameter of reinforcement
$D_{cl}$	: Chloride diffusion coefficient of concrete
E	: Applied potential
$E_{corr}$	: Corrosion potential
EIS	: Electrical Impedance Spectroscopy
erfc	: Complimentary error function
F	: Faraday's constant
$f_{cu}$	: Cube strength of concrete
H	: Depth of rebar penetration
HCP	: Half-cell potential
I	: Corrosion current
$i_{corr}$	: Corrosion rate

$i_{\text{corr, annual}}$	: Weighted average annual corrosion rate
$i_{\text{corr, dry}}$	: Corrosion rate measured when the steel-cementitious interface is dry
$i_{\text{corr, wet}}$	: Corrosion rate measured when the steel-cementitious interface is wet
ISE	: Ion specific electrode
k	: Multiplication coefficient to define stable data
LPR	: Linear Polarization Resistance
$M(t_p)$	: Median of corrosion propagation period
mACT	: Modified Accelerated Chloride Threshold
W/O	: Without
OCP	: Open Circuit Potential
OPC	: Ordinary Portland Cement
PDF	: Probability Density Function
PM	: Plain Mild
$P_r$	: Corrosion penetration rate
PS	: Prestressing
QST	: Quenched and Self Tempered (also known as TMT)
$R_{\text{cm}}$	: Resistance of cementitious system
RCPT	: Rapid Chloride Permeability Test
$R_p$	: Polarization resistance at steel-cementitious interface
$R_{\text{total}}$	: Bulk resistance of steel-cementitious system
SCE	: Saturated Calomel Electrode
SPS	: Simulated Pore Solution
t	: Duration of exposure
$t_{\Delta, X\%}$	: Time required for X % reduction in tensile strength of steel
$t_{\text{cr}}$	: Time required for corrosion-induced cracking of cover concrete
$t_i$	: Time required for corrosion initiation
TMT	: Thermo-Mechanically Treated (also known as QST)
$t_p$	: Time required for corrosion propagation
$t_r$	: Time to repair
W	: Equivalent weight of steel
x	: Depth considered to determine anion concentration

# 1 INTRODUCTION

## 1.1 PROBLEM STATEMENT

In reinforced concrete structures, the steel reinforcement (say, rebar) plays a vital role in carrying the structural load. Therefore, the steel embedded in concrete must be protected from corrosion such that the structure can have desired service life. However, premature corrosion of reinforced concrete structures have been observed worldwide due to many reasons. The key parameters that influence the corrosion initiation period ( $t_i$ ) and corrosion propagation period ( $t_p$ ) are chloride threshold ( $Cl_{th}$ ) and corrosion rate ( $i_{corr}$ ), respectively (Tutti 1982). The quantitative information or statistical distributions on these key parameters for various steel-cementitious can be helpful in selecting durable materials during the planning and design stages itself. However, such information and/or tools to obtain such information is not available, especially for new construction materials available in today's market.

Now-a-days, corrosion inhibiting admixtures (CIAs) are widely used to increase the  $Cl_{th}$  and corrosion resistance of steel-cementitious systems. In addition, CIAs based on various chemical families (nitrites, amines, etc.) and compositions are available in the market. However, the quantitative information on the effect of various types of CIAs on the  $Cl_{th}$ ; and hence, their effect on increasing  $t_i$  cannot be estimated. Also, many companies are producing Quenched and Self-Tempered (QST) steel. Note that in the Indian subcontinent, the QST steel is known as Thermo-Mechanically Treated (TMT) steel and is widely steel in the Indian construction industry. In particular, it is necessary to find the effect of various types of CIAs on the  $Cl_{th}$  of QST/TMT steel.

Currently available test methods to determine the  $Cl_{th}$  adopt the application of external potential gradient to accelerate the movement of chlorides towards the anode (rebar) in the test setup. Such application of potential difference may lead to the unwanted movement of anions in the CIAs (say, nitrites, amines, etc.) towards the anode. This leads to a change in the concentration of anions at or near the steel-cementitious interface. Such changes do not happen in concrete structures. Hence, the application of potential gradient may lead to an erroneous determination of  $Cl_{th}$  for real life systems with CIAs. Moreover, a suitable, short-term test

procedure to determine the  $Cl_{th}$  of steel-cementitious systems with CIAs is not available (Wu-Man et al., 2011). Therefore, engineers find it difficult to estimate the  $t_i$  for various material combinations and choose durable materials during the planning and design stage.

The estimation of residual service life is a challenging task and needed to decide the repair schedule and strategies. Corrosion propagation leads to the gradual loss of steel, which reduces the load carrying capacity of structures (Andrade et al., 2002). The corrosion rate ( $i_{corr}$ ) of steel is the parameter that leads to strength reduction of steel rebars. Different types of steel are used in construction industry and can have different  $i_{corr}$  and could lead to significant changes in the corrosion propagation period (Li et al., 2011). The existing inventory of concrete structures uses different types of steels. Engineers are in need of estimating the  $t_p$  for structures with different steel types and experiencing corrosion. Four such widely used steels are Plain Mild (PM), Cold-Twisted Deformed (CTD), Quenched and Self-Tempered (QST) and PreStressing (PS) steels. However, statistical distributions on the  $i_{corr}$  of these steels used/available in India are not well reported and engineers are not able to determine probabilistic  $t_p$  to decide the repair schedule and strategies.

Thus, statistical distributions of the two major service life parameters (say,  $Cl_{th}$  and  $i_{corr}$ ) need to be developed so that engineers can determine probabilistic  $t_i$  and  $t_p$  of reinforced concrete structures exposed to chloride environments. As a summary of all the problem stated, the following are the key questions citing the need for this research work,

- What is the effect of external potential application on the movement of nitrite ions through the cementitious system and how that will affect the estimation of  $Cl_{th}$  of systems with CIAs?
- Can a short-term test method be developed to estimate  $Cl_{th}$  of systems with CIAs?
- What is the effectiveness of bipolar type CIA's in increasing the  $Cl_{th}$  of steel?
- What is the difference in the rate of chloride-induced corrosion of different types of steels used in construction and how can they be modeled statistically?

## 1.2 DEFINITIONS

Definitions of some key terms used in this study are as follows:

**Service life ( $t_{sl}$ ):** Sum of corrosion initiation period ( $t_i$ ) and corrosion propagation period ( $t_p$ ).

**Corrosion initiation period ( $t_i$ ):** The time required to initiate corrosion of the embedded steel reinforcement.

**Corrosion propagation period ( $t_p$ ):** The time required, after corrosion initiation, to initiate the first crack in cover concrete due to prolonged corrosion.

**Chloride threshold ( $Cl_{th}$ ):** The minimum concentration of chloride at a depth of the reinforcement, which results in active corrosion of the steel.

**Chloride / Nitrite threshold, ( $Cl/NO_2$ ) $_{th}$ :** The ratio of the concentrations of chlorides and nitrites at steel surface required to initiate corrosion on steel.

**Corrosion rate ( $i_{corr}$ ):** The corrosion current density or the rate of degradation of metal due to electrochemical reactions.

**Chloride diffusion coefficient ( $D_{cl}$ ):** The amount of chloride moving across a unit area of a cementitious system in unit time.

## 1.3 RESEARCH HYPOTHESES AND ASSUMPTIONS

The following are the hypotheses of this research,

- Application of external potential gradient between the embedded steel specimen and the surface of mortar cover can lead to an increase in the concentration of anions/nitrites at the steel surface, which will affect the estimation of  $Cl_{th}$  of systems with CIAs.
- Short term  $Cl_{th}$  test without the application of potential gradient is possible.
- Use of CIAs can increase the  $Cl_{th}$ , which can be expressed as a normal distribution.
- Use of CIAs may increase the corrosion initiation period ( $t_i$ ).

- The  $i_{\text{corr}}$  of different types of steels embedded in similar chloride-contaminated mortar and exposed to long-term wet-dry and dry exposure conditions can be expressed as statistical distributions.
- Variation in the type of steel reinforcement can influence the  $t_p$ .
- It is assumed that the ‘wet’ in the term  $i_{\text{corr, wet}}$  indicates the steel-cementitious interface is in wet condition. Similarly, for the ‘dry’ in the term  $i_{\text{corr, dry}}$  indicates the steel-cementitious interface is wet condition.

#### 1.4 OBJECTIVES AND SCOPE

1. To study the effect of external potential application on the transport of anions through cementitious systems
  - Anions: Chloride, Nitrite
  - Potential applied: 20 Volts DC
  - Duration of potential applied: 6, 12, 36, and 48 hours
  - Mortar type: 0.45:1:2.25 (water:cement:sand)
  - Test name: Modified RCPT
2. To develop a test procedure to determine the critical chloride threshold ( $Cl_{\text{th}}$ ) of steel - cementitious systems with corrosion inhibiting admixtures (CIAs).
  - Steel type: Quenched and Self-Tempered (QST) steel
  - Mortar type: 0.45:1:2.25 (water:cement:sand)
  - Inhibitor types: Anodic and bipolar corrosion inhibitors
3. To determine the  $Cl_{\text{th}}$  of QST steel embedded in cementitious system with CIAs and estimate corrosion initiation period.
  - Steel type: Quenched and Self-Tempered steel
  - Mortar type: 0.45:1:2.25 (water:cement:sand)
  - Inhibitor types: Anodic and Bipolar corrosion inhibitor

4. To determine the corrosion rates of various types of steel reinforcement embedded in chloride contaminated mortar and to estimate the corrosion propagation period
  - Steel types: Plain Mild (PM), Cold-twisted and Deformed (CTD), Quenched and Self-Tempered (QST), and Prestressing (PS) steel
  - Mortar type: 0.5:1:2.25 (water:cement:sand)
  - Exposure conditions: 27 months wet-dry cycle and 9 months of standard room condition.

### 1.5 RESEARCH METHODOLOGY

Research methodology with the key steps involved in achieving the objectives are described in Figure 1.1. Two experimental programs are planned to facilitate the estimation of  $t_i$  and  $t_p$ .

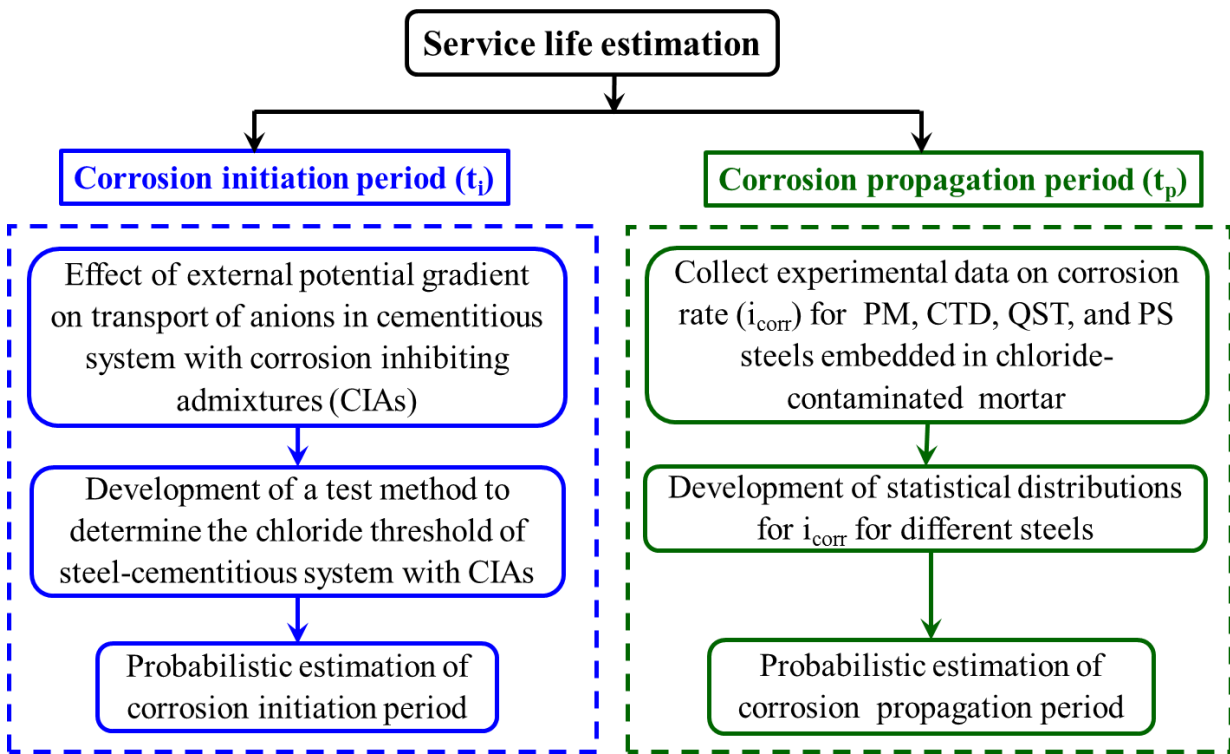


**Figure 1.1 Research methodology**

## **1.6 ORGANIZATION OF THESIS**

There are six sections in this thesis. The present section discusses the problem in general followed by the objectives, scope, and methodology of the research study. The second section gives a detailed review of the literature covering different aspects of corrosion and its effects pertaining to this study. The need for present research and its significance is described in the third section. The description of the materials, test procedures, and the experimental design are described in the fourth section. The results and discussion for each experimental program are presented in the fifth section. The concluding remarks followed by specific conclusions and scope for further research are presented in the sixth section.

## 2 LITERATURE REVIEW

### 2.1 INTRODUCTION

This section starts with a discussion on the basic mechanisms of corrosion. Then, the various phases of the service life of concrete structures and different mathematical models available to estimate the duration of these phases are discussed. Then a detailed review on the major parameters influencing the service life [i.e., chloride threshold ( $Cl_{th}$ ) and corrosion rate ( $i_{corr}$ )] is provided. Finally, different corrosion assessment techniques available to determine the  $Cl_{th}$  and  $i_{corr}$  are discussed.

### 2.2 BASIC MECHANISMS OF CORROSION

Corrosion is an electrochemical process, where the redox reactions take place at the surface of the steel in the presence of moisture and oxygen. The corrosion process involves two half-cell reactions, i.e., anodic and cathodic reactions (Jones 1996). For essential components of an electrochemical cell are (i) an anode, (ii) a cathode, (iii) an electronic conductor, and (iv) an ionic conductor. The following section explains the electrochemical reactions.

#### 2.2.1 Anodic reactions

At the anode, the oxidation of metal (say,  $Fe$ ) leads to corrosion, where the metal atom will be oxidized to an ion with the valance charge of  $n+$  and the release of  $n$  electrons. In steel rebar, the anodic reaction takes place as given in the Eq. 2.1, where the steel is oxidized to ferrous ions as shown in Figure 2.1.



The ferrous ions can subsequently get further oxidized to different forms through a series of complex reactions.

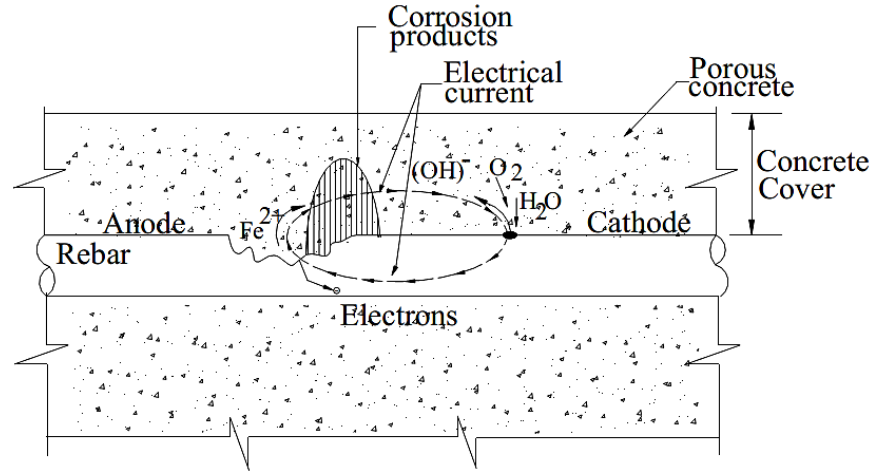


**Figure 2.1 Corrosion process on the surface of steel (Bentur et al., 1998)**

### 2.2.2 Cathodic reactions

At the cathode, the reduction reaction takes place by consuming the released electrons to produce hydroxyl ions. A typical cathodic reaction is given in Eq. 2.2.



The overall corrosion reaction is given in Eq. 2.3 in which the ferrous ions from the anode and the hydroxyl ions from cathode combine to form ferrous hydroxide.



The ferrous hydroxide can get further oxidized to hydrated ferric oxide, a red-brown rust as given in Eq. 2.4. and mentioned as “corrosion products” in Figure 2.1.



In the highly alkaline environment in uncontaminated concrete, the ferrous oxide may get oxidized to gamma ferric oxy-hydroxide, as given in Eq. 2.5, which is a stable passive film that protects the reinforcing steel from corrosion.



This passive film can be disrupted if the concentration of chloride exceeds the  $Cl_{th}$ , which leads to the corrosion initiation in the reinforcement. The chloride-induced corrosion mechanisms are briefly discussed in Section 2.4.2.1.

### 2.3 SERVICE LIFE OF CONCRETE STRUCTURES

The premature corrosion of reinforcement steel is the major reason for the reduction in the service life of the structure. Normally, the corrosion in reinforced concrete structures occurs due to the ingress of species (like oxygen, water, chloride, carbon dioxide etc.) through cover concrete. Many investigators like Tutti (1982), Schiessl (1987), Broomfield (2007), Amey et al. (1998), etc. have mentioned that the chloride-induced deterioration of a structure can be classified into two stages viz. (i) corrosion initiation period ( $t_i$ ), and (ii) corrosion propagation period ( $t_p$ ). Figure 2.2 shows a simplified representation [Tutti (1982)] of  $t_i$  and  $t_p$ , which end at corrosion initiation and crack initiation points, respectively. The sum of  $t_i$  and  $t_p$  can be defined as the overall service life. Sections 2.3.1 and 2.3.2 discuss  $t_i$  and  $t_p$ , respectively.

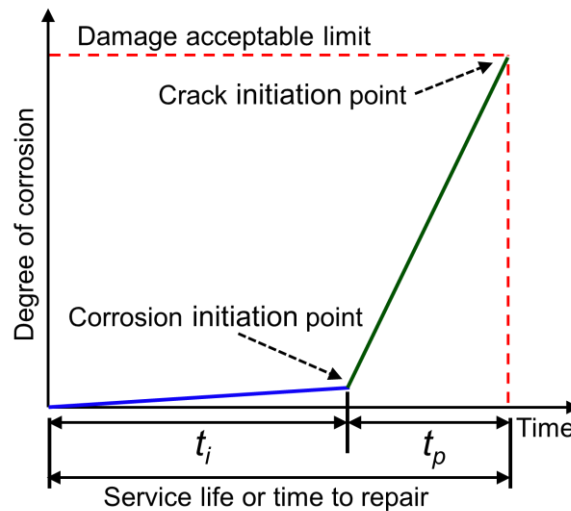


**Figure 2.2 Service life of a reinforced concrete structure exposed to chlorides  
(modified from Tutti, 1982)**

### 2.3.1 Corrosion initiation period ( $t_i$ )

During the corrosion initiation period, the chlorides can ingress through the cover concrete and progress towards the surface of the embedded steel. At this stage, there will be no or negligible corrosion activity on the steel rebars and the alkalinity of the concrete will be high [say,  $\text{pH} > 13$ ] (Bentur et al., 1998). The steel can lose its passivity when the chloride concentration exceeds the  $\text{Cl}_{\text{th}}$  level. In addition, the duration of  $t_i$  depends on the rate of ingress of chlorides through the cover-concrete, the thickness of the cover concrete, and the aggressiveness of the environment to which it is exposed (chloride, temperature, moisture conditions, etc.).

### 2.3.2 Corrosion propagation period ( $t_p$ )

During the corrosion propagation period, the corrosion of steel propagates and finally leads to cracking and spalling of cover concrete. The duration of  $t_p$  mainly depends on the  $i_{\text{corr}}$  of the reinforcement, the tensile strength of cover concrete, interconnectivity of pores in the cover concrete, etc. After cracking of the cover concrete, the reinforcement will be directly exposed to the aggressive environment, which will further increase the  $i_{\text{corr}}$ .

## 2.4 MODELING OF CORROSION INITIATION PERIOD

As the typical service life of a structure could be several decades, natural field exposure and long-term experimental studies cannot be the only solution to assess or estimate it. To assess  $t_p$ , the two important material parameters that needed to be determined are: (i) chloride diffusion coefficient of concrete ( $D_{\text{cl}}$ ) and (ii) critical chloride threshold of steel ( $\text{Cl}_{\text{th}}$ ). Accelerated and reliable laboratory based test method is necessary to acquire the data to assess the performance of the main influencing parameters that contribute to the service life of a reinforced concrete structure. In most such studies, aggressive exposure conditions and electrochemical techniques are used as time-saving methods.

## 2.4.1 Chloride diffusion coefficient of concrete ( $D_{cl}$ )

### 2.4.1.1 Fick's 2<sup>nd</sup> Law of diffusion

The ASTM C1556 (2016) is a well-established test method to determine the  $D_{cl}$ . The chloride ions from external sources like seawater, de-icing/anti-icing salts, etc. can penetrate into the cementitious system and reach the embedded steel. Also, internally available chlorides from the chloride-contaminated ingredients like aggregate, water, etc. can also be the source of chloride-induced corrosion. Most of the models estimate the rate of chloride penetration by assuming the concrete is homogenous at the macro-scale, and crack-free.

Fick's 2<sup>nd</sup> law of diffusion is most commonly used to estimate the chloride diffusion in concrete. While this is not strictly correct, it serves as a useful starting point for prediction. When chloride diffuses into the concrete, the concentration of chlorides and the apparent chloride diffusion coefficient ( $D_{cl}$ ) vary with respect to exposure period ( $t$ ) at a depth ( $x$ ) in concrete, due to the non-steady-state nature of chloride diffusion.

For a semi-infinite homogeneous medium, the law of diffusion may be stated as follows:

$$\frac{\partial C}{\partial t} = D_{cl} \frac{\partial^2 C}{\partial x^2} \quad \text{Eq. 2.6}$$

By assuming the one-dimensional diffusion into semi-infinite space, the diffusion coefficient can be obtained from the following mathematical expression. Carslaw and Jaeger (1947) provided solutions with various boundary conditions for the flow of heat in a semi-infinite solid media obtained using the Laplace transformation method. These solutions can be used to model the chloride migration in concrete with various boundary conditions as given in Table 2.1.

**Table 2.1 Diffusion equations for different boundary conditions [Carslaw and Jaeger 1947]**

<p>Case (i): For constant chloride concentrations at the concrete surface, the surface buildup rate, <math>\Phi(t) = C_0</math>,</p> $C(x,t) = C_i + (C_s - C_i) \cdot \operatorname{erfc}\left(\frac{x}{\sqrt{4Dt}}\right)$
<p>Case (ii): For cases where chloride concentration at the concrete surface varies linearly with the time of exposure, i.e., <math>\Phi(t) = kt</math>, then;</p> $C(x,t) = kt \left\{ \left(1 + \frac{x^2}{2Dt}\right) \cdot \operatorname{erfc}\left(\frac{x}{\sqrt{4Dt}}\right) - \frac{x}{\sqrt{\pi Dt}} \cdot \exp\left(-\frac{x^2}{4Dt}\right) \right\}$
<p>Case (iii): For cases where chloride concentrations at the concrete surface varies as a function of the square root of time of exposure, i.e. <math>\Phi(t) = k\sqrt{t}</math>, then,</p> $C(x,t) = k\sqrt{t} \left\{ \exp\left(-\frac{x^2}{4Dt}\right) - \frac{x\sqrt{\pi}}{\sqrt{4Dt}} \cdot \operatorname{erfc}\left(\frac{x}{\sqrt{4Dt}}\right) \right\}$
<p><math>C(x,t)</math> is the chloride concentration at depth, <math>x</math>, at exposure time, <math>t</math>  <math>C_i</math> is the initial chloride concentration at depth <math>x</math> (<math>t = 0</math>)  <math>C_s</math> is the surface chloride concentration (<math>t \geq 0</math>)  <math>\operatorname{erfc}</math> is the complementary error function has limit from 0 to <math>\frac{x}{\sqrt{4Dt}}</math>  <math>k</math> is a proportionality constant.</p>

By considering the boundary condition as the chloride concentrations is constant at the concrete surface, then the surface buildup rate,  $\Phi(t) = C_0$ , and the following equation is used to determine  $D_{cl}$ ,

$$C(x,t) = C_i + (C_s - C_i) \operatorname{erfc}\left(\frac{x}{\sqrt{4tD_{cl}}}\right) \quad \text{Eq. 2.7}$$

Note that the Eq. 2.7 is valid for a constant  $C_s$ . The commonly used diffusion equations with different boundary conditions are listed in Appendix E. The diffusion of chloride will be faster when the concrete is made with the higher water-binder ratio (Frangopol et. al., 1997). The higher water-cement ratio leads to more air-voids in concrete, which is more favorable for chloride diffusion. The  $D_{cl}$  of the concrete depends on many factors like presence of

micro-cracks, water-cement ratio, compaction, curing, mineral admixtures, surface chloride concentration, period of exposure, etc. and typically, it ranges from  $10^{-13}$  to  $10^{-10}$  m<sup>2</sup>/s (Song et. al., 2008). Page et al. (2009) showed that the increase in a water-cement ratio from 0.4 to 0.6 increases the  $D_{cl}$  from 4 to 6 times. Thus, the use of higher water-cement ratio will increase the diffusion rate and in turn, shortens the time required for the chloride to reach the steel and build up the  $Cl_{th}$  level. It should be noted that this thesis does not focus on the estimation of  $D_{cl}$ ; rather, it focuses on the estimation of  $Cl_{th}$ .

Also, literature provides other models based on the Fick's second law by simplifying the assumptions required. Richardson (2002) reported that most of the diffusion based chloride ingress models do not consider the effect of absorption on chloride transport and the combined mechanism of diffusion and absorption will result in a reduced estimation of service life than those estimated using diffusion models. The ingress of chlorides may vary by many parameters like water-binder ratio, binder content, binder type, temperatures, etc. Due to this, many studies have questioned the reliability of the estimations based on different models. However, the research is continuing to enhance the models to arrive at realistic estimates.

Life-365, CHLODIF, ClinConc, and DuraCrete are some of the existing models for service life estimation. List of tables in Appendix E provides the governing equation used in these models. Also, Table 2.2 provides a summary of the variables and modeling approaches used in these models (Pillai and Annapareddy, 2013). It should be noted that the major challenge remaining is in obtaining realistic estimates of the input variables for these models.

**Table 2.2 Different variables considered and the variation in the approaches adopted by various service life prediction models.**

<b>Variable / Approach</b>	<b>Life-365™</b>	<b>CHLODIF</b>	<b>ClinConc</b>	<b>DuraCrete</b>
Chloride binding coefficient			✓	
Temperature	✓	✓	✓	✓
Relative humidity		✓		✓
Corrosion inhibitor content	✓			
Type of steel /chloride threshold	✓			
Admixtures in concrete	✓	✓	✓	✓
Porosity			✓	
Effect of co-existing ions			✓	
Modelling approach	Empirical	Empirical	Physical	Empirical
Computational approach	Deterministic / probabilistic	Deterministic	Deterministic	Deterministic

#### 2.4.1.2 *Life-365 software programs*

Life-365™ is a freeware, widely used for service life estimation and life-cycle cost assessment of concrete structures exposed to different chloride environment (splash zone, immersed, etc.). Life-365™ model predicts  $t_i$  using the Finite Difference Approach and Fick's Second Law of Diffusion, considering the total chloride content as the driving force, and the  $Cl_{th}$  of steel as a condition for corrosion initiation (Life-365, 2014). The chloride diffusion coefficient of concrete is estimated as follows.

$$D(t, T) = D_{ref} \times f(t) \times f(T) = D_{ref} \times \left( \frac{t_{ref}}{t} \right)^m \times e^{\frac{U}{R} \left( \frac{1}{T_{ref}} - \frac{1}{T} \right)} \quad \text{Eq. 2.8}$$

where,  $D(t, T)$  is diffusion coefficient at time  $t$  and temperature  $T$ ;  $m$  is diffusion decay or age factor,  $D_{ref}$  ( $= D_{28}$ ) is the apparent chloride diffusion coefficient at time  $t_{ref}$  ( $= 28$  days) and temperature  $T_{ref}$  ( $= 293$  K);  $U$  is activation energy of the chloride diffusion process ( $35000 \text{ J} \cdot \text{mol}^{-1}$ ); and  $R$  is universal gas constant ( $8.31 \text{ J} \cdot \text{mol}^{-1} \text{K}^{-1}$ ), respectively. For practical considerations, the value of chloride diffusion coefficient of concrete is assumed to be constant after 25 years. The  $D_{28}$  is theoretically computed based on the water–cement ratio ( $w/c$ ) ( $D_{28} = 10^{-12.06 + 2.4(w/c)}$ ).

For estimating the service life of a concrete structure, the details on the geographic location (to choose temperature profile), dimensions of structure, nature of exposure, mixture proportion of concrete, statistical distribution of the depth of clear concrete cover (if possible), type of reinforcement, and corrosion protection strategies (corrosion inhibitors, epoxy coating, etc.) employed are needed. Default values are assumed for most parameters required in the analysis. It should be noted that Life-365™ is limited by the assumptions or simplifications made on the complex phenomena (such as chloride ingress, loss of passivity on embedded steel, corrosion of steel and subsequent damage of the cover concrete). The lack of sufficient knowledge restricts a rigorous and accurate analysis. However, it can provide reasonable estimates on service life and will be used in the case studies presented later in this thesis.

## 2.4.2 Chloride threshold ( $Cl_{th}$ ) of steel in cementitious systems

### 2.4.2.1 Chloride-induced corrosion mechanisms

Chloride threshold ( $Cl_{th}$ ) in this context is the minimum concentration of chlorides to be present at rebar level to overcome the passivity and initiate corrosion even at high pH environment (Taylor et al., 1999). Once the chlorides come in contact with the reinforcement, they damage the protective, passive film even at high pH level and increase the rate of corrosion (Gaidis [2004], Ann and Song [2007], Xu et al., [2011], Verbeck, [1987]). The oxide film theory postulates that the chloride ions disturb the oxide film, which leads to an easy breakdown

of the passive layer (ACI 222R, 2010). The overall chloride-induced corrosion mechanisms in concrete are schematically represented in Figure 2.3.

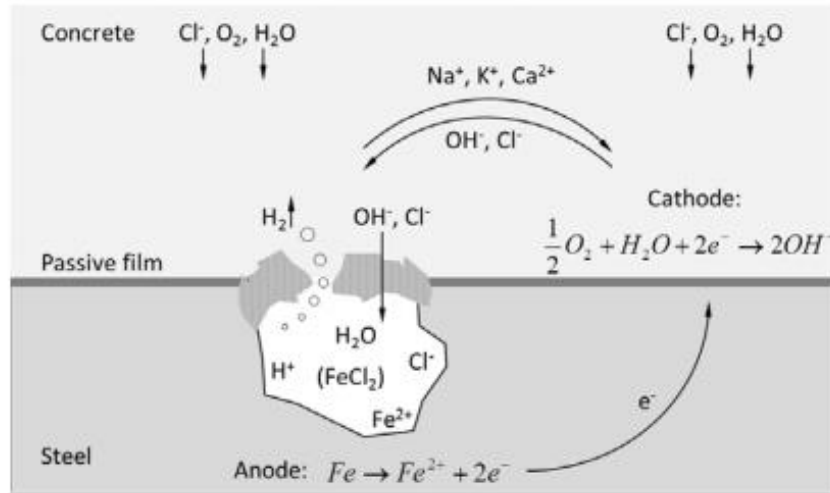


**Figure 2.3 Schematic of chloride-induced corrosion mechanisms (Silva et al., 2012).**

The reactions are given in Eq. 2.9 and Eq. 2.10 can take place while chloride-induced corrosion occurs on the steel surface (Neville, 1996).



Further, the chemical reactions continue to form rust, as catalytic reactions with chloride ions as catalysts. The concentration of chlorides required to sustain these catalytic reactions can be assumed to be the  $\text{Cl}_{\text{th}}$ . Significant research have been done to quantify the  $\text{Cl}_{\text{th}}$  of different types of steel embedded in the different cementitious environment. Angst et al. (2009b) provided a thorough review of the mechanisms of corrosion initiation and  $\text{Cl}_{\text{th}}$  in steel-cementitious systems.

2.4.2.2 Chloride threshold values and reasons for the large scatter

Significant research has been done to quantify the  $Cl_{th}$  of various types of steel reinforcement embedded in concrete. Figure 2.4 shows a bar chart with the  $Cl_{th}$  values reported in the literature. The ends of each bar indicate the minimum and maximum  $Cl_{th}$  (as percentage chloride by weight of cement [% bwoc]) obtained from the test conducted by the laboratory, field, and analytical results. Other units of representation of  $Cl_{th}$  are weight per unit of concrete ( $kg/m^3$ ), % by weight of the binder, chloride-to-hydroxyl ratio, etc.

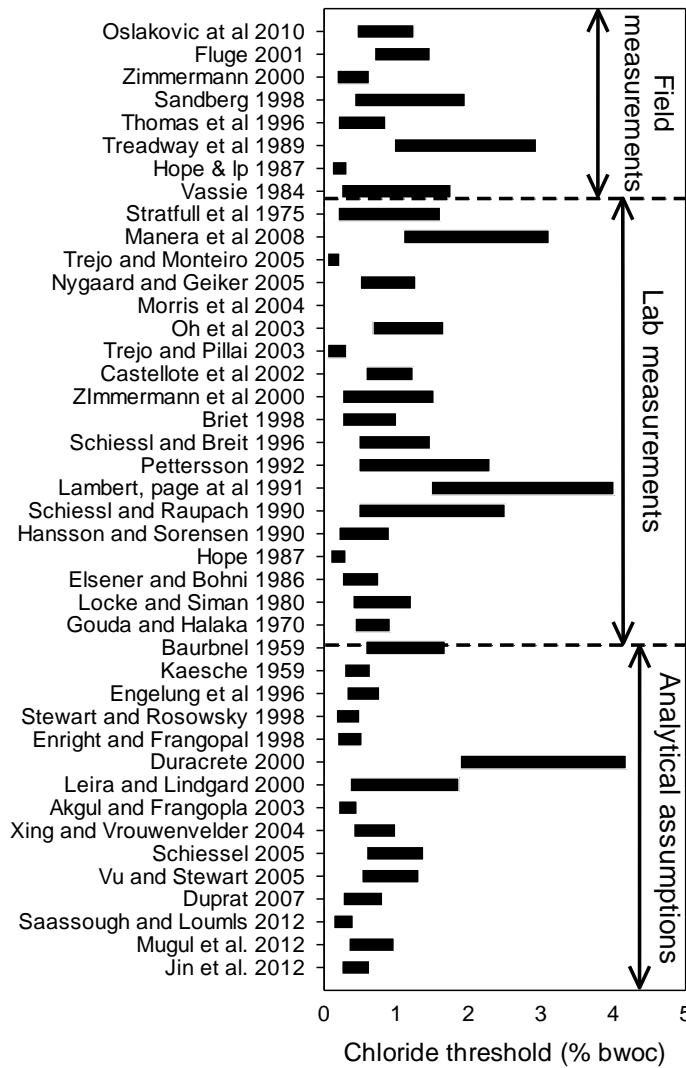


Figure 2.4  $Cl_{th}$  reported in literature (reproduced from Pillai and Annapareddy, 2013)

The  $Cl_{th}$  values shown in Figure 2.4 exhibit a huge scatter. Also, Cao et al. (2012) reported that the  $Cl_{th}$  of steel varies from 0.2 to 2.42 % by weight of the binder. Many researchers (Hausmann [1967], Goni and Andrade [1990], Venu et al. [1965], Li and Sagues [2001]) have reported that the  $Cl_{th}$  also depends on the available alkalinity of the concrete. Thus, the  $Cl_{th}$  is represented as the ratio of chloride and hydroxyl ions ( $Cl^-/OH^-$ ) which varies in the range of 0.01 to 4.5.

This scatters may be due to the variations in the influencing factors like binder type, water-binder ratio, steel type, exposure conditions, etc. The differences in the test methods followed by different researchers to detect the corrosion initiation may also be one of the reasons for the scatter among the reported values of  $Cl_{th}$ . Other reasons may be the differences in the composition of steel, ingredients in concrete, steel-cementitious interface, etc.

The report by the RILEM TC 235 CTC (2014) recommends a standard test method for determining  $Cl_{th}$  concentration. The test result shows that the duration to complete the test is around 900 days (about 3 years) for the specimens with 10 mm cover. Also, the difference in experimental procedures, experimental errors, and human errors can contribute significantly in the scatter for the determined  $Cl_{th}$ . Until now, a standardized or acceptable test method to detect the corrosion initiation and determine the  $Cl_{th}$  of steel embedded in concrete is not available. The accelerated chloride threshold (ACT) test method developed by Pillai and Trejo (2003) was an attempt towards the determination of  $Cl_{th}$  in short period of time. However, the suitability of this ACT method for the determination of  $Cl_{th}$  for the systems with anions (other than chlorides) is questionable (Karuppanasamy and Pillai (2016c)). This is because the ACT test method adopts external potential gradient, which can cause the unwanted movement of anions in the cementitious system (say, from corrosion inhibitors and other chemical admixtures) towards the embedded steel anode. However, such migration will not happen in the real concrete structures – leading to erroneous  $Cl_{th}$  measurements.

### 2.4.3 Recommended upper limit of chloride concentration in new concrete

To ensure long-term corrosion protection, many agencies have set upper limits for the chloride concentration in the new concrete, which is far less than the possible  $Cl_{th}$ . Table 2.3 shows a summary of various upper limits on chloride concentration in new concrete. For example, ACI 222R (2010) recommends an upper limit of 0.20 and 0.08%bwoc for conventionally reinforced and prestressed concrete systems. IS:456 (2000) recommends the chloride concentration less than 500 mg/l for reinforced concrete. The equivalent value in terms of %bwoc is not given in IS456 (2000).

**Table 2.3 Recommendations in international standards on upper limit of chloride content in concrete**

Standards	Maximum allowable chloride content in uncontaminated concrete (% by weight of cement)	
	Reinforced concrete	Prestressed concrete
BS 8110 (1997)	0.4	0.1
ACI 222R (2010)	0.20	0.08
CEB (2010)	0.4	0.2
IS 456 (2000)	Not given	Not given

### 2.5 MODELING CORROSION PROPAGATION PERIOD

The corrosion propagation period ( $t_p$ ) can be defined as the time required, after the corrosion initiation, to initiate a crack in the cover concrete. Depending on the oxidation level, iron can expand more than six times of its original volume as shown in Figure 2.5 (Gaidis and Rosenberg, 1987). Prolonged corrosion can lead to significant internal stresses and initiates crack in the cover concrete. When the corrosion products are deposited around the steel bar, they induce tensile stresses on the surrounding concrete, which cause cracking of cover concrete. These cracks can act as a path for the moisture, oxygen, and chloride to move towards the embedded steel surface. Figure 2.6 shows the sequence of corrosion propagation in a structural member. Most of the corrosion propagation models estimate the time required to

initiate an invisible crack. The different corrosion propagation models are discussed in the next section.

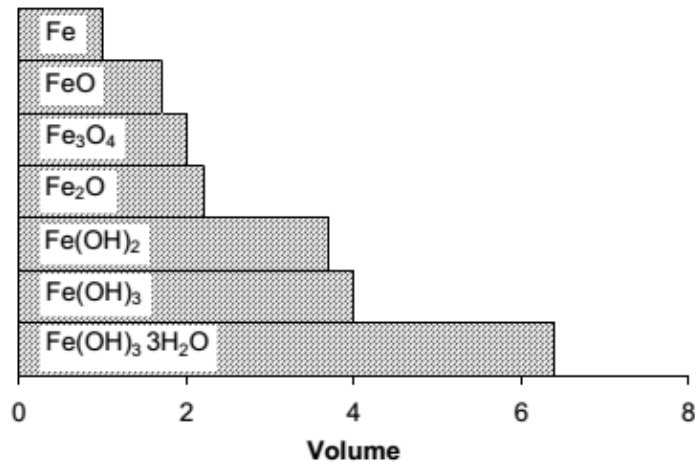


Figure 2.5 Relative volume of various corrosion products (Gaidis and Rosenberg, 1987)

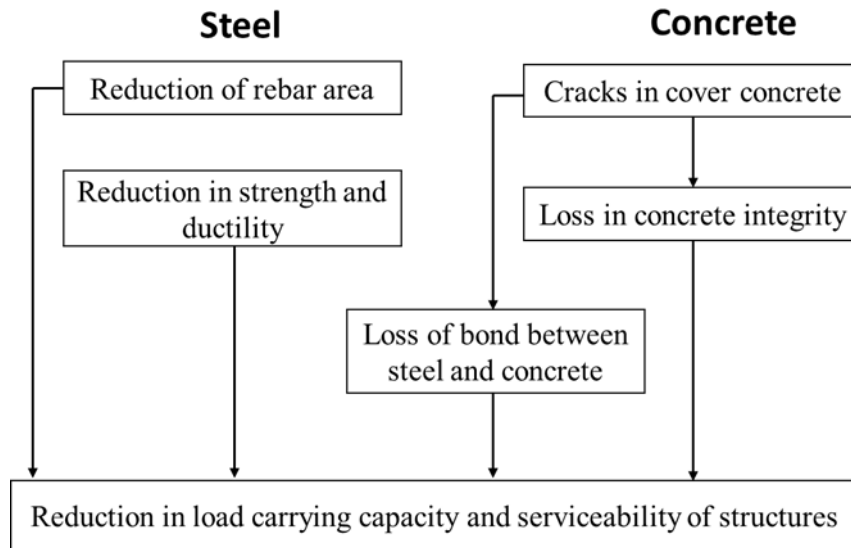


Figure 2.6 Effect of corrosion propagation on structural performance.

## 2.5.1 Existing models to predict the corrosion propagation period

In this section, some of the most commonly used corrosion propagation models are provided. Additional models and the corresponding mathematical formulations/empirical equations are provided in Appendix D.

### 2.5.1.1 Review of software programs and models for estimating $t_p$

Life-365™ is a freeware, widely used for service life prediction and to estimate the life-cycle cost of concrete structures exposed to different chloride environment. In this,  $t_p$  is assumed to be 6 years, immaterial of the steel-cementitious system. However, the  $t_p$  can vary with many factors like cover depth, amount of the corrosion product formed, tensile strength of the concrete, interconnectivity of pores, etc. Table 2.4 provides a summary of the parameters required for six different  $t_p$  models in literature. Note that each model requires different set of input parameters as per the assumed corrosion mechanism and crack initiation process.

Annexure D provides a list of models that can be used for directly estimating the  $t_p$ . Some of these models use FEM or long-term test results like creep coefficient, mass loss of steel, the thickness of pore band around the steel/concrete interface, etc (Reale and O'Connor, 2012). These are complex input parameters for a practicing engineer to determine in most cases. Ranjith et. al (2016) compared Bazant (1979) model, Morinaga (1990) model and Wang and Zhao (1993) model and found that the Wang and Zhao (1993) model provides a reasonable estimate. In this study, the Wang and Zhao (1993) model will be used for the estimation of  $t_p$  because it directly estimates  $t_p$  by using the input parameters that the practicing engineers can estimate fairly easily (i.e., compressive strength, corrosion rate, and cover depth).

**Table 2.4 Input parameters required for different propagation models**

Sl. No	Parameters considered	Bazant (1979)	Morinaga (1990)	Wang and Zhao (1993)	Liu (1996)	Stratfull (1957)	Clear (1976)
1	Initial diameter of steel rebar	✓	✓	✓	✓		
2	Corrosion rate of steel rebar	✓	✓	✓	✓		
3	Density of steel rebar	✓		✓	✓		
4	Equivalent weight of steel rebar	✓	✓	✓			
5	Faraday's constant	✓	✓	✓			
6	Perimeter of steel rebar	✓	✓				
7	Bar hole flexibility	✓					
8	Poisson ratio of concrete	✓					
9	Elastic modulus of concrete	✓					
10	Concrete creep coefficient	✓					
11	Thickness of cover concrete		✓			✓	✓
12	Crack expansion coefficient of concrete			✓			
13	Cube strength of concrete			✓			
14	Depth of rebar penetration			✓			
15	Density of corrosion product				✓		
16	Thickness of corrosion products to generate the tensile stress on concrete				✓		
17	Mass of steel rebar corroded				✓		
18	Thickness of pore band around steel-concrete interface				✓		
19	Chloride concentration at surface					✓	✓
20	Water-cement ratio					✓	✓
21	Time of exposure						✓

### 2.5.1.2 Wang and Zhao (1993) model

Wang and Zhao (1993) have developed an empirical model with an assumption of constant  $i_{corr}$  to estimate  $t_p$ . This model assumes that the  $t_p$  ends when the first corrosion-induced crack occurs, as defined earlier in this thesis. It is assumed that first crack occurs in concrete when the corrosion product reaches a certain quantity. Eq. 2.11 gives the empirical formula suggested by Wang and Zhao (1993) to estimate  $t_p$ .

$$t_p = \frac{H}{P_r}$$

$$H = \frac{\Delta}{\gamma} = \left[ \frac{\Delta}{0.33 \left(\frac{D}{C_v}\right)^{0.565} f_{cu}^{1.436}} \right] \quad \text{Eq. 2.11}$$

$$P_r = \left( \frac{W}{F \rho_{st}} \right) i_{corr}$$

where,  $t_p$  is time between corrosion initiation and the first cracking of cover concrete (years);  $H$  is the depth of rebar penetration (mm);  $\Delta$  is the thickness of corrosion product (mm);  $i_{corr}$  is the average corrosion rate (A/mm<sup>2</sup>);  $\gamma$  is the corrosion product crack expansion coefficient of concrete;  $D$  is initial diameter of the rebar (mm);  $C_v$  is the thickness of concrete cover (mm);  $f_{cu}$  is the cube strength of concrete (N/mm<sup>2</sup>);  $P_r$  is the penetration rate (mm/s);  $W$  is the equivalent weight of steel (g);  $F$  is the Faraday's constant (Coulombs);  $\rho_{st}$  is the density of steel (g/mm<sup>3</sup>). Wang and Zhao (1993) model assumed that the corrosion products will fill the steel-cementitious interface and develop an expansive pressure or tensile stress on the cover concrete, which will crack, when the exerted tensile stress from the expansive corrosion product exceeds the tensile strength of the concrete. This is empirically related to the compressive strength. The  $t_p$  can be predicted using this model using the  $i_{corr}$  data measured from the field and laboratory. In this study, the Wang and Zhao (1993) model that uses some of the most commonly and easily available parameters was considered for the estimation of  $t_p$ . Once the crack initiates, the estimation of corrosion propagation is more complex and the section 2.5.2

describes the influence of cracking on corrosion of steel. However, the corrosion of steel in cracked concrete is not considered for this study.

### 2.5.1.3 Andrade et al. (1989) model for the diameter loss of steel rebars

Andrade et al. (1989) derived an empirical formula (Eq. 2.12) which uses the  $i_{\text{corr}}$  to calculate the reduction in the diameter of steel rebar after long-term exposure.

$$\phi_t = D - 0.023 \times i_{\text{corr}} \times t \quad \text{Eq. 2.12}$$

$\phi_t$  is the diameter of the rebar at time ‘t’ after corrosion initiation and  $D$  is the initial diameter of reinforcement. Note that, Eq. 2.12 considers constant  $i_{\text{corr}}$ . However, this  $i_{\text{corr}}$  can vary with time, depending on the relative humidity and temperature variations prevailing in the different exposure conditions and inside concrete. Therefore, the prediction of  $t_p$  must consider the duration of wet and dry seasons prevailing at site – in order to get realistic estimates. IRC SP: 60 (2002) provides such a formulation that considers the seasonal effects to estimate the weighted average annual corrosion rate ( $i_{\text{corr, annual}}$ ), as given in Eq. 2.13.

$$i_{\text{corr, annual}} = \alpha \times i_{\text{corr, wet}} + (1 - \alpha) \times i_{\text{corr, dry}} \quad \text{Eq. 2.13}$$

where,  $i_{\text{corr, wet}}$  = corrosion rate in wet conditions,  $i_{\text{corr, dry}}$  = corrosion rate in dry conditions,  $\alpha$  = ratio of the duration of the rainy-to-summer season per year. The  $t_p$  estimated based on the  $i_{\text{corr, annual}}$  may better represent the corrosion propagation mechanism that occurs in the field.

## 2.5.2 Influence of cracking on corrosion of rebar

Corrosion in cracked concrete is a very complex phenomenon. A brief review on the corrosion in cracked concrete is provided next. However, it should be noted that this thesis does not focus on corrosion mechanisms in cracked concrete systems.

Generally, all concrete structures are cracked to some extent and the influence of cracking on long-term durability is a complex function governed by many parameters such as the composition of materials, exposure condition, crack width, etc. (Alonso et al., 1998; ACI 222R,

2010). Once the crack occurs, salt, air, moisture and other impurities will penetrate through the cracks – resulting in a non-uniform special distribution of these elements within the concrete. This can lead to differential conditions of pH, moisture, chloride, etc. along the steel-cementitious surface – leading to possible localized corrosion. Most codes of practice specify maximum permissible crack widths from the durability point of view, in general, crack width should not exceed 0.3 mm (BS 8110, 1997; IS 456, 2000). However, in many cases, cracks may appear at the surface but may not penetrate to the depth of the steel. As reported in Alexander et al. (2012), the corrosion behaviour in cracked concrete is complex and there are conflicting reports on the correlation between the corrosion rate and the influencing factors like crack width, crack frequency, crack orientation, crack dormancy or activity, etc.

## **2.6 CORROSION RATES OF STEEL REINFORCEMENT**

Table 2.5 shows the  $i_{\text{corr}}$  for different steel reinforcement types reported in the literature. These reported values exhibit significant scatter. Many researchers have followed the gravimetric mass loss method to obtain the average  $i_{\text{corr}}$  over the period of exposure (say, in mm per year). Nowadays, with the advancement of technology, the Linear Polarization Resistance (LPR) tests can be conducted to represent the instantaneous  $i_{\text{corr}}$  or corrosion current density (say, in  $\mu\text{A}/\text{cm}^2$ ).

**Table 2.5 Corrosion rate of steel specimen represented in literature**

<b>Steel type</b>	<b>Corrosion rate (<math>i_{corr}</math>)</b>	<b>Experimental details/environmental exposure conditions</b>	<b>Reference</b>
Black steel	2.54 $\mu\text{m}/\text{yr}$	OPC concrete exposed to NaCl solution	Spellman and Startfull (1968)
	94 $\mu\text{m}/\text{yr}$	RC structure exposed to marine environment for 25 years	Clear (1992)
	16 to 32 $\mu\text{m}/\text{yr}$	Compared available corrosion rates and developed equations	Hladky et al. (1989)
	0.025 to 1.620 $\mu\text{m}/\text{yr}$	OPC mortar exposed different NaCl concentration	Ismail and Ohtsu (2006)
	1 to 2 $\mu\text{m}/\text{yr}$	Embedded in different mortar with SCM, $i_{corr}$ measured at corrosion initiation time	Hansson and Sorensen (1990)
	0.026 to 1.575 $\mu\text{A}/\text{cm}^2$	OPC concrete with calcium nitrite exposed for 24 months	Berke et al. (1990)
CTD	3 to 4.2 $\mu\text{A}/\text{cm}^2$	Embedded in different mortar with SCM, $i_{corr}$ measured at corrosion initiation time	Pradhan and Bhattacharjee (2009)
	0.7 to 2.6 $\mu\text{A}/\text{cm}^2$	Embedded in OPC mortar exposed for three months	Firodiya et al. (2015)
QST	2.5 to 6 $\mu\text{A}/\text{cm}^2$	Embedded in different mortar with SCM, $i_{corr}$ measured at corrosion initiation time	Firodiya et al. (2015)
MS	0.5 to 1.7 $\mu\text{A}/\text{cm}^2$	Embedded in OPC mortar exposed for three months	Firodiya et al. (2015)
Galvanized steel	0.072 to 0.722 $\mu\text{A}/\text{cm}^2$	OPC concrete with calcium nitrite exposed for 24 months	Berke et al. (1990)
Chromate treated galvanized steel	0.025 to 1.091 $\mu\text{A}/\text{cm}^2$	OPC concrete with calcium nitrite exposed for 24 months	Berke et al. (1990)
Prestressing steel	3 to 9 $\mu\text{A}/\text{cm}^2$	OPC mortar; exposed for 10 months	Karuppanasamy and Pillai (2014)

The possible reasons for such huge scatter are the differences in (i) chemical composition of steel, (ii) specimen design, (iii) test methods, (iv) experimental setup, (v) exposure conditions, etc. across the studies. For example, Soylev and Richardson (2008) exposed the black steel rebar to 2, 3, and 4 % of sodium chloride solution and found the  $i_{\text{corr}}$  as 5.7, 6, and 10.7  $\mu\text{A}/\text{cm}^2$  respectively. Pradhan and Bhattacharjee (2009) reported that the  $i_{\text{corr}}$  of CTD reinforcement embedded in Ordinary Portland Cement (OPC) concrete with various water-cement ratios and different dosages of pre-mixed chlorides ranged from 3 to 4  $\mu\text{A}/\text{cm}^2$ . Pradhan and Bhattacharjee (2009) also reported  $i_{\text{corr}}$  for the QST steel reinforcement embedded in concrete is within the range of 2.5 to 6  $\mu\text{A}/\text{cm}^2$ . Thus, the literature confirms that the  $i_{\text{corr}}$  may vary for different steel types, cementitious system, exposure conditions, and testing methods. Also, the statistical distribution of  $i_{\text{corr}}$  of various steels is necessary for realistic estimation of  $t_p$ .

## **2.7 TYPES OF REINFORCEMENT USED IN REINFORCED CONCRETE**

A brief discussion on various types of steel that is used as reinforcement in concrete structures is described in this section.

### **2.7.1 Plain mild (PM) steel**

IS:432 (Part 1)-2004 provides the specification for the plain mild (PM) steel. A couple of decades ago, many structures were built with PM steels. Those structures are now experiencing premature corrosion. It is important to be able to assess the  $i_{\text{corr}}$  so that the  $t_p$  can be estimated to develop repair schedule and strategies. Nowadays, PM is used as a secondary reinforcement like stirrups and lateral ties.

### **2.7.2 Cold-twisted deformed (CTD) steel**

The hot rolled bars are allowed to cool under atmospheric conditions followed by twisting or work hardening method to increase the yield strength of the steel. IS:1786 (2008) provides the specifications for CTD steel, which has a characteristic yield strength of more than 415 MPa. The residual stress developed at the surface due to work hardening during the manufacturing process leads to stress-induced corrosion. Thus, the use of CTD bars is not recommended in many countries. However, there are many structures that are built using this steel (couple of

decades ago). Those structures are now experiencing significant corrosion and the assessment of  $t_p$  of those structures are very important to develop repair schedule and strategies.

### **2.7.3 Quenched and self-tempered (QST) or Thermo-mechanically-treated (TMT) steel**

In the Indian subcontinent, the Quenched and Self-Tempered (QST) steel is known as Thermo-Mechanically-Treated (TMT) steel. For making QST/TMT steel rebars, the hot rolled bars at around 1000 to 1100°C are quenched for about one or two seconds using a cooling water spray system. The quenching process converts the outer surface layer (a few millimeters) into a hard martensite, and the inner core remains as austenite. After quenching, the steel is allowed to cool naturally, on a cooling bed. This process creates a thermal gradient from the core to the surface. The heat from core radiates outward and tempers the outer layer of martensite to tempered-martensite. After prolonged cooling, the austenitic core changes to ferrite-pearlite. The tempered martensite contributes to the excellent tensile strength and toughness of the steel rebars and the ferrite-pearlite contributes to its ductility (with enhanced elongation of upto 20 %). IS:1786 (2008) provides the specifications for TMT steel bars.

### **2.7.4 Prestressing (PS) steel**

Prestressing steel can be manufactured by a different process like cold drawing, stress relieving, strain tempering, etc. to achieve high strength steel. The prestressing steel is used in different forms like wires, strands, tendons, cables, bars, etc. in high-rise buildings, bridges, and other special structures. With the need for slender and high strength-to-weight ratios, the use prestressing steel is increasing. The nominal tensile strength of the prestressing steel may be around 1800 MPa with less than about 5 % stress loss due to relaxation. The detailed specification is provided in IS:2090 (2004).

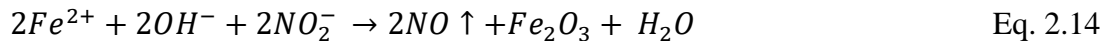
## 2.8 TYPES OF CORROSION INHIBITORS

### 2.8.1 Types of corrosion inhibiting admixtures (CIAs)

According to ISO 8044 – 1999, corrosion inhibitors can be defined as “A chemical substance that decreases the  $i_{\text{corr}}$  when present in the corrosion system at a suitable concentration, without significant change in the concentration of any other corrosion agent.” This definition excludes other corrosion protection methods such as coatings, pore blockers, and other material, which change the water, oxygen and chloride concentrations. However, some inhibitors also behave as pore blockers, which is a secondary property. The corrosion inhibiting admixtures (CIAs) offer a relatively economical as well as an easier way to increase the  $Cl_{\text{th}}$  of steel embedded in concrete (Hansson et al. [1998], Gaidis [2004], Ormellese et al. [2006], Morris and Vazques [2002], González [1998]). A variety of CIAs are available in the market for reinforced concrete applications. Calcium nitrite [ $Ca(NO_2)_2$ ] is a widely used anodic CIAs for concrete applications. Also, the bipolar CIAs are emerging in the construction industry. Following is a discussion on anodic and bipolar inhibitors.

#### 2.8.1.1 Anodic inhibitors

Various authors reported that the AN inhibitors produced better results in alkaline environments compared to other CIAs (Mammoliti et al., [1999], Ann et al., [2006], Berke and Hicks., [2004]). For example, the calcium nitrite inhibitor helps in forming a better passive film based on the reactions in Eq. 2.14 and Eq. 2.15 (El-Jazairi and Berke [1990], Gaidis [2004]).



At the anode, ferrous ( $Fe^{2+}$ ) ions (as soon as they form) are oxidized to ferric ions ( $Fe^{3+}$ ), which are very stable in the nitrite-rich environment. Also, the nitrite ions help in producing  $\gamma FeOOH$ , which are more stable than naturally formed passive layer and help in increasing the  $Cl_{\text{th}}$  value. These reactions form the basis for the inhibitive action by nitrites (Page et al. 1990). However, there exist mixed opinions on the effectiveness of nitrite-based anodic inhibitors.

It is reported that the effectiveness of the anodic inhibitor on complete protection against the depassivation always depends on the concentration of chloride ions present in the surrounding concrete (El-Jazairi and Berke, 1990). Montes et al. (2004) have reported that the effectiveness of calcium nitrite based CIAs is seen only in concrete with low water to binder ratio (i.e., less than 0.5). It was also found that the calcium nitrite based CIAs are not effective when chloride-to-nitrite ratio ( $Cl/NO_2$ ) is less than one (Rincon et al., 2002). Ann and Song (2007) found that CIAs are not suitable for concrete in immersed conditions, because the nitrite ions can leach out of the concrete and reduce the nitrite ion concentration inside the concrete. Note that the effect of this leaching on corrosion at the steel-cementitious interface depends on the cover thickness (Ramachandran, 1984). Although there are ambiguities regarding the performance of calcium nitrite based CIAs, it is still one of the most widely used CIAs (Vaysburd and Emmons, 2004). Also, quantitative and probabilistic information on their effect on  $Cl_{th}$  is required for realistic estimation of service life.

#### 2.8.1.2 *Cathodic inhibitors*

The cathodic inhibitors control or reduce the rate of corrosion process by decreasing the rate of cathodic reaction by reducing the availability of oxygen. The most commonly used cathodic inhibitors for reinforced concrete applications are sodium hydroxide and sodium carbonate (COIN 22-2010). These are supposed to increase the pH near the steel and reduce the oxygen availability by covering the steel surface. Phosphates, silicates, and polyphosphates are also used (Soeda and Ichimura, 2003). Based on long-term studies, Ormellese et al. (2006) reported that amine-esters, amino alcohols, and alkanolamines delay the onset of corrosion by reducing the penetration rate of chlorides and oxygen by filling the concrete pores and blocking the porosity of concrete by the formation of complex compounds.

#### 2.8.1.3 *Bipolar or Mixed inhibitors*

Bipolar inhibitors retard the corrosion process at both anodic and cathodic sites of a corrosion cell. The BP inhibitor acts by reducing the ferrous decomposition at the anodic site and restricts the availability of oxygen at the steel surface at the cathodic site (Nmai, 2004). BP inhibitors with the hydrophobic group that has polar groups such as Nitrogen (: N), Alkyl (R), and hydroxyalkyl (R-OH) are found to be effective in inhibiting corrosion (COIN 22-2010).

Organic polymer compounds such as amine and amino alcohol are commonly used in BP inhibitors. Soeda and Ichimura (2003). reported that the BP inhibitors could enhance the corrosion resistance of the steel by about six times. Rakanta et al. (2013) reported that the use of organic inhibitors of 2 % by weight of cement (%bwoc) could reduce the mass loss of steel by about 43 %. Also, the overall performance of organic based BP inhibitors in reducing the  $i_{\text{corr}}$  was better than the calcium nitrite based AN inhibitors (Virmani et al., 1998). Nmai et al. (1992) compared the performance of reinforced concrete slabs with the manufacturer recommended dosages of organic inhibitor, calcium nitrite, and no inhibitor. Active corrosion was observed on control specimens after 30 days of continuous exposure to 6 % chloride solution. The specimens containing calcium nitrite showed an active corrosion after 50 days. There was no sign of corrosion activity in the specimens with organic inhibitors even after 50 days. As these types of BP inhibitors were evolved recently, very limited quantitative and the probabilistic information is available on their performance. Such information is required for the realistic estimation of the service life of the reinforced concrete structure.

### **2.8.2 Migrating corrosion inhibitors (MCIs)**

The migrating corrosion inhibitors (MCIs) are used usually on existing structures. Upon application at the concrete surface, the vapours of MCIs penetrate into the concrete system (Ormellese et al. 2006) – hence, also known as vapour phase inhibitors. Mackechnie et al. (2004) reported that the rate of transport of MCIs can decline as the depth of penetration increases. Also, it was reported that the effective inhibition may not be possible if the chloride concentration at the steel-cementitious interface is more than 1% by mass of cement. This may be one of the reasons why the use of MCIs is limited in the reinforced concrete applications. This thesis will focus on the performance assessment of two CIAs – one anodic and one mixed CIAs.

## **2.9 CORROSION MEASUREMENT TECHNIQUES**

During 1950's, non-destructive test methods were developed to detect the corrosion of steel embedded in concrete. The test method to develop the  $i_{\text{corr}}$  were developed by studying the

electrochemical reactions happening on the metal in an aqueous solution (Stratfull [1957], Jones and Greene [1966], Monfore [1968]). The method of detecting the corrosion initiation may have a high influence on the corresponding  $Cl_{th}$  determined for the material (Karadakis, 2010). This section discusses the different corrosion measurement techniques followed by the researchers and practicing engineers.

### 2.9.1 Hall-cell potential test

The ASTM C876 (2015) standard provides the broad classification on the probability of occurrence of corrosion using the measured OCP. In this method, the reinforcing steel acts as the working electrode, concrete acts as an electrolyte and the standard copper-copper sulphate electrode (CSE) acts as a reference electrode as shown in Figure 2.7. The interpretation of the measured potential is classified as given in Table 2.6. The classification indicates the level of corrosion activity in the localized areas of the reinforcing steel.

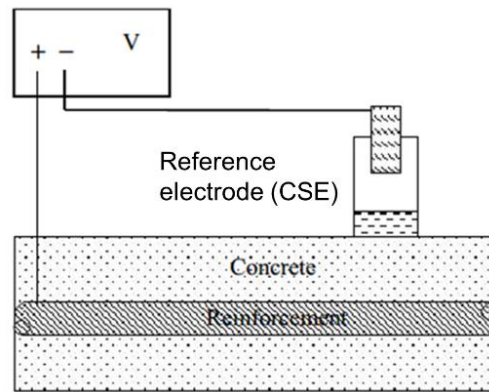


**Figure 2.7 Schematic half-cell potential test setup**

**Table 2.6 Interpretation of corrosion potential readings [ASTM C 876 (2015)]**

Potential Reading (mV versus CSE)	Probability of Corrosion
$E_{corr} \geq -200$	< 10 percent
$-200 > E_{corr} > -350$	Indeterminate
$E_{corr} \leq -350$	> 90 percent

The potential measured is the corrosion potential ( $E_{\text{corr}}$ ) [also known as Open-Circuit Potential, OCP] is a measure of electron charge transfer between the steel, concrete, and the steel-concrete interface, not only the potential of steel by itself (Hansson, 1984). In half-cell potential tests, the resistivity (saturation level) and the cover thickness of the concrete leads to the variation in the  $E_{\text{corr}}$  measured (Elsener et al., 2003). The resistivity of concrete and cover depth are the major influencing parameters, which lead to possible errors in the potential measurements. Pour-Ghaz et al. (2009) showed that, for the same  $i_{\text{corr}}$ , the corrosion potential varies with the difference in the concrete resistivity. Also, the  $E_{\text{corr}}$  value will not provide details about the corrosion kinetics (say,  $i_{\text{corr}}$ ) of the steel.

### 2.9.2 Linear polarization resistance (LPR) technique

The three-electrode linear polarization resistance (LPR) technique given in ASTM G59 (2014) can be used to measure the polarization resistance of the steel-cementitious interface ( $R_p$ ), and hence the kinetics or rate of corrosion. The LPR test setup consists of the corrosion cell with a working electrode (WE), a counter electrode (CE), and a reference electrode (RE) as shown in Figure 2.8.

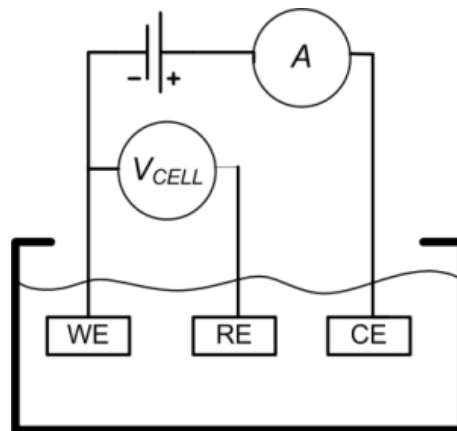


**Figure 2.8 Typical linear polarization resistance test setup (Jaime et al., 2013)**

Andrade and Alonso (1996) summarized that the  $i_{\text{corr}}$  was less than  $0.1 \mu\text{A}/\text{cm}^2$  and greater than  $0.2 \mu\text{A}/\text{cm}^2$  denote the passive and active states of corrosion, respectively. Since the 1970s, LPR technique has been accepted as a commonly used test method to measure the instantaneous  $i_{\text{corr}}$  in the solution as electrolytes with low electrical resistance. By applying a

series of offset potential ( $E$ , in volts) with reference to open circuit potential (OCP), the corresponding current ( $I$ , in amperes) is measured. In 1957, Stern and Geary (1957) formulated a linear relationship established between applied potential ( $E$ ) and measured corrosion current density ( $i$ ), as given in Eq. 2.16.

$$R_p = \left| \frac{\Delta E}{\Delta i} \right|_{E \rightarrow E_{corr}} \quad \text{Eq. 2.16}$$

The polarization resistance is inversely related to the  $i_{corr}$  and expressed in corrosion current density ( $i_{corr}$ ,  $\mu\text{A}/\text{cm}^2$ ) (Tait 1994). The  $i_{corr}$  of steel can be calculated by applying the polarization resistance data in Stern-Geary equations, as given in Eq. 2.17.

$$i_{corr} = \frac{B}{R_p} \quad \text{Eq. 2.17}$$

Andrade et al., (1984) suggested that the  $i_{corr}$  calculated using by considering  $B = 52 \text{ mV}$  would be larger than the calculated. Therefore, the assumption of  $B = 52 \text{ mV}$  will not be an appropriate for calculating the  $i_{corr}$  of passive steel, which underestimates the  $i_{corr}$ . ASTM C59 (2014) provides guidelines to conduct LPR test. Figure 2.9 shows a typical LPR plot.

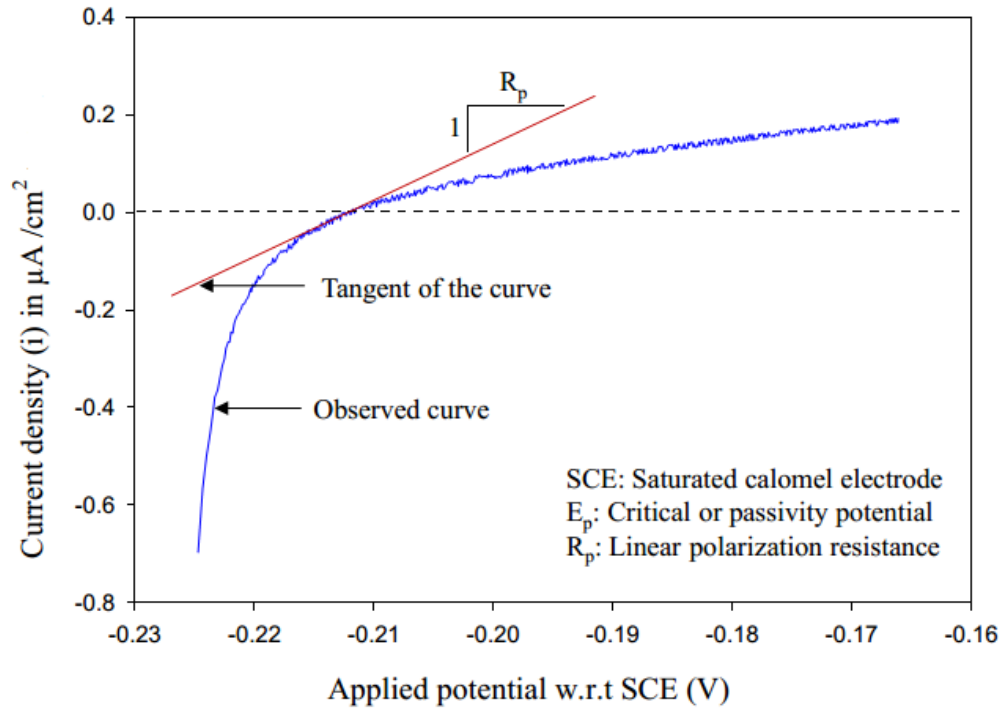


**Figure 2.9 A typical LPR plot**

Cigna et al. (1993) compared the corrosion resistance, electrical resistivity, the polarization resistance, and concluded that the  $E_{\text{corr}}$  is not as good as a parameter like  $i_{\text{corr}}$  to detect the corrosion initiation. Andrade and Alonso (1996) determined  $i_{\text{corr}}$  in terms of corrosion current density ( $i_{\text{corr}}$ ) of steel embedded in concrete exposed to chlorides. They classified that the  $i_{\text{corr}}$  values less than  $0.1 \mu\text{A}/\text{cm}^2$  and more than  $0.2 \mu\text{A}/\text{cm}^2$  denote the passive and active state of corrosion, respectively. The highly chloride contaminated concrete can exhibit  $i_{\text{corr}}$  values of up to  $100 \mu\text{A}/\text{cm}^2$ .

The LPR technique has been accepted as a commonly used technique to measure instantaneous  $i_{\text{corr}}$  since the 1970s. However, it has its own limitations (Baweja et al., [(2003), Ahmad [2003]). If the liquid electrolyte like sodium chloride solution, simulated pore solution (SPS) was used for the corrosion study, the bulk electrical resistance of the liquid electrolyte could be negligible (Yonezawa et al., 1988). However, concrete as an electrolyte can exhibit high electrical resistance ranging from  $0.01$  to  $10^3 \text{ k}\Omega\cdot\text{cm}$ . Note that this would depend on the saturation level of concrete. Also, the total resistance ( $R_{\text{total}}$ ) measured by the LPR technique which includes the cementitious cover and will vary from the polarization resistance ( $R_p$ ) at the

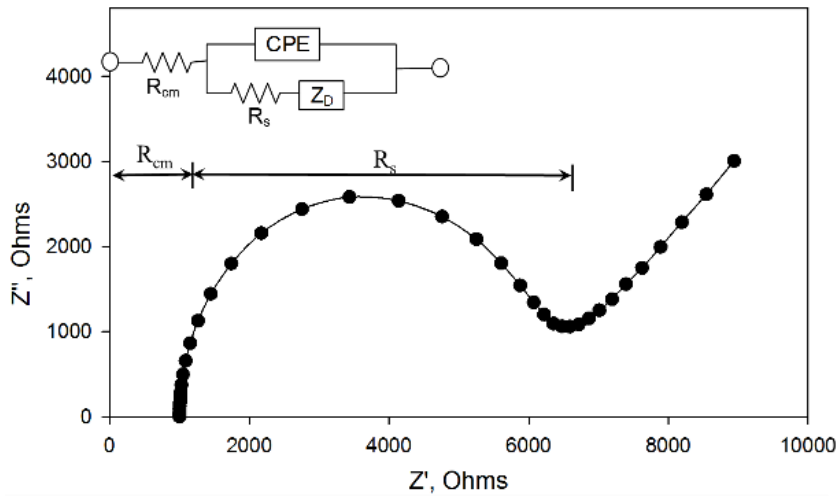
steel-cementitious interface. To account for this, the error in ohmic drop due to the bulk electrical resistance of concrete electrolyte ( $R_{cm}$ ) have to be compensated while measuring LPR value. Bouteiller et al. (2012) assumed that the ohmic drop is negligible when the specimen is exposed to chloride and wet condition. To be precise, the electrical impedance spectroscopy (EIS) could be used to find the bulk resistance of concrete.

### **2.9.3 Electrical impedance spectroscopy (EIS)**

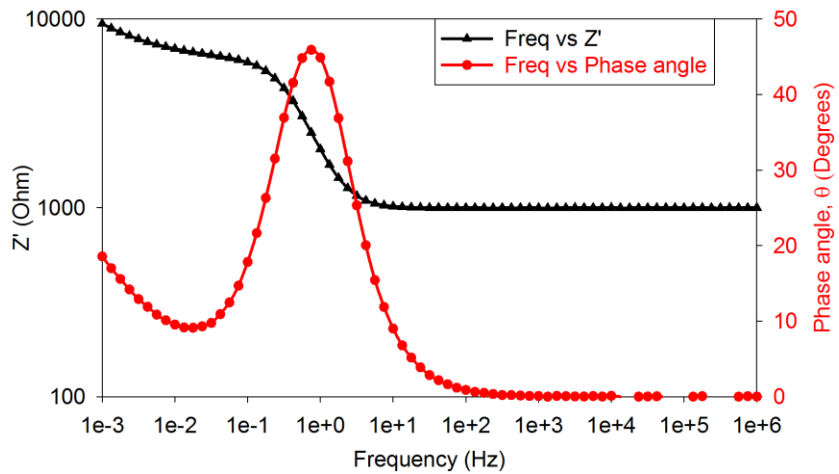
#### *2.9.3.1 Principle*

Electrochemical impedance spectroscopy (EIS) is a non-destructive laboratory technique which is widely used for studying the electrochemical systems. It is considered as one of the reliable techniques in monitoring corrosion process in the reinforcement steel [Dong et al. 2014, Poupard 2004, Hachani et al. 1992, Husain et al. 2004, Andrade et al. 1995, Pradhan and Bhattacharjee 2009, Ismail et al. 2006, Zhang et al. 2010]. In the EIS tests, a spectrum (typically 1 kHz to 5 MHz) of external AC voltage (in the range of 0 to 20 mV) is applied to the specimen and the electrical response is measured. The response of the system is recorded and analyzed using Nyquist plot and (2) Bode's plot [Zhang et al. 2010]. The Nyquist plots (See Figure 2.10 a) are commonly used because it allows an easy assessment of circuit elements and their properties. However, as mentioned in Section 2.9.3.3, challenges exist in modeling of the equivalent circuit and interpretation of the EIS data, especially for a complex steel-cementitious system.

Figure 2.10 (b) shows a typical Bode plot for the same system as shown in Figure 2.10 (a). The real impedance ( $Z'$ ) and the phase angle ( $\theta$ ) are plotted against the frequency. The  $Z'$  versus  $\theta$  curve can be used to determine the  $R_p$  and  $R_{cm}$ . The  $Z'$  can become independent of frequency at both very high and very low frequencies. At very high frequencies, the ohmic resistance controls the impedance and  $R_{cm}$  can be determined by fitting the data in the equivalent circuit. Similarly, from the data corresponding to the low frequency, the  $(R_p+R_{cm})$  can be determined. The Bode format provides a more understandable information for the frequency dependent behaviour of electrochemical systems (Princeton Applied Research, 2000).



**(a) Nyquist plot and equivalent electrical circuit (inset)**



**(b) Bode plot**

**Figure 2.10 Nyquist and Bode plots for a typical steel-cementitious system**

### 2.9.3.2 Developing an equivalent electrical circuit model

To interpret the EIS data, it is needed to develop an equivalent electrical circuit model for the system being studied, such that the circuit model represents the physical system of sample material and interfaces being studied. Before developing the equivalent electrical circuit for the electrochemical system of a given system, a thorough understanding of the actual physical model of that system is necessary. Since the steel-cementitious interface is a complex system,

several models have to be studied so that the best fitting model for the data obtained can be identified [Zhang et al. 2010, Andrade et al. 1984, Husain et al. 2004, Duarte, 2014]. In the reinforced concrete system, the physical model of steel-concrete interface can be developed using various phenomenon such as diffusion control, movement of species, passive film formation, corrosion product formation, etc. [Cesiulis et al., 2016, Yoon et al. 2006]. Feliu et al. (1998) presented a modified Randle's circuit (shown in Figure 2.11) that represents a typical steel-cementitious system.

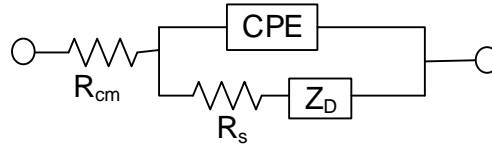


**Figure 2.11 Equivalent electrical circuit for a typical steel-cementitious system**

The equivalent circuit has individual components representing the bulk resistance of cementitious system ( $R_{cm}$ ), Charge transfer resistance of steel-cementitious interface ( $R_s$ ), Constant Phase Element (CPE) replacing the double layer capacitance of steel-cementitious interface ( $C_{dl}$ ), and the Warburg element for the non-steady steady chloride diffusion ( $Z_D$ ). The values of  $R_s$  and  $R_{cm}$  can be obtained by regressing the experimental data using Eq. 2.18

$$Z = R_{cm} + \frac{R_s}{1 + j\omega R_s C_{dl}} \quad \text{Eq. 2.18}$$

where,  $Z$  is the Ohmic resistance,  $\omega$  is the angular frequency ( $\omega = 2\pi f$ ),  $j$  is the imaginary unit of  $\sqrt{-1}$ . At higher frequency, the second term in Eq. 2.18 approaches zero and the response data represents the concrete resistance ( $R_{cm}$ ).

### 2.9.3.3 Difficulties in using EIS to detect corrosion initiation

Impedance spectroscopy is used for several years to obtain information about corrosion rate, electrochemical mechanisms, reaction kinetics etc. in various systems. However, compared to other techniques like LPR, the EIS is considered as a complex method to analyze and interpret the data. This is because, the reliable results can be obtained only when the complete physical system of the sample being tested, is understood well and modeled as an equivalent electrical

circuit. The determination of  $R_p$  for a very small area with active corrosion is difficult due to the presence of diffusion phenomena and double layer effects at the interface (John, 1981). In the chloride-induced corrosion tests, there can be a change in the ratio of the passive/active areas during the test duration. This scenario makes it necessary to modify the model during the test, which requires expertise and is cumbersome (Noggerath and Bohni, 1992). Moreover, the analysis of EIS results is complexity due to the overlapping phenomenon at interface, and noise in the measurement resulting from the heterogeneity of the specimen (Ribeiro and Abrantes, 2016). Considering these difficulties, this study proposes the use of LPR method for corrosion detection. However, there is a need to identify a method to extract the information on the bulk resistance of the cementitious system ( $R_{cm}$ ) from the  $R_{total}$  values obtained using the LPR tests. As shown in Figure 2.10 (a), the Nyquist plot can directly provide the  $R_{cm}$ . Further details are given in Section 4.3.3.

## **2.10 EXISTING TEST METHODS TO DETERMINE $Cl_{th}$ OF STEEL IN SYSTEM WITH CIAS**

The Japanese Industrial Standard JIS A6205 (2013) provides a test procedure for assessing the performance of CIAs used in concrete. In this method, a bare steel specimen is kept directly in contact with the simulated pore solution (SPS) or saline water (i.e., immersed in salt water) and the corrosion initiation is detected by visual observation. Poursae and Hansson (2007) reported that the corrosion performance of steel immersed in solution might be different from that embedded in concrete. Therefore, the results from JIS A6205 test may not replicate the performance of steel reinforcement embedded in cementitious mortar or concrete. On the other hand, the ASTM G109 (2016) test method uses measurements on steel rebars embedded in the cementitious system – mimicking the situations in real structures. This method suggests assessing the efficiency of CIAs based on the changes in the half-cell potential value (ASTM C876 [2015]) and macrocell corrosion current measurements during the cyclic wet-dry exposure using 3.5 % sodium chloride solution. Although the ASTM G109 (2016) test method does not provide direct guidance on the determination of  $Cl_{th}$ , many researchers have used this method for monitoring corrosion performance and determined  $Cl_{th}$  of same specimens with further testing. It should be noted that better the CIAs, the more will be the duration of  $Cl_{th}$  tests. Depending on the system, it may take many years to complete the ASTM G109 testing,

which is not acceptable by most of the engineers, designers, and clients, who want to select the materials during the planning and design stage itself.

To overcome these issues, Trejo and Miller (2002) developed and patented an accelerated chloride threshold (ACT) test method to detect the corrosion initiation in plain cementitious systems. Later, Trejo and Pillai (2003) refined it to reduce the variations in the measured test parameters. In this, an external potential (20 V) was applied across the 38 mm thick mortar cover to drive the chlorides towards the embedded steel surface. In the ACT method, OCP and LPR tests were conducted at regular intervals. The *t*-score statistical approach was followed to detect corrosion initiation by considering all the inverse polarization resistance ( $1/R_p$ ) measured from the beginning of the test. There are limitations in adopting this method for evaluating the  $Cl_{th}$  of systems with CIAs. This will be discussed next.

#### **2.11 ISSUES WITH THE APPLICATION OF POTENTIAL GRADIENT IN EVALUATING THE PERFORMANCE OF CIAS IN STEEL-CEMENTITIOUS SYSTEMS**

It should be noted that the ACT test method (Trejo and Pillai, 2003) was developed for determining the  $Cl_{th}$  of steel embedded in plain cementitious systems. The ACT test method uses an external potential gradient of 20 V to accelerate the movement of chlorides towards the embedded steel in plain cementitious systems. When the mortar contains CIAs with anions (say, nitrite), the external potential drives both the chlorides and the other anions towards the embedded steel surface (Andrade and Rebolledo, 2012). This potential application can increase the nitrite concentration at the steel-cementitious interface, during testing. Such increase, in turn, reduces the  $Cl^-/NO_2^-$  ratio at the steel-cementitious interface. Such increase in the nitrite concentration at the steel surface does not occur in real structures (Qian et al., 2008). In other words, the concentration of nitrites will be uniform throughout the cementitious system and will not change as a function of exposure time. Therefore, a test method that does not induce changes in nitrite concentration during the course of exposure and testing is required. Also, the effect of potential application on the migration of chlorides and nitrites needs to be quantified. Also, it should be noted that the  $Cl^-/NO_2^-$  ratio should be greater than one to initiate corrosion in steel (Rincon et al., 2002).

## 2.12 RESEARCH NEEDS

Considerable research has been carried out in the laboratory and existing reinforced structures to characterize the corrosion behavior of steel. The theoretical background and literature review provided in this section brings out the following main research gaps that form the basis of this thesis work. The literature review shows that test methods are available to measure the corrosion characteristics of plain steel-cementitious systems. Nowadays, corrosion inhibiting admixtures (CIAs) are used to increase the  $Cl_{th}$  of steel. Recently, many types of CIAs are being introduced into the market. The effectiveness of these materials in enhancing  $Cl_{th}$  need to be assessed before they are used in projects. However, there is no standardized, short-term test method available to determine the  $Cl_{th}$  of steel embedded in the cementitious system with CIAs. Such a test is required to be able to select durable materials during the planning and design stages. Also, statistical distributions of  $Cl_{th}$  are required to estimate probabilistic corrosion initiation period ( $t_i$ ).

Many structures are experiencing premature corrosion and engineers need to assess the residual service life (say, time until the first crack) so that suitable repair schedule and strategies can be adopted. The major parameter determining the time to corrosion crack is corrosion rate ( $i_{corr}$ ), which is a random variable and need to be modeled as statistical distribution so that probabilistic estimates of corrosion propagation period ( $t_p$ ) can be obtained. Also, such statistical distributions for the  $i_{corr}$  of various types of steels used in the construction and statistical tools to obtain  $t_p$  for various steel types are needed.

## 2.13 SUMMARY

The literature review helped in understanding the mechanisms and the factors influencing the  $Cl_{th}$ ,  $i_{corr}$ ,  $t_i$ ,  $t_p$ , etc. The various phases of the service life of concrete structures and different models to estimate the  $t_i$  and  $t_p$  were discussed. Then a detailed review on the major parameters influencing the service life [i.e., chloride threshold ( $Cl_{th}$ ) and corrosion rate ( $i_{corr}$ )] was provided. Finally, different corrosion assessment techniques available to determine the  $Cl_{th}$  and  $i_{corr}$  were discussed. Also, the issues associated with some of the available  $Cl_{th}$  tests were discussed.



### 3 RESEARCH SIGNIFICANCE

Steel rebars embedded in reinforced concrete structures can be susceptible to corrosion when exposed to the marine environment. The corrosion of steel reinforcement will lead to the reduction in overall service life of the structure. The service life of a structure can be defined as a sum of corrosion initiation period ( $t_i$ ) and corrosion propagation period ( $t_p$ ). The initiation of corrosion of rebars can influence the durability of the structure based on the service life parameters. By appropriately selecting materials during the design and construction stages, the premature corrosion can be avoided, the maintenance and repair costs can be minimized, and the service life can be enhanced.

There are many theoretical models available to estimate the  $t_i$  of structures. The chloride threshold ( $Cl_{th}$ ) is one of the key input parameters for these models. Moreover, the use of Corrosion Inhibiting Admixtures (CIAs) based on various chemical families (nitrites, amines, etc.) are increasing in the construction industry. Engineers want to quantify (during the planning and design stage itself) the effect of such CIAs on the service life of concrete structures. For this, the  $Cl_{th}$  of steel-cementitious systems with CIAs needs to be determined. However, no suitable, short-term test methods are available to determine the  $Cl_{th}$  of steel-cementitious systems with CIAs. This study develops a suitable, short-term test procedure for this by modifying an existing Accelerated Chloride Threshold (ACT) test method. The developed short-term test method (known as mACT) would be useful for the engineers and clients to determine the effect of CIAs on the  $Cl_{th}$  in about 120 days, which in turn will help engineers in selecting appropriate type and dosage of CIAs during the planning and design stage itself - to ensure that the desired service life could be achieved.

The corrosion  $t_p$  mainly depends on the  $i_{corr}$  of the steel reinforcement. Many existing concrete structures are built using Plain Mild (PM), and Cold Twisted Deformed (CTD) steel bars. Also, Quenched and Self-Tempered (QST) and Prestressing (PS) steel reinforcement are extensively used in today's construction. The statistical distribution of  $i_{corr}$  are necessary for probabilistic estimation of  $t_p$ . However, very limited information is available on the  $i_{corr}$  of PM, CTD, QST, and PS steel reinforcement – making it difficult to estimate the  $t_p$ . Current practice is to assume similar  $i_{corr}$  for PM, CTD, QST, and PS steel, which may give erroneous estimations

of probabilistic  $t_p$ . In addition, many software programs inadequately assume deterministic values for  $t_p$ , irrespective of the type of materials used in the structure. This study provides experimental data and statistical distributions on  $i_{\text{corr}}$  of PM, CTD, QST, and PS steel reinforcement embedded in chloride-contaminated mortar. These statistical distributions and probability density functions developed can be very valuable to budget and plan the maintenance, monitoring, and repair activities for the structures experiencing corrosion.

## 4 MATERIALS AND METHODS

### 4.1 INTRODUCTION

Based on the research objectives provided in Section 1.4, three different experimental programs have been developed. This section discusses the materials used, experimental design, test methodology, and the experimental program. The test setup and the accessories required to Rapid Migration test, modified Accelerated Chloride Threshold (mACT) test, and the  $i_{\text{corr}}$  measurement are explained in this section.

### 4.2 OBJECTIVE 1: DETERMINATION OF THE EFFECT OF EXTERNAL POTENTIAL ON ANION TRANSPORT THROUGH MORTAR

#### 4.2.1 Introduction

An investigation was done to study the effect of external potential on the migration of anions in cementitious systems. The Rapid Migration (RM) test was used. In particular, the possible migration of chloride and nitrite ions through a 15 mm thick mortar cylinder was studied. The issues associated with the migration of anions (say, nitrites) in the CIAs along with the chlorides were discussed in Section 2.11. Further details of the modified RCPT test program is discussed next.

#### 4.2.2 Specimen design and preparation

The dimension of the test specimen is 100 mm diameter and 15 mm length is sliced from the 100 mm diameter and 200 mm length mortar cylinders. The mixture proportion of the mortar was 0.5:1:2.25 (water: cement:sand). Oxide composition of Ordinary Portland Cement (OPC) (IS:12269-2008) was determined by X-Ray Fluorescence (XRF) Spectroscopy is presented in Table 4.1. Physical characteristics of cement were determined as per IS:4031-2005 and fineness were determined as per ASTM C204 (2016) and results are given in Table 4.2.

**Table 4.1 Chemical composition of Ordinary Portland Cement (OPC)**

<b>Chemical component</b>	Al <sub>2</sub> O <sub>3</sub>	CaO	Fe <sub>2</sub> O <sub>3</sub>	K <sub>2</sub> O	MgO	Na <sub>2</sub> O	SiO <sub>2</sub>	SO <sub>3</sub>
<b>Concentration (%)</b>	4.51	66.67	4.94	0.43	0.87	0.12	18.91	2.5

**Table 4.2 Physical Properties of Ordinary Portland Cement (OPC)**

<b>Characteristics</b>	<b>Value obtained</b>	<b>Relevant standard</b>
Specific gravity	3.16	IS 4031-Part 11-2005
Fineness (m <sup>2</sup> /kg)	310	ASTM C204-16
Consistency (%)	30	IS 4031-Part 4-2005
Initial setting time (min)	52	IS 4031-Part 5-2005
Final setting time (min)	265	IS 4031-Part 5-2005

Silica sand of Grades I, II and III (IS:383-1970) with the particle size as shown in Table 4.3 was used as fine aggregate. An equal volume of each grade is used for making all the mortar specimens. Distilled water was used for the preparing all the mortar specimens.

**Table 4.3 Particle size distribution of sand used for cement mortar**

<b>Grade of Sand</b>	<b>Particle size range</b>
Grade - I	1 mm to 2 mm
Grade -II	1 mm to 500 microns
Grade -III	500 microns to 90 microns

Table 4.4 shows the properties of calcium nitrite based anodic (AN) corrosion inhibitor and the combination of Nitrite and amine based bipolar (BP) corrosion inhibitors are used in the research program. AN inhibitor which has a high concentration of nitrite is used to assess the effect of potential gradient. A calcium nitrite based AN type inhibitor (29 % solid content) was used at a manufacturer recommended dosage of 5.4 ml/kg of cement.

**Table 4.4 Typical properties of AN and BP corrosion inhibitor**

Property	AN inhibitor	BP inhibitor
Appearance	Light brown liquid	Light brown liquid
Specific gravity	1.27 to 1.30 at 20 °C	1.2 at 25 °C
Compositions	Minimum 30%	Nitrite and Amine
Recommended dosage	5.4 ml per kg of cement	5 ml per kg of cement

The cement mortar cylinders of size the 100 mm diameter and 200 mm length mortar cylinders were cast and cured for 28 days at standard laboratory condition. Then, the specimens were sliced to 15 mm length and used for further testing.

#### 4.2.3 Test setup to apply external potential

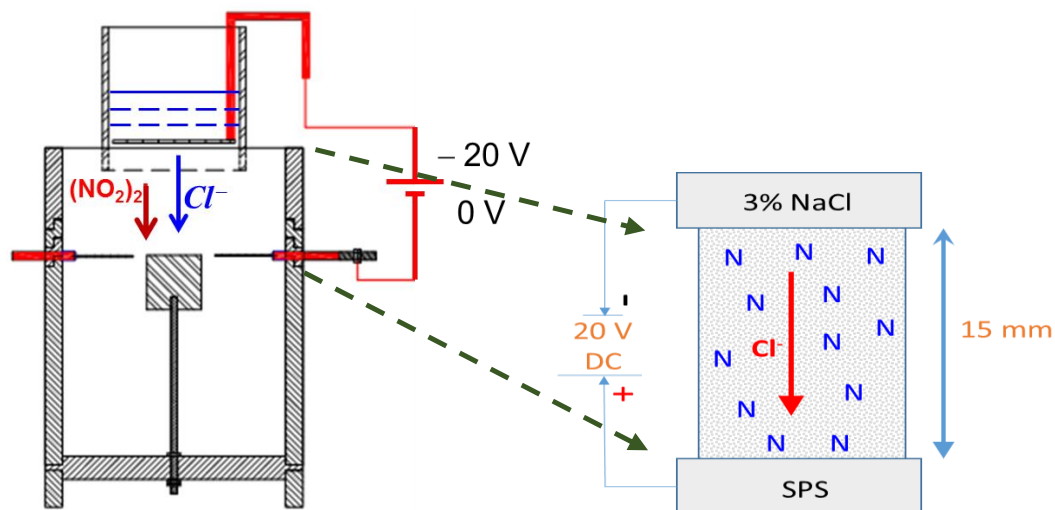


**Figure 4.1 Comparison of ACT specimens with modified RCPT test**

Figure 4.1 shows the ACT test setup (left) developed by Pillai and Trejo (2003) to determine the  $Cl_{th}$  of steel embedded in plain mortar. The cell arrangement and the mortar specimen in between the sodium chloride (NaCl) and Simulated Pore Solution (SPS) cell (right side) replicate the configuration of ACT setup. Figure 4.2 shows the schematic of the test setup which replicates the RCPT test setup (ASTM C1202-2012). These tests were performed to quantify the effect of external potential on the transport of anions (say, chlorides and nitrites) through cement mortar systems. Mortar cylinder specimens (100 mm diameter; 15 mm long) was assembled to the cell containing 3 % NaCl solution and simulated pore solution (SPS) on either side. The chemical composition of SPS is given in Table 4.5. The positive terminal of the DC potential source [Agilent E3611A] (See: Figure 4.3), was connected to the cell with SPS and the negative terminal to the cell with NaCl solution. An external potential of 20 V was applied continuously for 6, 12, 36, and 48 hours on three specimens each (total 12 specimens).

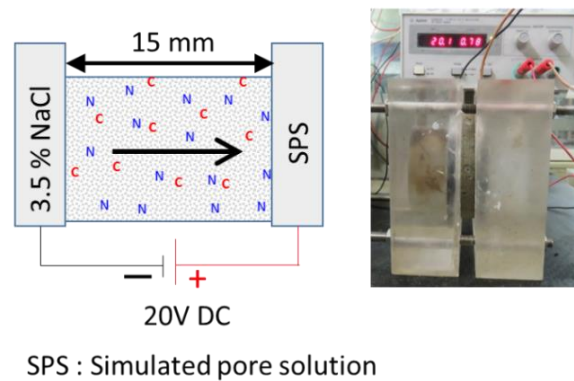


**Figure 4.2 Test setup to study the effect of anion migration due to external potential**

**Table 4.5 Chemical composition of Simulated Pore Solution (SPS)**

Constituents	Concentration (g/l)
H <sub>2</sub> O	966.08
Ca(OH) <sub>2</sub>	0.3
NaOH	10.4
KOH	23.23



**Figure 4.3 DC potential source used for this study (Agilent E3611A)**

#### **4.2.4 Determination of chloride and nitrite concentration**

At the end of the potential application for the specified periods, the mortar powder from different depths (3, 7, 11, and 13 mm) was collected from each specimen as shown in Figure 4.4.

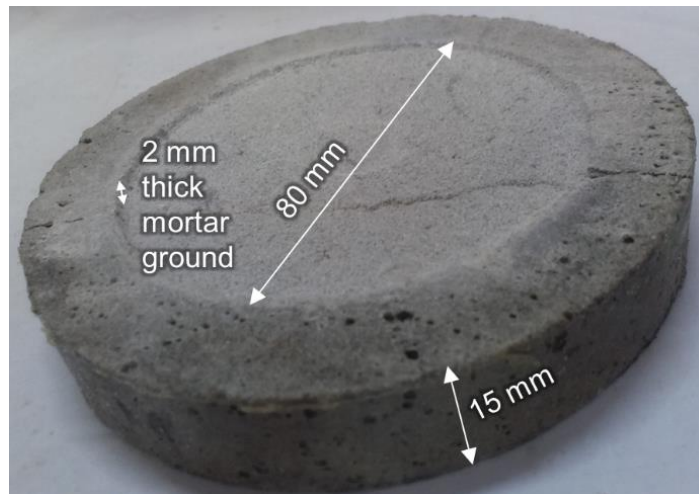


**Figure 4.4 Mortar powder ground at the steel-mortar interface**

Then, the chloride concentrations in the collected mortar powder was determined using chloride ion selective electrode as specified in SHRP-330 (1993). A chloride ion specific electrode (ISE) [Cole-Parmer Model: 27504-08] is used to measure the concentration of chloride in aqueous solutions. Figure 4.5 shows the chloride ISE connected to conductivity meter (Thermo Scientific CyberScan pH510). Appendix B provides a detailed procedure to determine the chloride concentration from cementitious powder.



**Figure 4.5 Chloride ion specific electrode connected to conductivity meter**

The concentration of nitrite in the collected mortar powder was determined using the UV-Visible spectrometer. UV-Visible spectrometer (Agilent Cary 100 UV-Vis) shown in Figure 4.6 is used to determine the concentration of nitrite in the mortar powder. Iron (II) sulfate heptahydrate (Hanna Instruments: HI 93708) is the reagent used. A detailed test procedure to nitrite concentration in cementitious powder is provided in Appendix C. The ratio between the chloride and nitrite ions (denoted as  $Cl/NO_2$  herein) was calculated, and the obtained results are discussed in Section 5.2.



**Figure 4.6 UV-Visible spectrometer**

### **4.3 OBJECTIVE 2: DEVELOPMENT OF MODIFIED ACT (MACT) TEST METHOD**

This section discusses the development of a modified ACT (known as mACT herein) test procedure to determine the  $Cl_{th}$  of steel embedded in cementitious systems with CIAs. Based on the findings from RM test, it was decided not to use the external potential in the mACT test procedure – to avoid the migration of anions in CIAs during the course of testing. The details of the mACT test specimen, corrosion measurement technique, and the statistical approach to detect corrosion initiation are discussed next.

Trejo and Miller (2002) patented Accelerated Chloride Threshold (ACT) test method, which was later refined by Trejo and Pillai (2003). The ACT method was developed for plain cementitious systems (i.e., without CIAs). This study provides a “modified” version of ACT (denoted as ‘mACT’ herein) test with the following modifications: (1) avoiding the application of potential gradient (2) reducing the cover depth, (3) increasing the concentration of NaCl solution from three to 15 %, and (3) modifying the statistical method of corrosion detection. The details of the (i) test specimen design and materials used (ii) curing and chloride exposure conditions, (iii) repetitive corrosion measurements, (iv) statistical methods to identify the stabilized data and to detect the corrosion initiation, and (v) determination of chloride concentration are presented in the following subsections.

#### **4.3.1 Specimen configuration and materials used**

Figure 4.7 and Figure 4.8 show the schematic and photograph of the mACT test setup. The setup consists of three-electrode corrosion cell system (WE, CE, and RE), an electrochemical workstation, and a computer as shown in Figure 4.8. Figure 4.7 and Figure 4.9 show the schematic and photograph of the mACT mould. The mACT moulds with features to place appropriately various electrodes (embedded in the mortar) were designed and fabricated. A 100 mm diameter Polyvinyl chloride (PVC) cylinder (Item 8 in Figure 4.7) is the mould for holding the cement mortar. Figure 4.10 shows a 25 x 25mm square Nickel-Chromium mesh made of 0.3 mm diameter wires and with 3 mm opening was used as a counter electrode (CE). The CE is held by a copper rod (3 mm diameter to hold in place and maintain the distance between the working electrode).

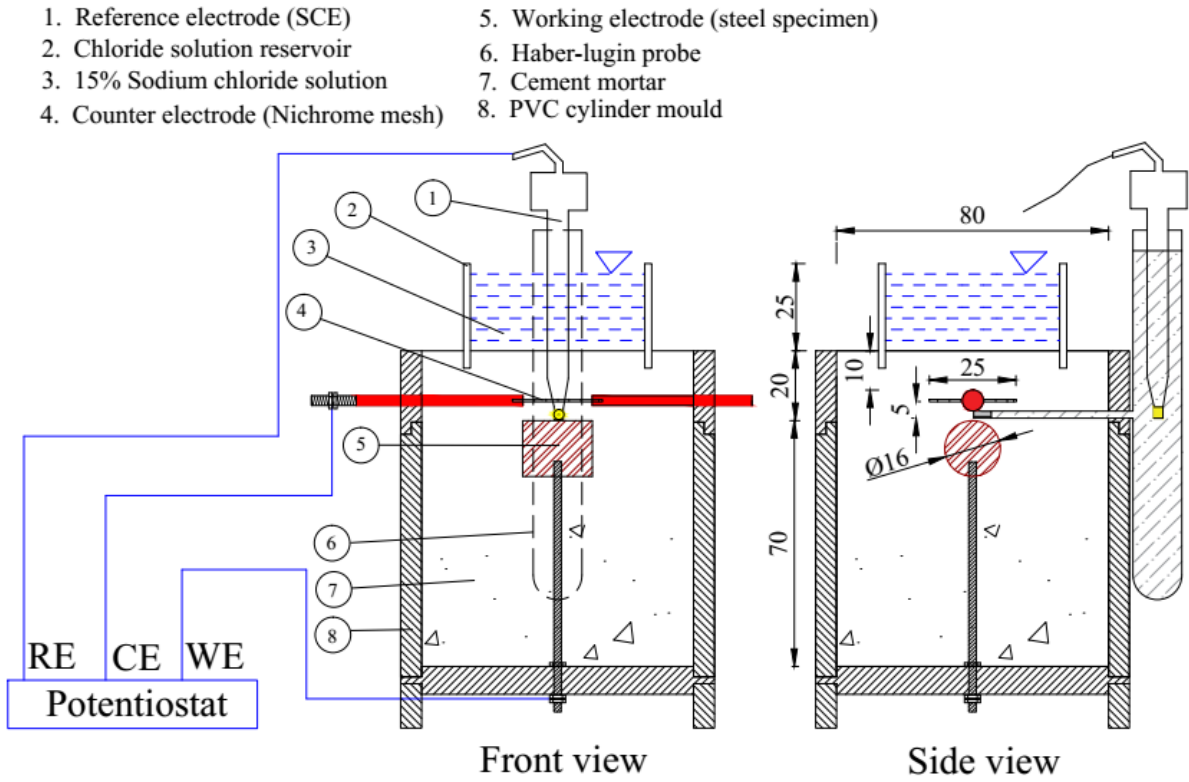


**Figure 4.7 Schematic of the mACT test setup**



**Figure 4.8 Photograph of the mACT test setup in the laboratory**

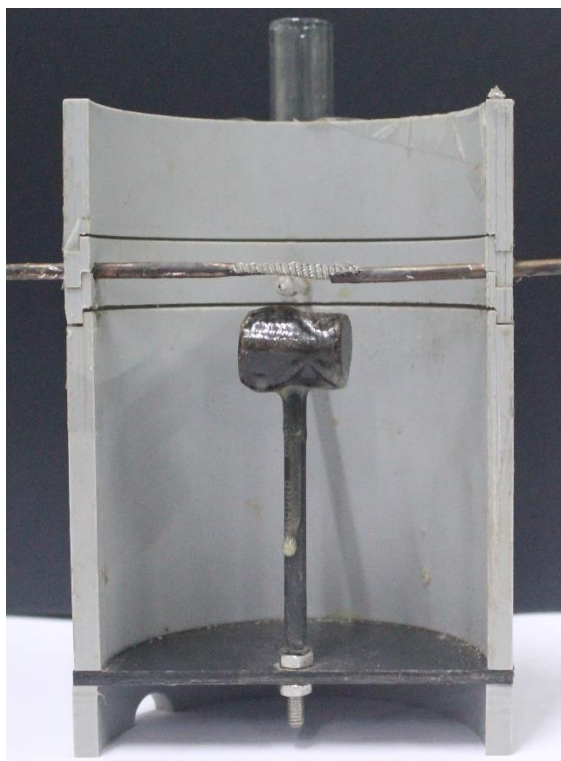


**Figure 4.9 Cross section of the mACT mould**

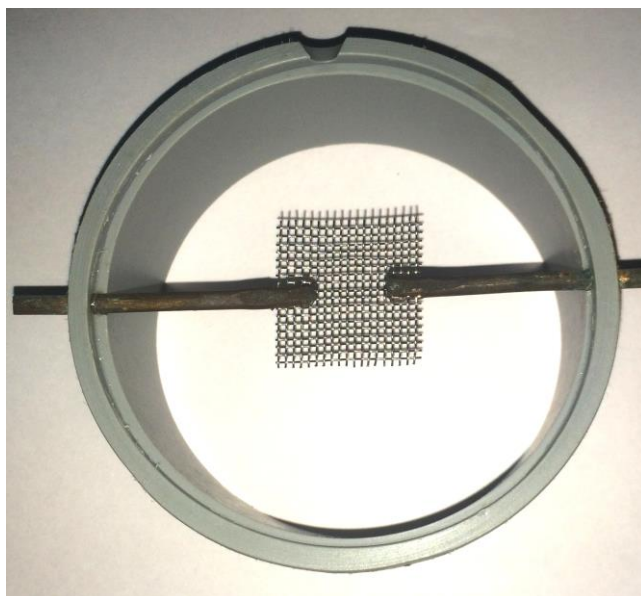


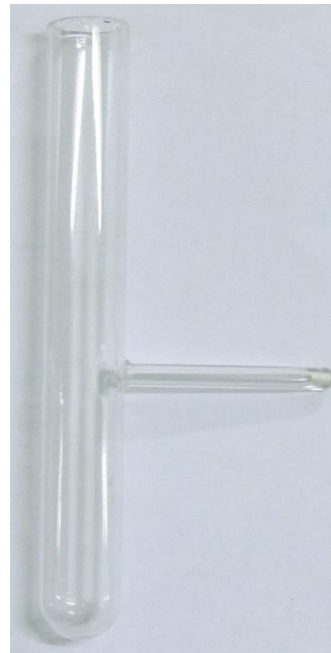
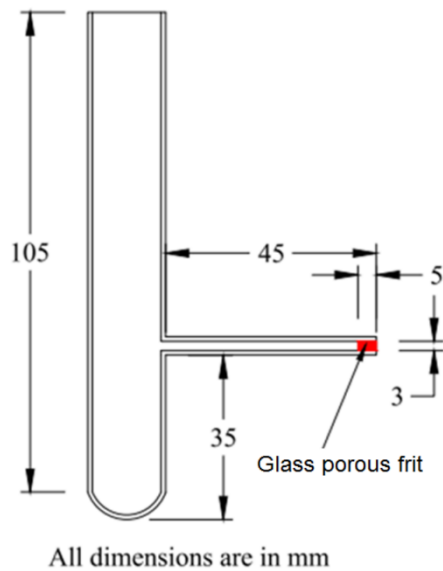
**Figure 4.10 Nichrome mesh connected with copper rod**

A Haber-luggin probe was used for placing the reference electrode. A glass luggin probe (See Figure 4.12 ) containing saturated potassium chloride (Sat. KCl) solution and with a

ceramic frit at the tip act as a salt bridge between the reference electrode and the steel-cementitious system. The mACT moulds have provisions made to place the luggin probe, such that the tip of the luggin probe will be placed at a distance of less than 5 mm from the working electrode. The Saturated calomel electrode (SCE) shown in Figure 4.11 is used as a reference electrode (RE). A 16 mm diameter QST steel rebar was cut to 20 mm length and used (Item 5) as working electrode (WE) as shown in Figure 4.13. The chemical composition of different steel used for this research program is shown in Table 4.6. For this study, the QST steel is used.



**Figure 4.11 Saturated calomel reference electrode**



(a) Schematic figure of luggin probe

(b) Typical luggin probe used

**Figure 4.12 Haber-Luggin probe**



**Figure 4.13 A typical working electrode used for mACT testing**

**Table 4.6 Chemical composition (% by weight) of different steel rebars**

Element	Cu	Co	Al	Ni	Mo	Cr	S	P	Mn	Si	C	Fe
<b>PM</b>	0.27	-	-	0.09	0.02	0.08	0.05	0.06	0.64	0.26	0.19	Re.
<b>CTD</b>	0.09	0	0	0.07	0.01	0.07	0.27	0.09	0.45	0.23	0.13	Re.
<b>QST</b>	0.16	0	0	0.15	0.06	0.24	0.01	0.08	0.63	0.24	0.2	Re.
<b>PS</b>	0.02	0	0	0.02	0	0.27	0	0.06	0.83	0.29	0.84	Re.

Re. – Remaining

The Ordinary Portland Cement (53 Grade) was used (see Table 4.1 for chemical composition). The standard silica sand classified as Grade III in IS:383 (1970) was used (see Section 4.2). Mortar with cement:sand ratio of 1:2.25 and a water-cement ratio of  $0.45 \pm 0.05$  was used. Distilled water was used for preparing the mortar. Ten specimens without inhibitor (W/O) as mentioned in Table 4.7, were tested to develop the mACT test method and determine the  $Cl_{th}$  of QST steel rebars in a plain mortar (i.e., W/O).

**Table 4.7 Experimental design for the mACT tests**

Corrosion Inhibitor type	Dosage (ml/kg of cement)	Number of specimens
Without inhibitor (W/O)	0	10
Anodic inhibitor (AN)	5.4	10
Bipolar inhibitor (BP)	5	10

### 4.3.2 Casting, curing, and chloride exposure

The mACT test specimens were cast according to the procedures given in Appendix A. The solution reservoir was filled with distilled water after the final setting time. The specimens were then cured for 28 days in a laboratory environment with  $65 \pm 5$  % relative humidity (RH) and  $25 \pm 2$  °C temperature. After the curing period, the solution reservoir (Item 2) on the top of each specimen was filled with 15 % sodium chloride solution (150 g of NaCl in 850 g of deionised water). This will significantly help in accelerating the  $Cl_{th}$  testing without affecting the chloride transport mechanisms inside the mortar (unlike the application of potential gradient). The solution level was maintained at 30 mm above the mortar surface. The solution in the reservoir was replaced at an interval of 10 days with a freshly prepared solution to maintain the chloride concentration.

### 4.3.3 Corrosion measurements

The setup consists of three-electrode corrosion cell system (WE, CE, and RE), an electrochemical workstation, and a computer as shown in Figure 4.8. The OCP and LPR were conducted on each mACT specimen using an electrochemical workstation (Solartron Models - SI 1287/1260). At first, the OCP of WE was measured. Then, the LPR test was conducted by sweeping the potential from  $-15$  mV to  $+15$  mV with respect to OCP at a scan rate of  $0.1667$  mV/s. Then, the electrical impedance spectroscopy (EIS) test with a stable AC potential of  $10$  mV and frequency ranging from  $1$  MHz to  $0.1$  Hz was conducted to determine the total resistivity (say,  $R_{total}$ ) of the steel-cementitious interface and the  $10$  mm thick mortar (or cementitious material) layer between the embedded electrodes. The  $R_{total}$  was calculated as the slope of the applied potential ( $E$ ) versus measured current density ( $i$ ) curve at the zero corrosion current, as shown in typical graph (Figure 4.14) and expressed mathematically as follows:

$$R_{total} = \left( \frac{\Delta E}{\Delta i} \right)_{E \rightarrow E_{corr}} \quad \text{Eq. 4.1}$$

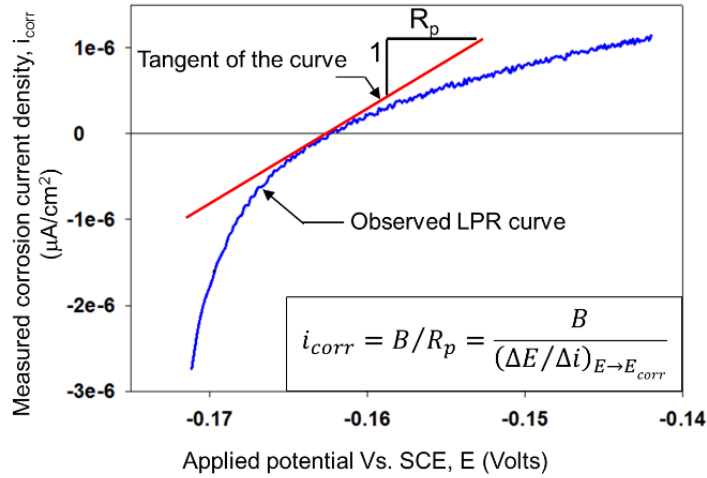


**Figure 4.14 A typical linear polarization resistance (LPR) curve**

The Figure 4.15 shows the expected equipotential and equicurrent lines between WE and CE while conducting the LPR and EIS test. The resistance of 10 mm thick steel-cementitious interface and the cementitious cover leads to IR drop. The bulk resistivity of the mortar layer between the electrodes (say,  $R_{cm}$ ; the subscript 'cm' stands for cementitious material) was calculated by fitting the EIS data in the modified Randles circuit, as given in Figure 2.11.

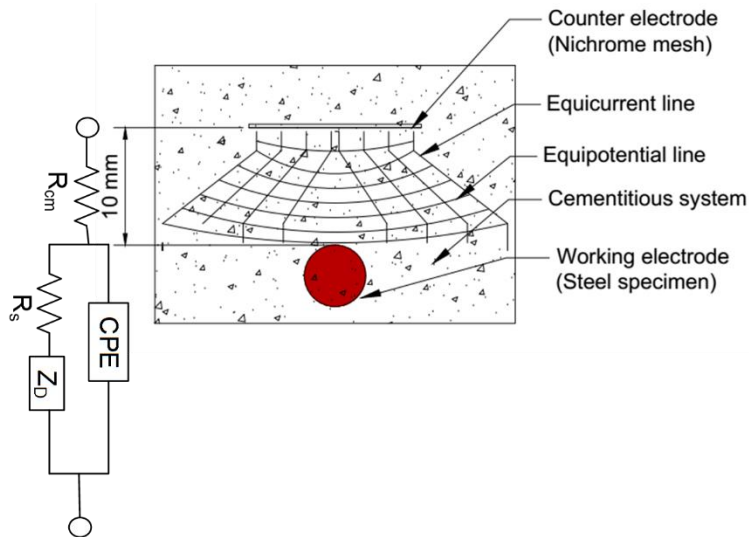


**Figure 4.15 Equipotential and equicurrent lines between WE and CE**

The Nyquist plot in the Figure 2.10(a) shows the corrosion behaviour of the steel cementitious interface. The beginning of the curve at  $10000 \Omega$  relates the cementitious properties at high frequency. The intermediate frequency at  $6500 \Omega$  attributes to the steel-cementitious system interface. The low frequencies corresponding to the inclined line at the end show the availability of oxygen at the interface. The diameter of the semicircle represents the charge transfer ( $R_s$ ) which is equivalent to the polarization resistance of steel ( $R_p$ ). Large the diameter of the semicircle means higher the polarization resistance ( $R_s$ ) of steel and lower the corrosion rate ( $i_{corr}$ ). However, the charge transfer along the steel specimen (20 mm) which indicates the corrosion process is very small. In this study,  $R_{cm}$  was calculated and the  $R_s$  was not considered from EIS data. The resistance of cementitious system ( $R_{cm}$ ) was calculated by fitting the EIS data using Nyquist plot with the equivalent circuit provided in Figure 2.11.  $R_{total}$  was the total resistance of steel-cementitious interface and the cementitious cover obtained from LPR test. The absolute polarization resistance of steel ( $R_p$ ) was calculated by subtracting  $R_{cm}$  from  $R_{total}$ .

Figure 4.16 shows that the  $R_{cm}$  value as a function of the exposure period. It shows that the  $R_{cm}$  decreases as a function of the exposure period and becomes negligible by about 30 days of exposure to chloride solution.

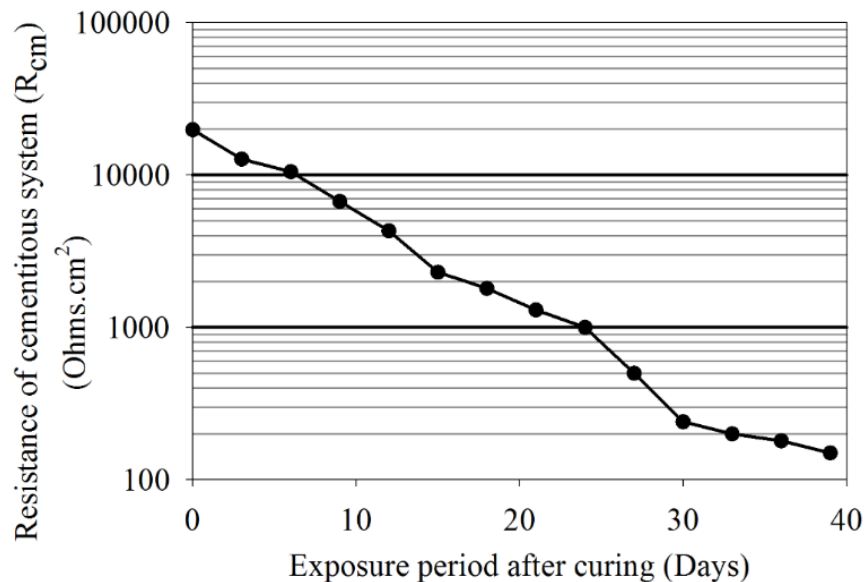


**Figure 4.16 Plot showing  $R_{cm}$  with respect to time for a specimen**

Thus, the polarization resistance of steel-cementitious interface ( $R_p$ ) can be assumed to be equal to  $R_{total}$ , as follows.

$$R_{total} \approx R_p \quad \text{Eq. 4.2}$$

The  $R_p$  changes as a function of the change in corrosion activity. The  $R_p$  values are monitored at every  $72 \pm 3$  hours until the detection of active corrosion initiation. To confirm the corrosion initiation, at least one more  $R_p$  is measured and analyzed. The following statistical approach was adopted to detect and define corrosion initiation.

#### 4.3.4 Statistical approach to detect corrosion initiation

Figure 4.17 shows the flowchart of the test procedure to conduct mACT test and obtain  $Cl_{th}$ . Considering the large scatter in the corrosion data, the  $(1/R_p)$  values observed at the beginning of the exposure period may have significant scatter, which can lead to erroneous interpretation of data. This randomness/scatter is depicted in Figure 4.18. Typically, the randomness reduces and the  $(1/R_p)$  gets stabilized as a function of exposure time. In this study, a ‘stable’ set of five  $(1/R_p)$  values (i.e., with acceptable scatter) is identified as follows.

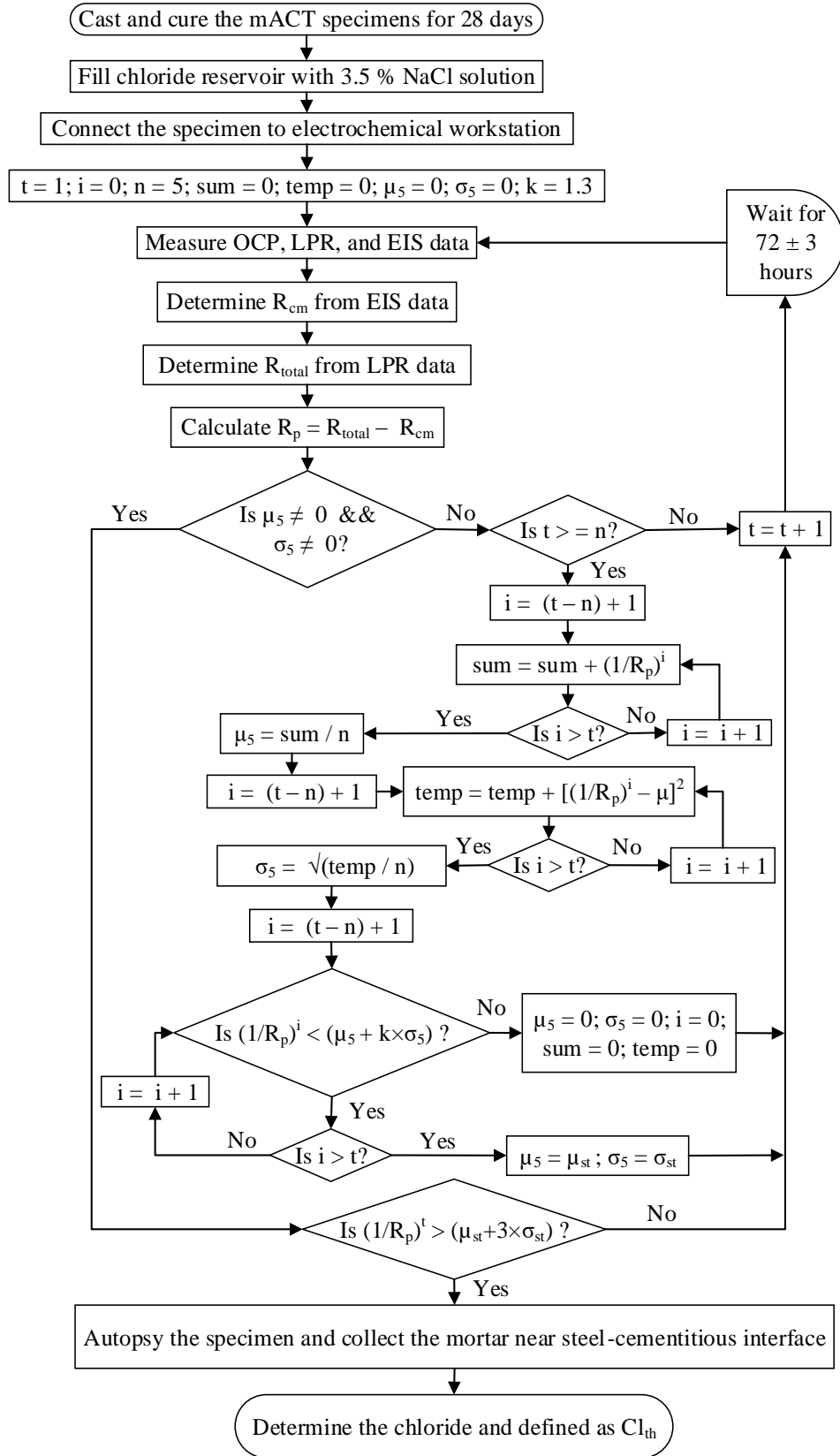
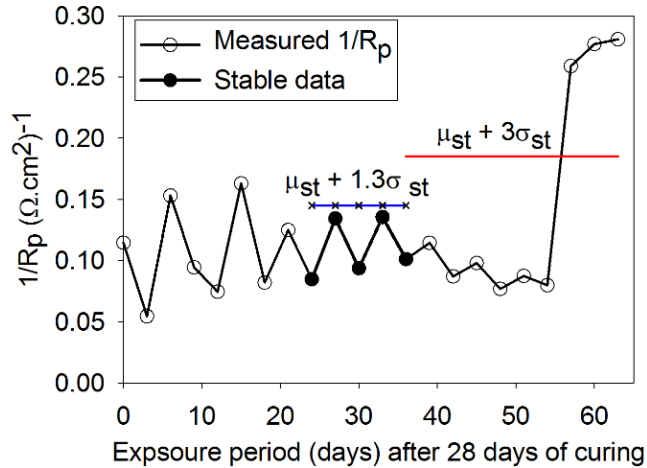


Figure 4.17 Flowchart to conduct mACT test



**Figure 4.18 Statistical approach used in mACT method to detect corrosion initiation**

First, the mean and standard deviation of the first five consecutive  $(1/R_p)$  values (denoted as  $\mu_5$  and  $\sigma_5$ ) are calculated. This data set is considered as ‘stable’ if all the five  $(1/R_p)$  values are less than  $(\mu_5 + k \sigma_5)$ , where  $k$  is defined to be 1.3. Otherwise, the next five consecutive  $(1/R_p)$  values are checked for the stable data condition. This will be continued until a stable data set is identified. Once the stable  $(1/R_p)$  data set is identified, the terms corresponding  $\mu_5$  and  $\sigma_5$  will be defined as  $\mu_{st}$  and  $\sigma_{st}$ . In short, the stable data limit is shown by the horizontal line with cross markers [i.e., at  $(\mu_{st} + 1.3 \sigma_{st})$ ] in Figure 4.18. Then, the LPR tests are continued until the corrosion initiation is detected. Corrosion is defined to be initiated when the  $(1/R_p)$  value exceeds the  $(\mu_{st} + 3\sigma_{st})$ . This statistical approach can be followed for detecting corrosion of each specimen. It should be noted that in most cases, the specimens may not exhibit visible corrosion. In other words, the corrosion initiation were detected before significant quantity of rust that is visible with naked eyes was formed. In some cases, very small rust spots were observed at or near the ribs and away from the epoxy coating.

The value of  $k$  was determined using a different analysis on  $(1/R_p)$  values (not discussed in this document). It was found that  $k = 1.3$  yielded reasonable number of test specimens with ‘stable’ data set. When the  $k$ -value was less than 1.3, many specimens were not able to exhibit ‘stable’ data set. On the other hand, keeping the  $k$ -value above 1.3 led to other challenges in detecting corrosion initiation. In short,  $k = 1.3$  was found suitable and used in this study.

#### 4.3.5 Method to determine the chloride and nitrite concentration

Once the corrosion is initiated, the specimens are autopsied at the level of steel surface to determine the chloride and nitrite concentration. As shown in Figure 4.19 the powdered mortar between the reference electrode and the working electrode was used to determine the chloride and nitrite content. The mortar was collected at about 2 mm above and 30 mm diameter from the top center of the steel specimen using the profile grinder shown in Figure 4.20, and the chloride concentration was determined, as per SHRP-S-330 (1993) procedure and the detailed steps provided in the Appendix B. This chloride concentration is defined as the  $Cl_{th}$  of the steel-cementitious system being tested. Additional details about the mACT test method are provided in Appendix A. Additional details about the accessories required for the mACT test are provided in Trejo and Pillai (2003) and the modified test procedure is provided in Appendix A.



**Figure 4.19 Specimen autopsied across the steel mortar interface**



**Figure 4.20 Concrete profile grinder (Germann Inc. Model No. PF-1100)**

#### **4.4 OBJECTIVE 3: DETERMINATION OF CHLORIDE THRESHOLD OF QST STEEL EMBEDDED IN SYSTEMS WITH CIAS**

The purpose of the mACT method is to determine the effect of AN and BP type CIAs on the  $Cl_{th}$  of QST (or Thermo-Mechanically Treated (TMT)) steel embedded in cementitious systems. The experimental procedures are discussed in Section 4.3. Table 4.7 provides the experimental design used to determine the  $Cl_{th}$  of QST steel rebars using mACT test method. In this study, a total of 30 mACT test specimens with QST steel pieces embedded in mortar without inhibitors ('W/O') and with anodic and bipolar inhibitors ('AN' and 'BP') were tested – 10 specimens each of W/O, AN, and BP were tested. The manufacturer recommended dosage of 5.4 ml/kg of cement was adopted for the calcium nitrite based AN inhibitor. The manufacturer recommended dosage of 5 ml/kg of cement was adopted for the calcium nitrite and amino alcohol based BP inhibitor.

## 4.5 OBJECTIVE 4: DETERMINATION OF CORROSION RATES OF DIFFERENT STEELS

### 4.5.1 Introduction

Most of the reinforced concrete structures are built using PM, CTD, QST, and PS steel as reinforcing steel. The corrosion of reinforced concrete structures exposed to chloride environment may not be neglectable, which in turn reduces the overall service life of the structure. Due to prolonged corrosion, the cover concrete can crack and leads to spalling. This can further lead to the higher rate of deterioration, which leads to the reduction in the structural load carrying capacity, as indicated by the increase in the slope of the curve in Figure 4.21.

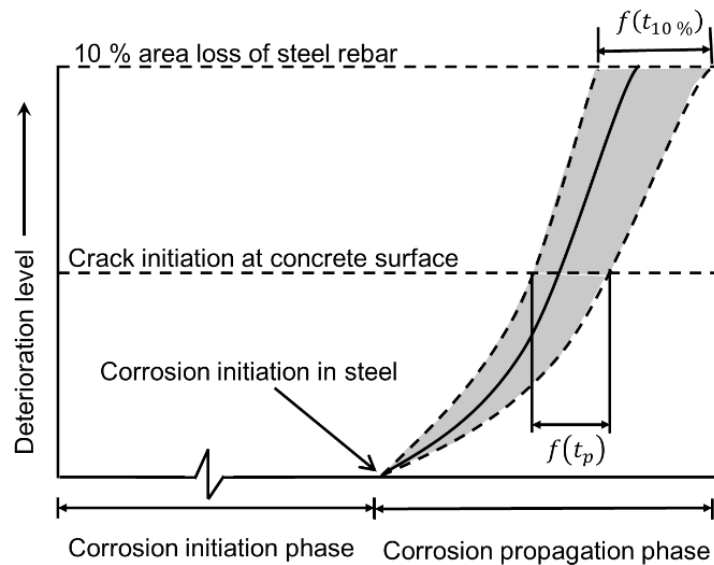


**Figure 4.21 Representation of probabilistic corrosion propagation period**

The corrosion propagation period ( $t_p$ ) is critical, and the corrosion rate ( $i_{\text{corr}}$ ) is one among the major influencing parameters. However, very limited information is available on  $i_{\text{corr}}$  for PM, CTD, QST, and PS steel rebars – making it difficult to estimate the service life. Current practice is to assume similar  $i_{\text{corr}}$  for PM, CTD, QST, and PS steel, which may give erroneous estimations of service life. Also, software programs like LIFE-365<sup>TM</sup> inadequately assume a deterministic value of 6 years for  $t_p$ , irrespective of the type and quality of materials used in the structure. This study provides experimental data and its statistical distributions of  $i_{\text{corr}}$  of PM, CTD, QST and PS steel bars. Using these data, the probabilistic  $t_p$  values for concrete systems

with different steel rebars are estimated using the models available in the literature. These findings can be very valuable to budget and plan repair strategies for the structures experiencing corrosion.

A comprehensive corrosion test program was conducted to determine the probabilistic corrosion rate ( $i_{\text{corr}}$ ) of four types of steel reinforcement. Twenty-five specimens of each steel type, adding to a total of 100 specimens, were cast. The cast specimens were cured for 28 days and then, subjected to cyclic wet-dry exposure using 3.5 % sodium chloride solution for 24 months. Every month, at the end of the wet period, the corrosion rate ( $i_{\text{corr, wet}}$ ) of each specimen was measured using linear polarization technique. Also, the specimens were then allowed to dry in the standard laboratory environment until the end of the 33<sup>rd</sup> month. The corrosion rate ( $i_{\text{corr, dry}}$ ) were measured at 27<sup>th</sup> and 33<sup>rd</sup> month. These data were used to develop a statistical distribution of  $i_{\text{corr, wet}}$  and  $i_{\text{corr, dry}}$ , which are later used to estimate probabilistic  $t_p$ . The details of the materials used, casting, exposure conditions, and test procedure, etc. are described next.

#### **4.5.2 Specimen design and preparation**

The schematic of the specimen is shown in Figure 4.22. The PM, CTD, and QST steel reinforcement (with 16 mm diameter and 420 mm long) and king wire (5.2 mm diameter and 420 mm long) removed from a 7-wire PS strand were used to prepare the test specimens. The steel reinforcement was cleaned by immersing in ethanol and using an ultrasonic cleaner for 5 minutes – to maintain ‘as received condition’. To facilitate corrosion measurements, an insulated copper wire (300 mm long) was fastened to one end of the steel specimen using a metallic screw. Then, the steel bar (except the 50 mm length at the center) and the screw were coated with two thin layers of a low viscosity epoxy (Sikadur<sup>®</sup>-52 UF). The steel reinforcement was then embedded in mortar. For prestressing steel specimens, the diameter of the steel piece and mortar cylinder were 5.2 and 29.2 mm, respectively. For PM, CTD and TMT steel specimen, the diameter of the specimen is 16 mm and the cover thickness is 12 mm.

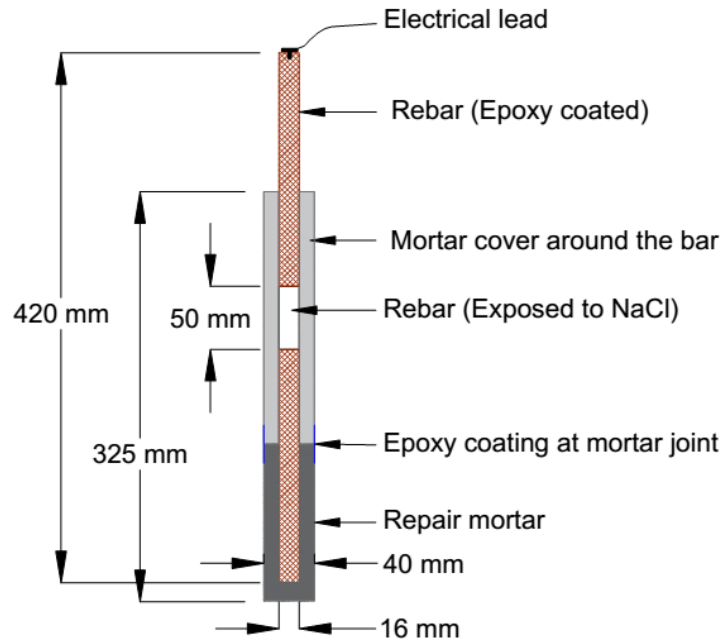


**Figure 4.22 Corrosion test specimen with a steel bar embedded in mortar**

### 4.5.3 Curing and exposure conditions

The test specimens were cured in a laboratory environment (ambient temperature =  $25 \pm 3^\circ\text{C}$  and relative humidity =  $65 \pm 5\%$ ) for  $24 \pm 1$  hours after casting. After this, the specimens were immersed/cured by immersing in saturated limewater for additional 27 days. Then, the cured specimens were subjected to cyclic wet-dry exposure (i.e., seven days wetting followed by seven days drying) using 3.5 % sodium chloride solution and in a laboratory environment with ( $\sim 65\%$  RH and  $\sim 25^\circ\text{C}$ ). During the wet period, the specimens were kept in a plastic container with sodium chloride solution. This container was covered with a plastic lid to avoid evaporation. During the dry period, the specimens were placed out of this container. The wet-dry exposure was continued for a period of 24 months under the laboratory environment. Later, the specimens were completely allowed to dry and the corrosion rates were measured at 27<sup>th</sup> and 33<sup>rd</sup> month. It is assumed that the ‘wet’ indicates the steel-cementitious interface is wet. Similarly, for the ‘dry’ condition.

The study shows that the corrosion rate was reduced to half the time when the cover depth is increased from 15 mm to 35 mm (Schiessl and Raupach, 1997). The increase in cover

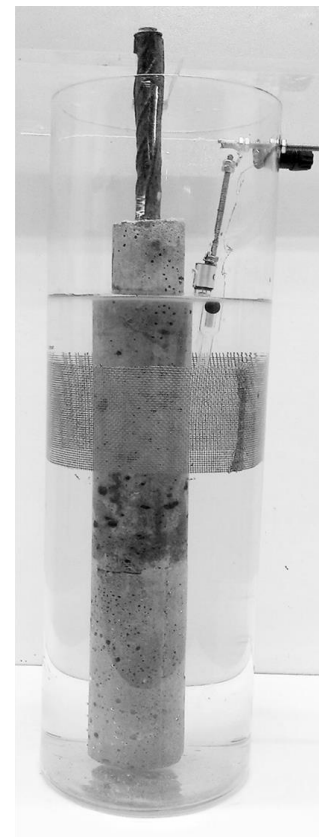
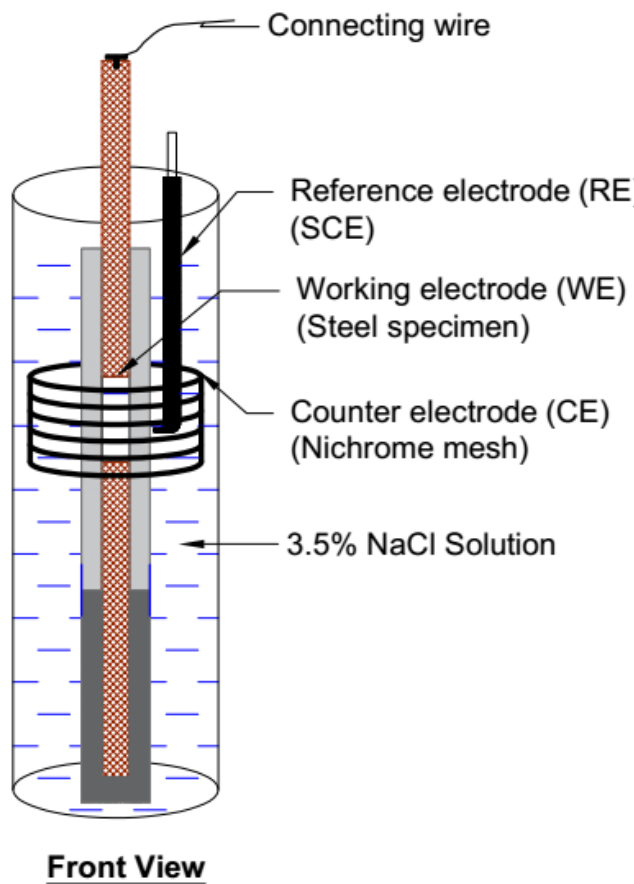
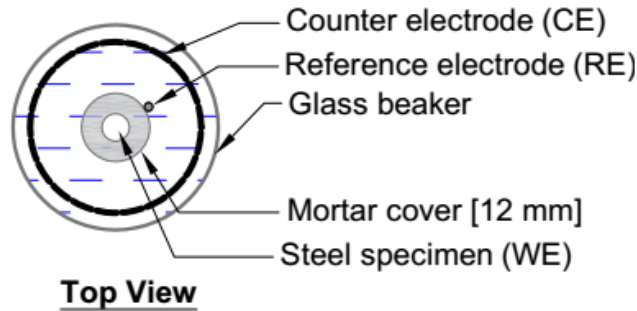
depth will reduce the availability of oxygen to the cathode. In addition, higher the cover depth will delay the drying at the steel surface (Alexander et al., 2012). Thus, the cover thickness of 12 mm was maintained for all the steel type to compare the corrosion performance in a severe exposure condition. ASTM G109 recommends 15 days wet and 15 days dry cycle to accelerate chloride ingress through cover concrete. In this study, 7 days wet and 7 days dry cycle was followed to increase the ingress rate of chlorides

Unfortunately, after ten months of exposure, the 2-layers of epoxy coating at the bottom end portion of the steel specimens (a lower region with no mortar cover; see Figure 4.22) failed/cracked and led to severe under-film or crevice corrosion (i.e., beneath the epoxy layer). This was due to the poor long-term performance of epoxy coating; the specimens exhibited large scatter in the  $i_{\text{corr}}$  data. The  $i_{\text{corr}}$  data obtained during this period does not truly represent the actual corrosion rate at the predefined exposed surface (center 50 mm long) of the specimen. Therefore, the damaged epoxy coating was removed using dichloromethane and the under-film or crevice corrosion products were removed by following the procedure given in ASTM G1-11 (Designation C.3.5 in Table A1.1) and re-coated with two new layers of epoxy. To avoid further failure/cracking of the epoxy coating, the bottom part of the epoxy coated steel was covered with cement mortar (denoted as ‘repair mortar’ in Figure 4.22). The interface between the old and new mortar was also sealed with epoxy. After 28 days of curing of the repair mortar, the repaired specimens were again exposed to cyclic wet-dry conditions using 3.5 % sodium chloride solution and corrosion rate measurement was resumed after 18<sup>th</sup> month. During the period from 10<sup>th</sup> to 18<sup>th</sup> months of exposure, the specimens were stored in the laboratory environment (~65% RH and ~25°C). However, it should be noted that the  $i_{\text{corr}}$  measured from 19<sup>th</sup> to 24<sup>th</sup> and 27<sup>th</sup> to 33<sup>rd</sup> month only used for the development of statistical distribution for  $i_{\text{corr, wet}}$  and  $i_{\text{corr, dry}}$  respectively, in this study.

#### **4.5.4 Corrosion test setup and corrosion rate measurements**

Figure 4.23 shows the three-electrode corrosion cell with a working electrode (WE), a counter electrode (CE), and a reference electrode (RE). All the electrodes were placed in a glass beaker with 3.5 % sodium chloride solution. This corrosion cell setup was then connected to a potentiostat and computer, as shown in Figure 4.24. The central 50 mm long uncoated region

of the steel piece was considered as the WE. A 90 mm diameter and 50 mm long pipe (annular setup) made of Nichrome wire mesh (24 wires of 0.5 mm diameter per inch) was used as the CE. The test specimen was placed at the center of the annular CE. The saturated calomel electrode (SCE) was used as the RE and placed near the surface of mortar cylinder (near the uncoated steel portion at the center 50 mm).



**Experimental setup**

**Figure 4.23 Schematic of the 3-electrode corrosion cell setup**

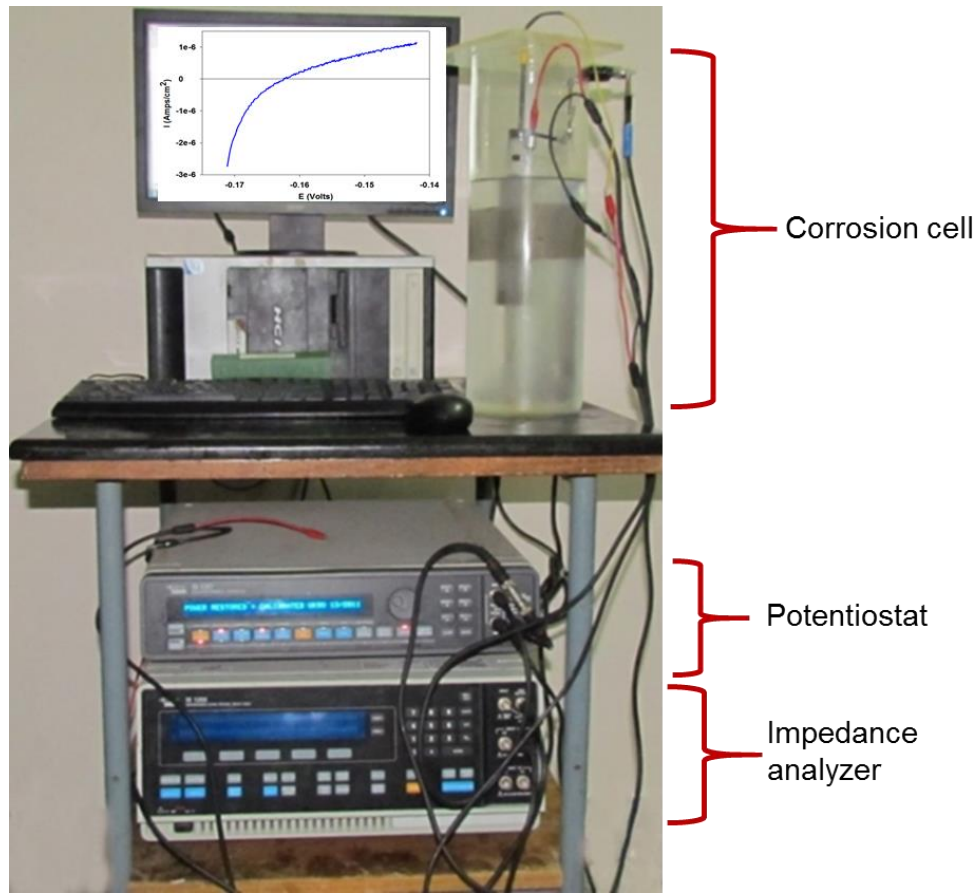


**Figure 4.24 Corrosion test setup with corrosion cell, potentiostat, and computer**

Corrosion measurements were made at the end of the alternate wetting period (say, once in a month). At first, the Open Circuit Potential (OCP) of the steel specimen was measured. Immediately after measuring the OCP, the LPR test was conducted with a scan range of +15 to -15 mV with respect to the measured OCP and at a scan rate of 0.1667 mV/s. During the forward scan in the LPR test, once the applied potential crosses the zero-current axis and sufficient data (say, about +5 mV Vs. OCP) is collected for obtaining the  $R_p$ . After this, the scanning/sweeping were manually terminated to avoid the application additional overpotential to the steel surface. The measured corrosion current density ( $i$ ) was plotted with respect to the applied potential ( $E$ ) to generate the LPR curve (see Figure 4.14 for a typical LPR curve). In the present investigation, though a scan range of  $\pm 15$  mV Vs OCP is adopted, only the linear data near the zero-current axis (linear region) is considered for determining the  $R_p$  values in this investigation. The  $i_{\text{corr}}$  was calculated as follows,.

$$i_{corr} = \frac{B}{R_p} = \frac{B}{\left(\frac{\Delta E}{\Delta i}\right)_{E \rightarrow E_{corr}}} \quad \text{Eq. 4.3}$$

where,  $B$  is the Stern-Geary coefficient,  $R_p$  is the polarization resistance,  $E$  is the applied potential,  $i$  is the measured corrosion current density.  $B$  is assumed as 26 mV for all the measurements.

#### 4.5.4.1 Corrosion rate measured during the wet-dry cycle and the dry period

The specimens were exposed to seven days wet and seven days dry cycle after the repairing the damaged epoxy coating as discussed in Section 4.5.3. The  $i_{corr}$  values measured at the ends of every 2<sup>nd</sup> wet cycle from 19<sup>th</sup> to 24<sup>th</sup> month are used as corrosion rate during wet period (denoted as  $i_{corr, wet}$ ). From 25<sup>th</sup> to 33<sup>rd</sup> month, the specimens were allowed to dry in a laboratory environment (Temperature =  $25 \pm 3^\circ\text{C}$  and RH =  $65 \pm 5\%$ ) and the  $i_{corr}$  were measured at 27<sup>th</sup> and 33<sup>rd</sup> month. These were considered as corrosion rate for dry period (denoted as  $i_{corr, dry}$ ). Note that the dry specimens were wetted by placing in a glass beaker with 3.5% sodium chloride solution for 30 minutes prior to the electrochemical testing. Only the  $i_{corr, wet}$ , and  $i_{corr, dry}$  data were used for estimating  $t_p$ , provided in Section 5.5.4.

## 4.6 SUMMARY

The details of the materials used, experimental design and the procedures of different experiments used in this study were described in this section. The details presented include the properties of the materials used for making cement mortar, exposure conditions, corrosion rate measurement procedures, and test variables.

## 5 RESULTS AND DISCUSSIONS

### 5.1 INTRODUCTION

Section 5.2 presents the results from the experimental programs on the effect of potential gradient on the movement of anions (say, nitrites) through the mortar. Section 5.3 discusses the development of mACT test method. Following this, Section 5.4 discusses the results on the  $Cl_{th}$  of steel-cementitious systems with W/O, AN, and BP inhibitors and their effects on  $t_i$  are presented. Then, Section 5.5 presents the corrosion rates of four different types steels (PM, CTD, QST, and PS) and their effects on the  $t_p$ .

### 5.2 OBJECTIVE 1: DETERMINATION OF THE EFFECT OF EXTERNAL POTENTIAL ON THE MIGRATION OF ANIONS THROUGH MORTAR

Figure 4.2 shows the modified RCPT setup used for this study to migrate the chloride in cementitious system. The change in the concentration of anions near the SPS cell (at right side) is the focus of this study (i.e., at 13 mm from the chloride solution cell). The potential-induced changes in the concentrations of chlorides and nitrites, and the chloride-nitrite ratio are discussed next.

#### 5.2.1 Migration of chloride ions

Figure 5.1 shows the chloride concentration (in %bwoc; by weight of cement) at different depths of the 15 mm thick mortar specimens exposed to the external potential of 20 Volts for 6, 12, 36, and 48 hours.

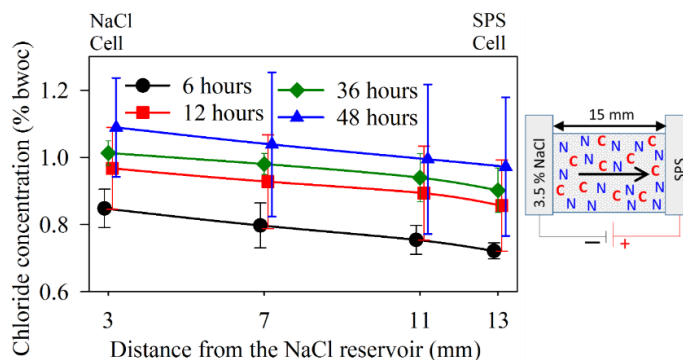
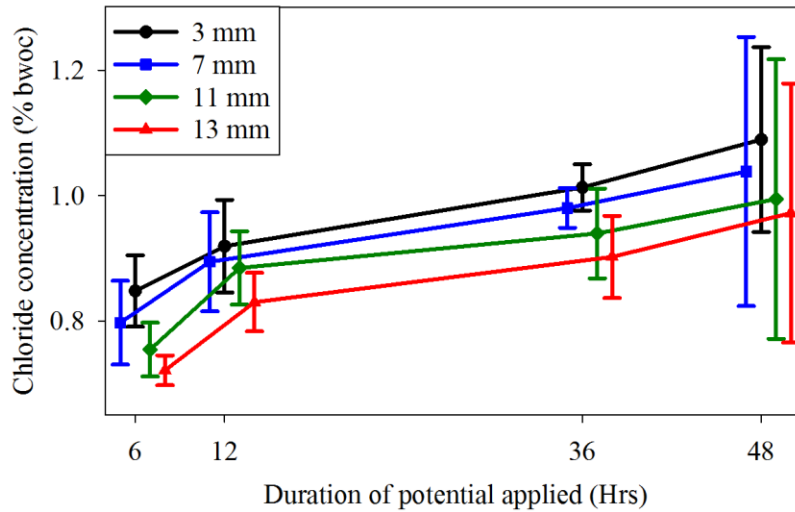


Figure 5.1 Variation in chloride due to application of external potential

The concentration of chlorides in the mortar near the SPS cell is about 0.7 %bwoc after 6 hours of potential application (circular markers at right end). The concentration of chlorides increases linearly with increase in the duration of potential applied. After 48 hours of potential application, chloride concentration in the mortar near the SPS cell (at right end) increases to about 1.1 %bwoc (triangular marker). Figure 5.2 shows the same data shown in Figure 5.1. Figure 5.1. shows ‘distance from the NaCl reservoir’ as the abscissa whereas Figure 5.2 shows the ‘duration of potential applied’ in the abscissa.

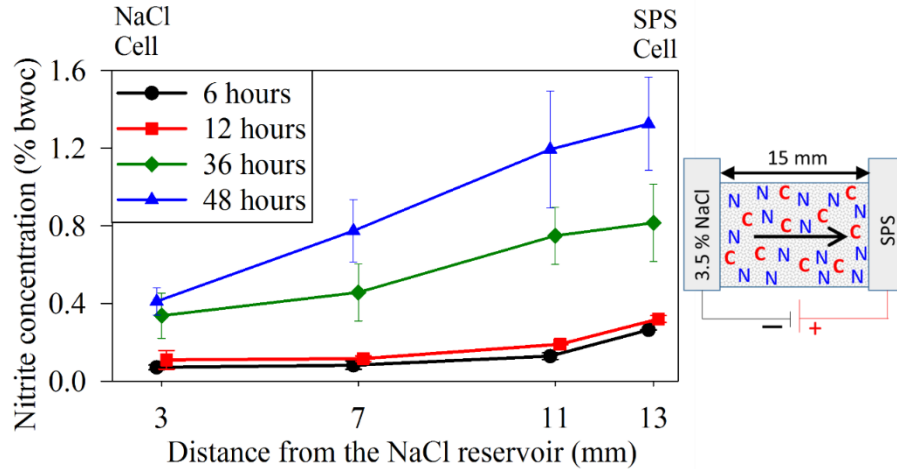


**Figure 5.2 Variation in chloride at different depth w.r.t potential applied**

Each curve in Figure 5.2 shows the concentration of chloride at a particular depth as a function of the duration of potential applied. For the case at 13 mm, the concentration of chloride is around 0.7 %bwoc at the beginning, increases to 0.84 and 0.98 %bwoc at 12 and 48 hours, respectively. Similarly, after 48 hours of potential application, the average chloride concentrations at 3, 7, 11, and 13 mm are about 1.1, 1.04, 1, and 0.98 %bwoc, respectively. Thus, the external potential application helps in migrating the chlorides through mortar within a short duration. However, it also helps in the migration of nitrite ions, as discussed next.

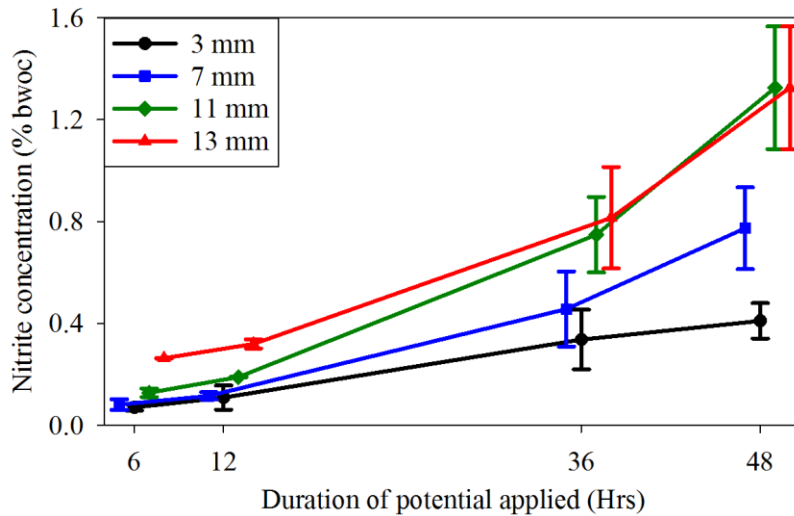
### 5.2.2 Migration of nitrite ions (anions)

Figure 5.3 shows the concentration of nitrites at different depths in mortar with respect to the duration of application of 20 V potential gradient.



**Figure 5.3 Variation in nitrite due to application of external potential**

The concentration of nitrites in mortar near the SPS cell is about 0.3 %bwoc even after 12 hours of potential application (see the square marker at right end). However, this concentration has increased to about 1.2 %bwoc after 48 hours of potential application (see the triangular marker at right end). Figure 5.4 shows the same data shown in Figure 5.3. Figure 5.3 shows ‘distance from the NaCl reservoir’ as the abscissa whereas Figure 5.4 shows the ‘duration of potential applied’ in the abscissa.



**Figure 5.4 Variation in nitrite at different depth w.r.t potential applied**

Each curve in Figure 5.4 shows the concentration of nitrite at a particular depth as a function of the duration of potential applied. For the case at 13 mm, the concentration of nitrite

is around 0.25 %bwoc at the beginning, increases to 0.32 and 1.34 %bwoc at 12 and 48 hours, respectively. Similarly, after 48 hours of potential application, the average nitrite concentrations at 3, 7, 11, and 13 mm are about 0.4, 0.78, 1.31, and 1.34 %bwoc, respectively. A scatter in results was observed after 36 hours of potential application. The difference in the pattern of changes in the chloride and nitrite concentrations along the depth is probably because the initial concentration of the former in the mortar is negligible; whereas the initial concentration of the latter is uniform and significant. This indicates that the concentration of nitrites near the steel working electrode in the ACT test specimen would experience a significant increase if the external potential is applied. This increased nitrite concentration at the steel surface can lead to a delay in corrosion initiation – but, such increase in nitrite (or anion) concentration will not happen in real structures. Therefore, it can be concluded that the application of external potential can lead to erroneous estimation of the  $Cl_{th}$  of steel-cementitious systems with CIAs.

### 5.2.3 Variation in the chloride-nitrite ratio

Figure 5.5 shows the  $Cl/NO_2$  ratio at different depths in mortar with respect to the duration of application (6, 12, 36, and 48 hours) of 20 V potential gradient.

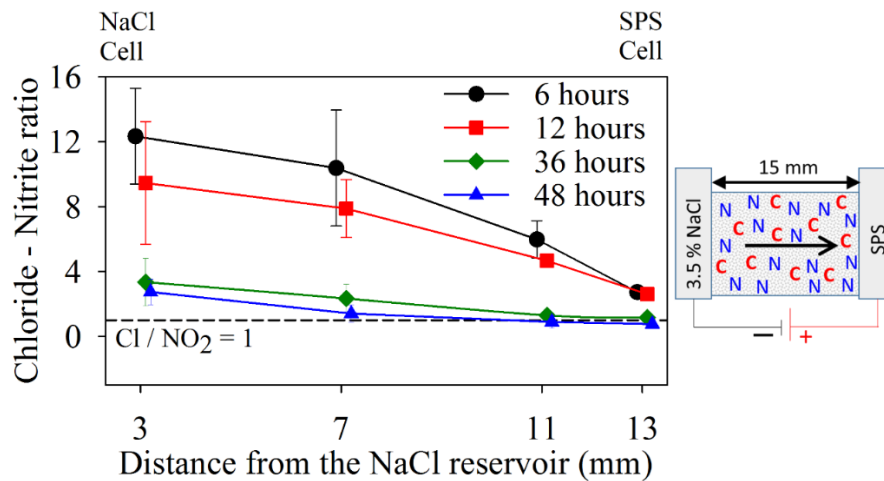


**Figure 5.5 Variation in chloride-to-nitrite ratio due to application of external potential**

With the increase in the duration of application of 20 V, the  $Cl/NO_2$  ratio reduces to a value below one, which is reported as the threshold value for corrosion initiation (Gaidis, 2004).

Figure 5.6 shows the same data shown in Figure 5.5. Figure 5.5 shows ‘distance from the NaCl

reservoir’ as the abscissa whereas Figure 5.6 shows the ‘duration of potential applied’ in the abscissa.

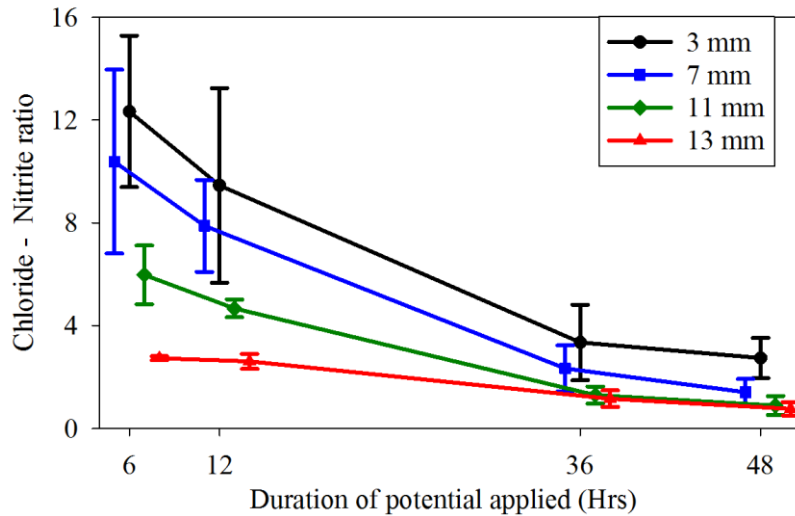


**Figure 5.6 Variation in chloride-nitrite ratio at different depth w.r.t potential applied**

Each curve in Figure 5.6 shows the chloride-nitrite ratio at a particular depth as a function of the duration of potential applied. At 7 mm from the NaCl cell, the chloride-nitrite ratio is about 10.5 at the beginning, decreases to 8.6 and 2.8 at 12 and 48 hours, respectively. Similarly, after 48 hours of potential application, the chloride-nitrite ratio at 3, 7, 11, and 13 mm is about 5, 2.8, 1.34, and 1.2, respectively. Prolonged application of nitrites could lead to a chloride-nitrite ratio of less than unity at the steel surface – leading to a highly corrosion resistant system. This artificial change in nitrite concentration (at the steel surface) during the ACT test will not happen in real life. Hence, test methods that use the external potential to drive the chlorides cannot be used for estimating  $Cl_{th}$ . In short, the application of an external potential to drive the chlorides towards the surface of the embedded steel alters the steel-cementitious interface chemistry and provide erroneous test results. Thus, an alternate  $Cl_{th}$  test method, which will not alter the anion concentrations near the steel surface during the course of the testing is required to assess the  $Cl_{th}$  of systems with CIAs containing various anions.

#### 5.2.4 Summary of test results (Objective 1)

Based on the potential-induced, rapid chloride penetration study conducted on 15 mm thick mortar cylinders, the following conclusions are made.

- Significant transport of nitrite ions can occur upon the application of potential gradient of 20 V across a 15 mm thick mortar cylinder. This transport and a corresponding change in nitrite concentration at the steel surface do not happen in structures experiencing natural chloride ingress.
- Upon the application of 20 V potential gradient for about 12 hours, ( $\text{Cl}/\text{NO}_2$ ) at the surface of the steel embedded inside the cementitious matrix can reduce to a value less than one – resisting corrosion initiation; although the chloride concentration might be high.
- The application of potential gradient can change the chemical composition at the steel-cementitious interface and hence, is not a suitable technique while determining the chloride threshold for steel-cementitious systems with corrosion inhibitors containing anions.

### **5.3 OBJECTIVE 2: DEVELOPMENT OF MACT TEST METHOD**

The author could not find a standardized short-term test method to directly determine the  $\text{Cl}_{\text{th}}$  of steel-cementitious systems with CIAs. However, researchers have used some of the existing corrosion test methods and further testing to indirectly determine the  $\text{Cl}_{\text{th}}$ . However, these indirect methods either take a long time (say, years) for test completion or apply the potential gradient. The application of potential gradient may alter the anion concentrations (say, nitrites) at the steel-cementitious interface – leading to erroneous results. However, determination of  $\text{Cl}_{\text{th}}$  of steel cementitious systems with corrosion inhibitors is necessary for service life prediction. This study experimentally develops a test procedure to detect the corrosion initiation and chloride threshold of the steel embedded in the cementitious systems with corrosion inhibitors – in a reasonable period of about 4 months. This test method would be useful to the engineers and clients in selecting appropriate corrosion inhibitor from the various products available in the market, during the planning and design stages.

### 5.3.1 Inverse polarization resistance data for specimens without inhibitors

Figure 5.7 shows the variation of inverse polarization resistance ( $1/R_p$ ) as a function of exposure period for specimens without inhibitors (W/O). The unfilled star marker towards the end of each curve indicate the corrosion initiation point for that particular specimen. Corrosion initiation was detected using the method discussed in Section 4.3.4. For example, Specimen W/O-S8 shows stable data in the early time periods and exhibits a significant increase in ( $1/R_p$ ) at about 30 days of exposure. Similarly, other specimens also showed corrosion initiation between about 24 and 36 days. The measurements were continued for at least one more reading after the star markers. This was done so to confirm that the active corrosion is propagating. In general, all specimens showed stable data and corrosion initiation in reasonable period of time.

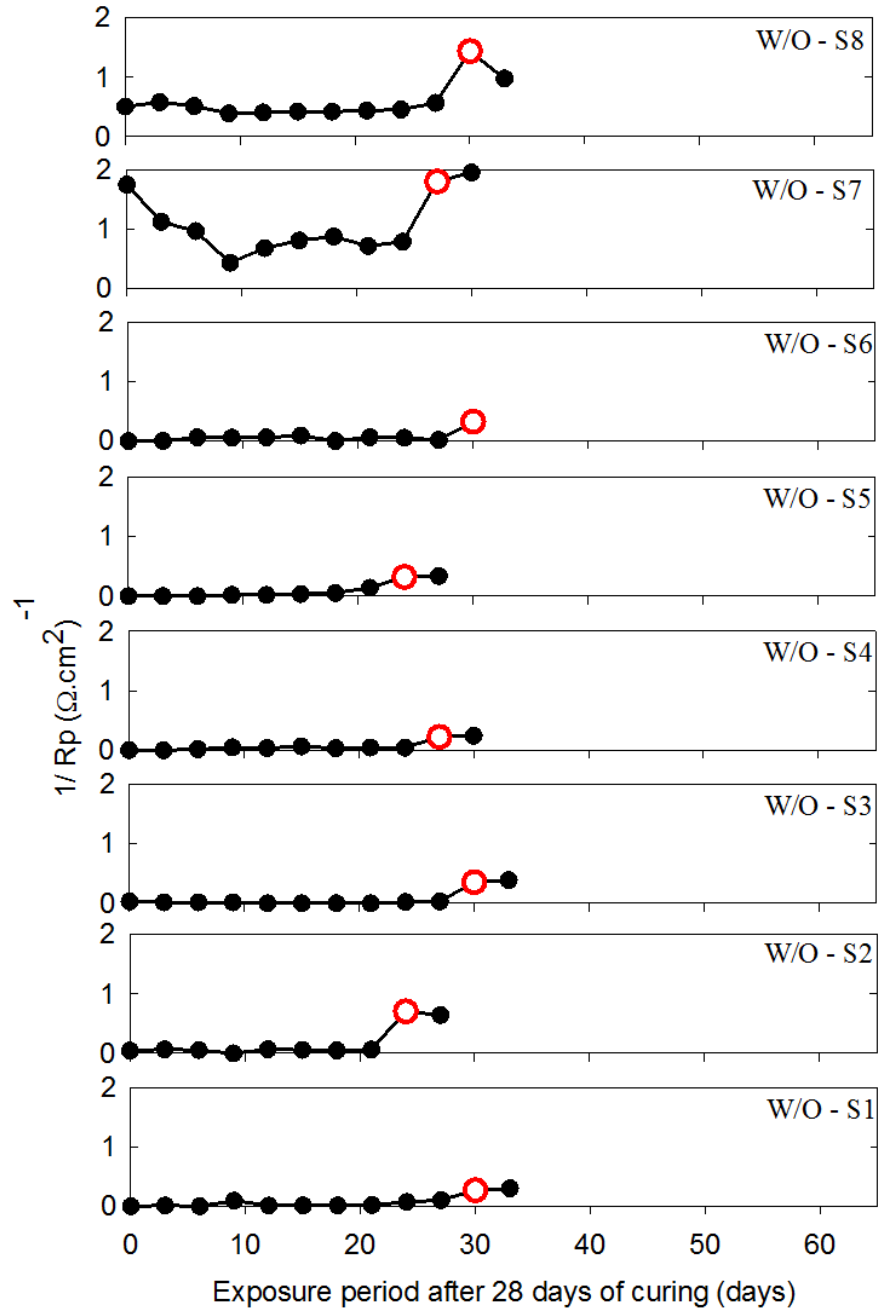


**Figure 5.7 Inverse polarization resistance Vs chloride exposure time for systems without inhibitor (W/O)**

### 5.3.2 Cl<sub>th</sub> for specimens without inhibitor and validation of mACT test method

The first column in Figure 5.8 shows the Cl<sub>th</sub> of steel embedded in cementitious systems without inhibitors (determined using the mACT test method). The average Cl<sub>th</sub> of QST steel is

found to be about 1.12 %bwoc (indicated by the solid horizontal line) and the standard deviation is 0.5 %bwoc.

To validate the developed mACT test method, it would be ideal to compare the determined  $Cl_{th}$  values with those determined using a long term test method with the identical steel-cementitious systems. However, such tests could not be performed. Therefore, the  $Cl_{th}$  values (for steel-cementitious systems without inhibitors) reported in the literature over a period of 50 years (see Figure 2.4) were collected and compared with the results obtained from the mACT method. The data points shown in the second column of Figure 5.8 are the average  $Cl_{th}$  values reported in the literature and is about 0.8 % by weight of cement (%bwoc) and standard deviation of 0.4 %bwoc. A statistical assessment was done with these two data sets for specimens without inhibitor case. Both the  $Cl_{th}$  data reported in the literature and those determined using the mACT test method passed the normality test (Shapiro - Wilkinson method). Further, Student's t-test using the two data sets concluded that, at a significance level of  $\alpha = 0.05$ , there is no evidence to reject the null hypothesis. This indicates that there is a statistical similarity between the two data sets. This validates that the mACT test can produce good estimates of  $Cl_{th}$ .

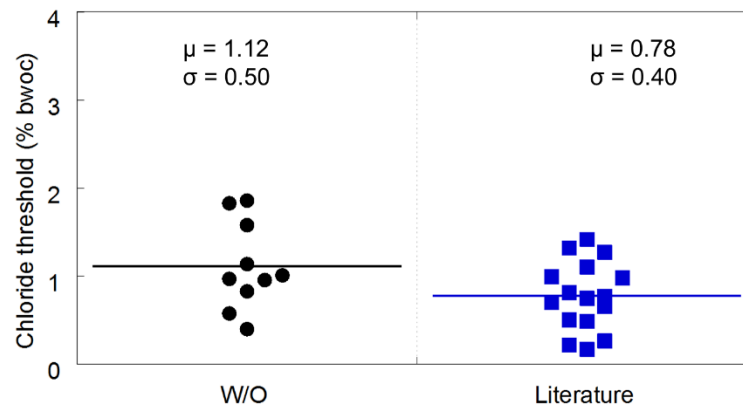


**Figure 5.8  $Cl_{th}$  of QST steel in systems without CIAs (plain mortar)**

### 5.3.3 Summary of test results (Objective 2)

- The mACT test method is developed for determining  $Cl_{th}$  of steel-cementitious systems with CIAs containing anions is developed. The time required to complete the mACT test is about 4 months. However, it should be noted that the better the inhibitors, the longer would be the test duration.
- The specimens without inhibitors exhibited  $Cl_{th}$  of about 1.12 %bwoc, which is similar to the range of the reported values in the literature (0.8 %bwoc). Considering the inherent variations in corrosion mechanisms and large scatter in measurements reported in the literature, it can be concluded that the mACT test method is a reasonably valid procedure.

## 5.4 OBJECTIVE 3: DETERMINATION OF CHLORIDE THRESHOLD OF QST STEEL EMBEDDED IN SYSTEMS WITH CIAS

This subsection provides the  $Cl_{th}$  of ten specimens each with QST steel embedded in cementitious systems with AN and BP inhibitors.

### 5.4.1 Inverse polarization resistance data for specimens with AN and BP inhibitors

Similar to Figure 5.7 for the case of W/O inhibitors, Figure 5.9 and Figure 5.10 shows the variation of  $(1/R_p)$  as a function of exposure period for specimens with ‘AN’, and ‘BP’ inhibitors, respectively. The unfilled star marker towards the end of each curve indicate the corrosion initiation point for that particular specimen.

For example, Specimen AN-S4 in Figure 5.9 shows stable data (as discussed in Section 4.3.4) in the early time periods and exhibits a significant increase in  $(1/R_p)$  at about 40 days of exposure. Similarly, other specimens also showed corrosion initiation between about 30 and 60 days of exposure.

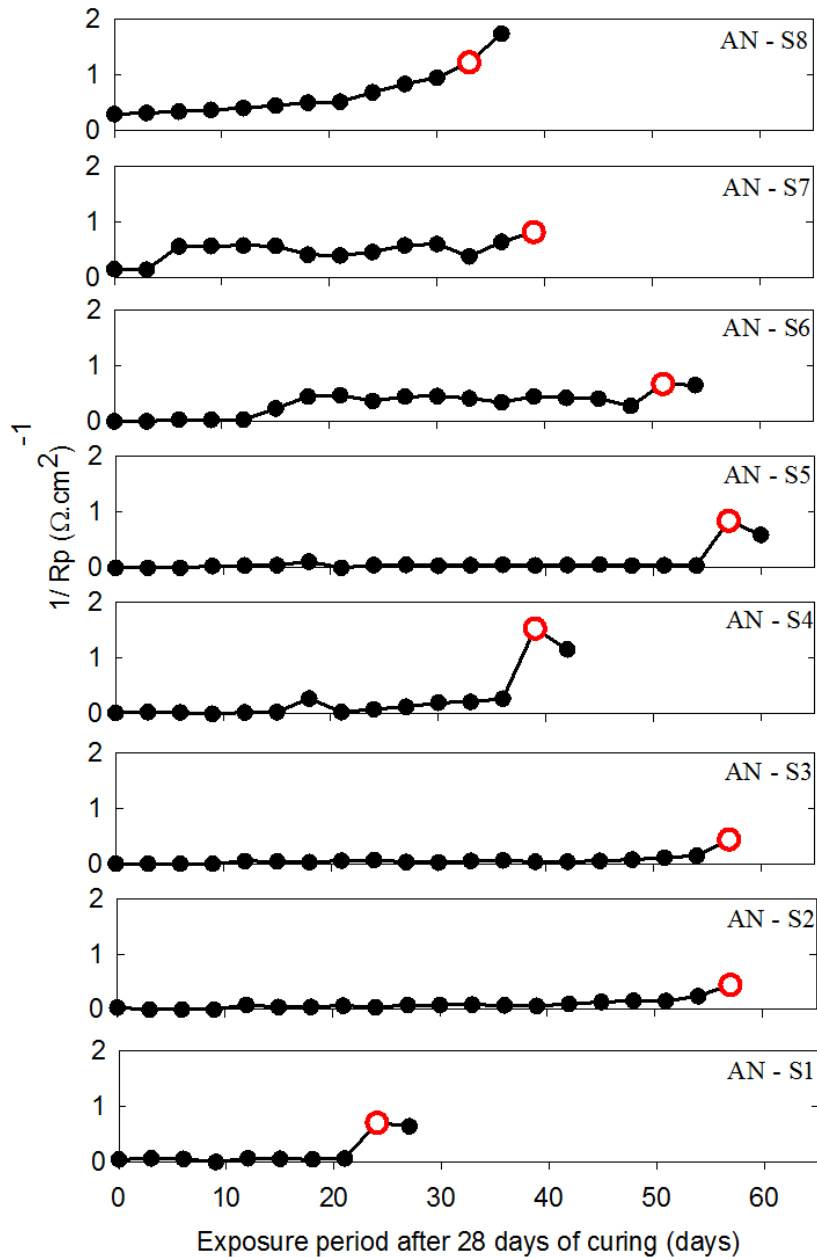


**Figure 5.9 Inverse polarization resistance Vs chloride exposure time for systems with anodic inhibitor (AN)**

In the case of Specimen BP-S2 in Figure 5.10, corrosion initiation is detected at about 55 days of exposure. To confirm that the active corrosion is propagating, the LPR measurements were repeated for at least one more time after the star markers. Specimens AN-S7 and BP-S9 exhibited more significant scatter in the beginning as compared to the other specimens and were defined as bad specimens. The reason for this unusual data was unknown. Note that the data for these two bad specimens are not shown in Figure 5.9 and Figure 5.10.

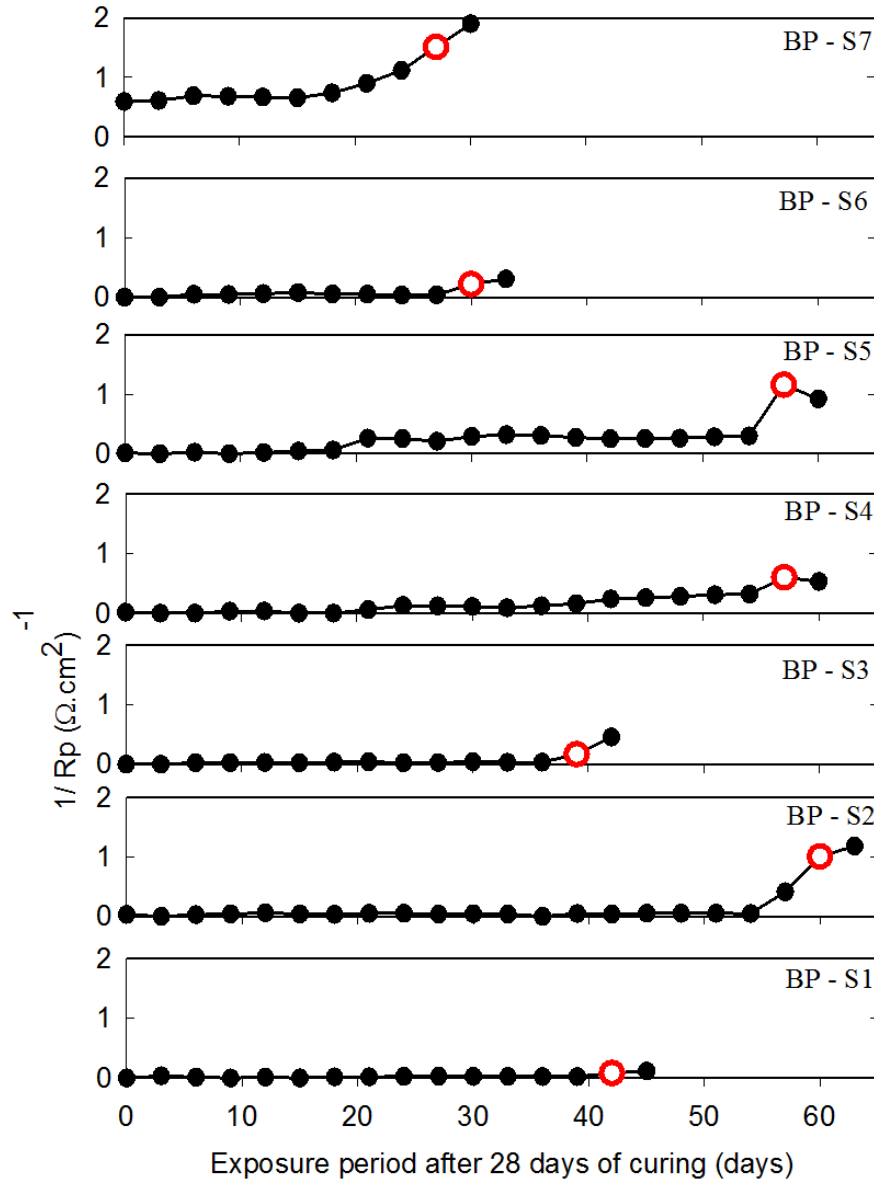


**Figure 5.10 Inverse polarization resistance Vs chloride exposure time for systems with bipolar inhibitor (BP)**

#### 5.4.2 $Cl_{th}$ of QST steel embedded in systems with CIAs

Figure 5.11 shows the  $Cl_{th}$  values of QST steel embedded in mortar with W/O, AN, and BP inhibitors.

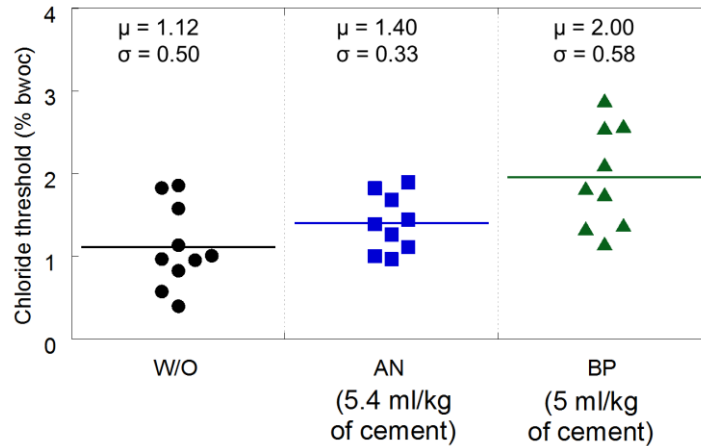


**Figure 5.11  $Cl_{th}$  of QST steel in systems with and without CIAs**

Table 5.1 shows the  $Cl_{th}$  value obtained for each specimen. The  $Cl_{th}$  of QST steel embedded in a cementitious system with W/O, AN, and BP inhibitors can be expressed as normal distributions as follows:  $\sim N(1.12, 0.5)$ ,  $\sim N(1.4, 0.33)$ , and  $\sim N(2, 0.6)$  %bwoc, respectively. At 95% confidence level ( $\alpha = 0.05$ ), there is no significant difference ( $p$ -value = 0.167) between the  $Cl_{th}$  for systems with no inhibitors (W/O) and with anodic inhibitors (AN). However, the  $Cl_{th}$  for systems with anodic inhibitors (AN) and with bipolar inhibitors (BP) were statistically significantly different ( $p$ -value = 0.032). The average  $Cl_{th}$  of specimens with CIAs exhibited higher  $Cl_{th}$  values than that of specimens without inhibitors shown in Column 1 in Figure 5.11. Moreover, the  $Cl_{th}$  values of many specimens with BP inhibitors are higher than the average  $Cl_{th}$  of the specimens without inhibitor and AN inhibitor.

**Table 5.1 Chloride threshold of QST steel embedded in cementitious systems with and without CIAs**

Specimen Number	Cl <sub>th</sub> of steel in mortar		
	Without inhibitor (W/O)	Anodic Inhibitor (AN)	Bipolar inhibitor (BP)
1	0.40	1.01	1.83
2	0.58	1.39	2.12
3	0.96	1.83	2.56
4	1.14	1.90	1.34
5	1.83	1.39	1.38
6	0.83	1.12	1.76
7	1.58	–	2.89
8	1.01	1.45	2.58
9	1.86	0.97	–
10	0.97	1.27	1.16
Equivalent normal distribution, ~N( $\mu$ , $\sigma$ )	~N(1.12, 0.5)	~N(1.4, 0.33)	~N(2, 0.6)

### 5.4.3 Duration of mACT testing for systems with and without CIAs

Figure 5.12 shows the exposure period (after 28 days of curing) required for specimens to initiate corrosion on the QST steel when embedded in cementitious systems with different CIAs. The mACT specimens without inhibitor took about 28 days to initiate corrosion. The mACT specimens with AN and BP took an average of 42 and 54 days, respectively, to initiate corrosion. Based on these results, it can be concluded that the average time required to initiate corrosion will be around 70 days. It indicates that the total time (including specimen preparation, casting, curing, etc.) to determine the Cl<sub>th</sub> using the developed mACT test method could be around 4 months. Therefore, the mACT test method could be preferred to other long term test methods, if it is required to determine Cl<sub>th</sub> of systems with new steel and CIAs and estimate service life during the planning and design stage itself.

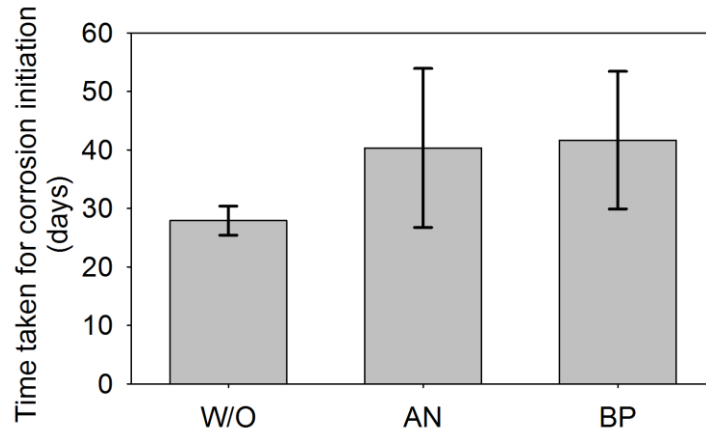


**Figure 5.12 Exposure period required to initiate corrosion in QST steel**

#### 5.4.4 Practical application of the mACT

The main focus of this study is to facilitate the assessment of the effect of CIAs in increasing the overall service life of structures by increasing the corrosion initiation period ( $t_i$ ). In the present study,  $t_i$  for a reinforced concrete column made of OPC concrete ( $w/b = 0.5$ ) with a cover depth of 50 mm and different CIAs are estimated using Life-365<sup>TM</sup> software program. The  $Cl_{th}$  values for systems with different CIAs determined using the mACT test method were used. The chloride diffusion coefficient of concrete was assumed to be  $3 \times 10^{-12} \text{ m}^2/\text{s}$  (considered for typical concrete) exposed to marine splash zone. The probability density functions (PDFs) of the  $t_i$  for the three systems (W/O, AN, and BP inhibitors) are shown in Figure 5.13. The vertical lines within each PDF indicate the median of the estimated  $t_i$  [denoted as  $M(t_i)$ ]. The systems without inhibitors may exhibit an  $M(t_i)$  of 19 years, whereas the systems with AN and BP inhibitors could exhibit an  $M(t_i)$  of 25 and 34 years, respectively. Also, note that the scatter of the PDF for the cases with anodic and bipolar inhibitors is larger than that of the case without inhibitor. This is because the LIFE 365<sup>TM</sup> software program assumes a constant Coefficient of Variation of 0.2 for the chloride threshold. This indicates that the larger the chloride threshold, the larger will be the standard deviation. Hence, the scatter of the PDF is more in the case of cases with larger chloride threshold. Also, this is expected in reality. Thus, it may be concluded that the use of AN and BP inhibitors can delay the  $M(t_i)$  by about 1.5 and 2 times, respectively, when compared to a system without any CIAs.

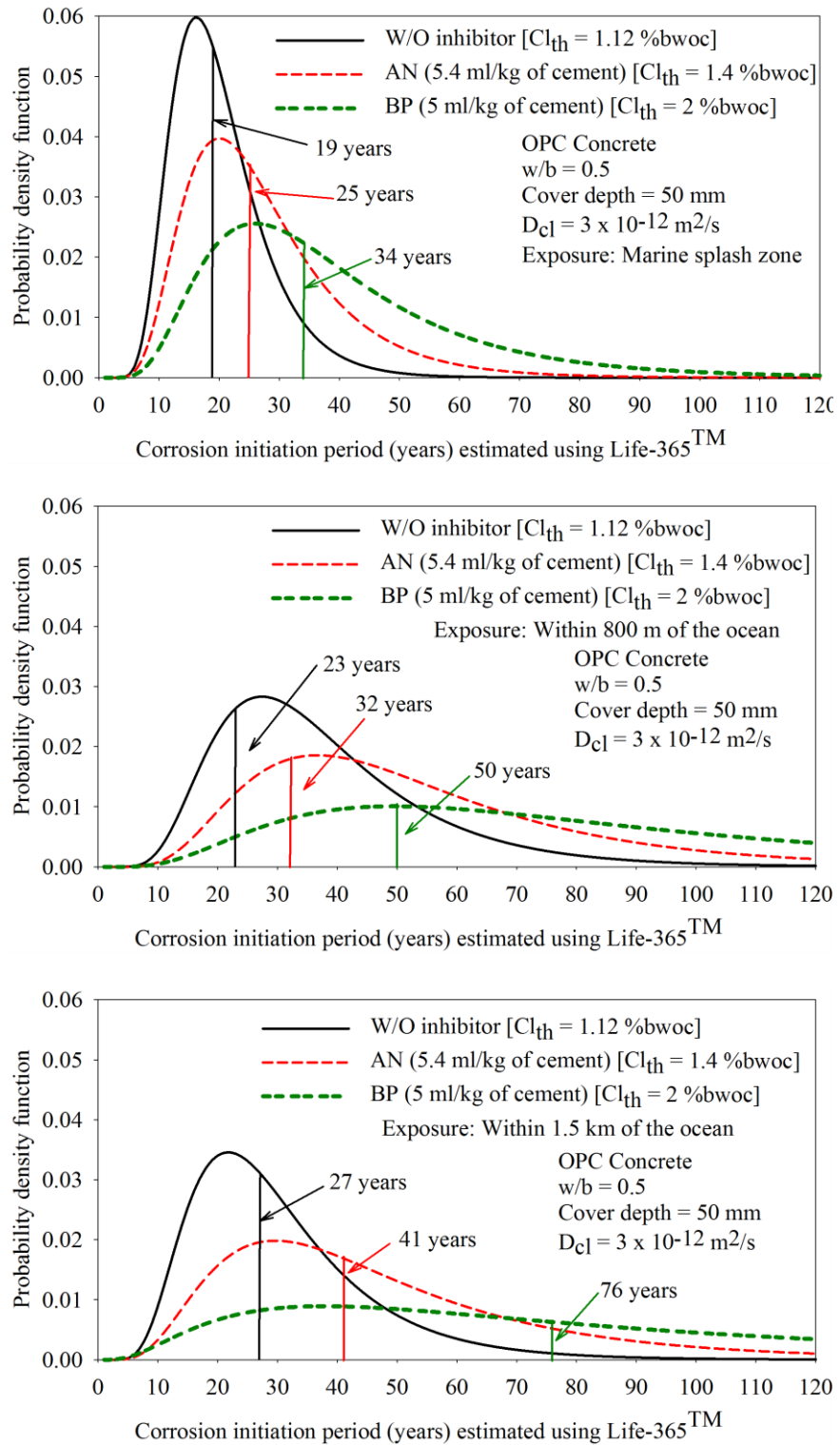


**Figure 5.13 Effect of CIAs on  $t_i$  of concrete with  $D_{cl} = 3 \times 10^{-12} m^2/s$  and located at (a) marine splash zone, (b) within 800 m from the ocean, and (c) within 1.5 km from the ocean**

Similarly, the  $M(t_i)$  was estimated for a structure with different CIA's located at around 800 m and 1.5 km from the ocean. Figure 5.13 (b) shows the  $M(t_i)$  of a typical structure with W/O, AN, and BP inhibitors located at around 800 m may have the  $M(t_i)$  as 23, 32, and 50 years respectively.

Figure 5.3 (c) shows that the  $M(t_i)$  of a typical structure with W/O, AN, and BP inhibitors located at around 1.5 km may have the  $M(t_i)$  as 27, 41, and 76 years respectively. This clearly shows that the surface concentration of chloride plays a major role in reducing the service life of a structure. Thus, a good quality cover concrete and a corrosion resistance steel will increase the service life of structure for 1.5 to 2 times. Similarly, the  $M(t_i)$  was estimated for a structure with different CIA's located at around 800 m and 1.5 km from the ocean by assuming the  $D_{cl}$  of concrete as  $2 \times 10^{-12} \text{ m}^2/\text{s}$ .

Figure 5.14 (a) shows the  $M(t_i)$  of a typical structure with W/O, AN, and BP inhibitors located at marine splash may have the  $M(t_i)$  as 28, 37, 51 years respectively. Figure 5.14 (b) shows the  $M(t_i)$  of a typical structure with W/O, AN, and BP inhibitors located at around 800 m may have the  $M(t_i)$  as 34, 48, and 75 years respectively. Figure 5.14 (c) shows the  $M(t_i)$  of a typical structure with W/O, AN, and BP inhibitors located at around 1.5 km may have the  $M(t_i)$  as 41, 62, and 114 years respectively. This clearly shows that the surface concentration of chloride plays a major role in reducing the service life of a structure. Thus, a good quality cover concrete and a corrosion resistance steel will increase the service life of structure for 2 to 3 times.

As discussed earlier,  $D_{cl}$  and  $Cl_{th}$  are two major parameters for influencing the corrosion the initiation period. From the results shown in Figure 5.13 and Figure 5.14, where the location of the structure is similar but with the change in the  $D_{cl}$  improves the service life by 1.5 to 2 times. Thus, it gives a clear insight to the practicing engineers about the importance of quality of the cover concrete and the use of effective corrosion inhibitors to delay the corrosion initiation and to enhance the overall service life of the structures.

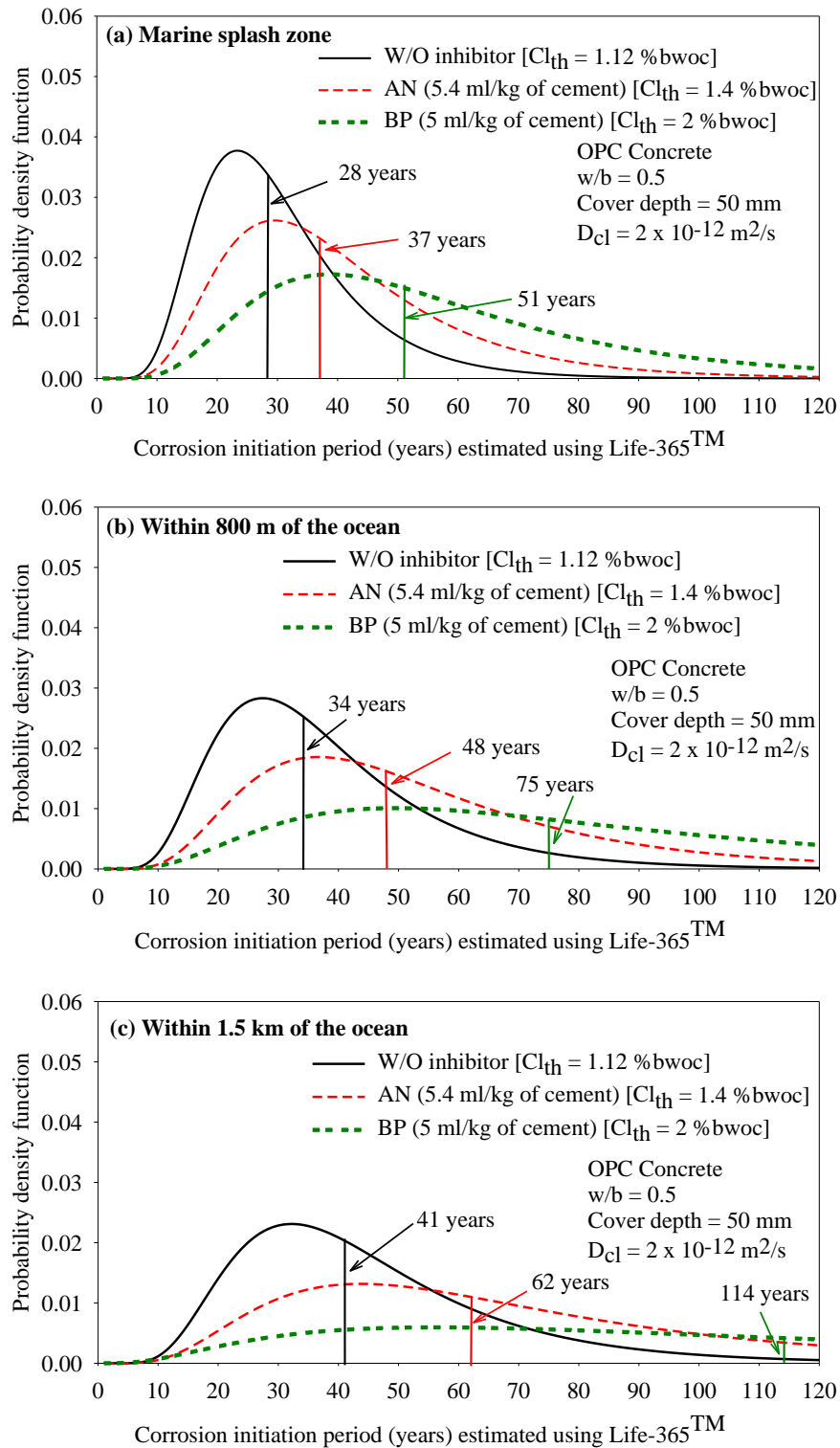


**Figure 5.14** Effect of CIAs on  $t_i$  of concrete with  $D_{Cl} = 2 \times 10^{-12} \text{ m}^2/\text{s}$  and located at (a) marine splash zone, (b) within 800 m from the ocean, and (c) within 1.5 km from the ocean

**Table 5.2  $t_i$  (years) for systems with CIAs Chloride threshold of QST steel embedded in cementitious systems with and without CIAs**

	$D_{cl} = 3 \times 10^{-12} \text{ m}^2/\text{s}$					$D_{cl} = 2 \times 10^{-12} \text{ m}^2/\text{s}$				
	$t_i$ (years)			Increase in $t_i$ wrt W/O (Fraction)		$t_i$ (years)			Increase in $t_i$ wrt W/O (Fraction)	
Exposure from sea	W/O	AN	BP	AN	BP	W/O	AN	BP	AN	BP
Marine splash zone	19	25	34	1.3	1.8	28	37	51	1.3	1.8
800 m away	23	32	50	1.4	2.2	34	48	62	1.4	1.8
1.5 km away	27	41	76	1.5	2.8	51	75	114	1.5	2.2

Table 5.2 shows the summary of the  $t_i$  estimated for system exposed to different marine exposure. The structures with a cementitious system containing AN and BP may have around 1.5 and 2 times more  $t_i$  when compared to the structures with the cementitious system without inhibitors.

#### 5.4.5 Limitations of the mACT test method

Following are some of the major limitations of the mACT test method.

**Specimen size:** The length of steel specimen used for the study is only 20 mm. Such a small specimen may not sometimes allow sufficient cathodic area to be developed to sustain the active corrosion. This could lead to a longer time for corrosion initiation and the subsequent active corrosion rates could be lower (Angst et al. 2009). However, note that this test adopts repeated measurements of instantaneous corrosion rates on same

specimen (similar to a typical metallographic specimen) and statistical comparison to detect if there are any statistically significant changes. Therefore, the results may still be reasonable. Further studies are required to quantify the effect of the specimen size and electrode configuration.

**Specimen preparation:** It is very crucial to ensure that the distance between the electrodes in the 3-electrode mACT specimen is maintained as prescribed. This requires a delicate, careful, and meticulous approach of casting the specimen. Also, the epoxy used for coating the side faces of the steel specimen must be very good and resistant to the alkaline environment - so that the chances of under film/crevice corrosion is minimal.

**Test procedure:** The mACT procedure detects the corrosion initiation by conducting the repeated LPR tests followed by a statistical approach. The data analysis involved in this process may be complex for some technicians.

**Application:** The determined  $Cl_{th}$  might be suitable only for the structures experiencing high moisture conditions (say, submerged or saturated conditions). The direct application of the results to other moisture conditions may be appropriate. However, Frederickson (1996) provides useful information for such extrapolations.

The mACT procedure detects the corrosion initiation by conducting the repeated LPR tests followed by a statistical approach may seem to be complex for some technicians.

#### 5.4.6 Summary of test results (Objective 3)

- The specimens with anodic and bipolar inhibitors exhibited  $Cl_{th}$  of 1.4 and 2 %bwoc, respectively. Based on this, it can be concluded that the use of CIAs can potentially delay the onset of corrosion in concrete structures in immersed conditions.
- The use of anodic and bipolar CIAs can delay the corrosion initiation by about two and three times, respectively, when compared to that of steel embedded in the cementitious system without any corrosion inhibitor.

## 5.5 OBJECTIVE 4: DETERMINATION OF CORROSION RATES OF DIFFERENT STEELS

Most of the reinforced concrete structures are built using PM, CTD, QST, and PS steel as reinforcing steel. The corrosion of reinforced concrete structures exposed to chloride environment may not be neglectable, which in turn reduces the overall service life of the structure. The corrosion propagation period ( $t_p$ ) is critical, and the corrosion rate ( $i_{\text{corr}}$ ) is one among the major influencing parameters. However, very limited information is available on  $i_{\text{corr}}$  for PM, CTD, QST, and PS steel rebars – making it difficult to estimate the service life. Current practice is to assume similar  $i_{\text{corr}}$  for PM, CTD, QST, and PS steel, which may give erroneous estimations of service life. This section provides experimental data and its statistical distributions of  $i_{\text{corr}}$  of PM, CTD, QST, and PS steel bars.

### 5.5.1 Corrosion rate of different steels in laboratory

As mentioned earlier, this study focuses only on  $t_p$ , which mainly depends on the  $i_{\text{corr}}$  of embedded steel reinforcement embedded in mortar. Figure 5.15 shows the average open circuit potential (OCP) of PM, CTD, QST, and PS steel reinforcement measured until 33<sup>rd</sup> month. After two months of exposure, corrosion potential ( $E_{\text{corr}}$ ) values are more negative than -276 mV vs SCE (equivalent to -350 mV versus Cu/CuSO<sub>4</sub> electrode) and exhibits a significant reduction in OCP when compared to initial readings. This indicates that the specimens are possibly experiencing ‘active’ corrosion. This also indicates that the chlorides took about 2 months to penetrate through the mortar cover of 12 mm and reach steel surface. By this time, the passive layer could have formed. Also, all the steels exhibit similar OCP values. Figure 5.16 shows the average  $i_{\text{corr}}$  of the different steels exposed to chloride environment. After 5 months of exposure, the  $i_{\text{corr}}$  of steel specimens started showing huge scatter in the measured  $i_{\text{corr}}$ . This phenomenon is due to the failure of the epoxy coating provided at the bottom portion of the steel bar. Later, the specimens were repaired as described in Section 4.5.3 and the corrosion testing was resumed from 18<sup>th</sup> month onwards and continued until 33 months. At the end of 33 months of exposure, corrosion stains were visible on the surface of test specimens. However, they did not exhibit cracking – even with severe corrosion. The probable reasoning could be as follows. The overall/effective permeability of concrete could be less than that of mortar with similar paste quality; due to the presence of impermeable

coarse aggregates occupying about 70% of volume. In the case of test specimens, the corrosion products could easily permeate through the relatively more permeable 12 mm thick mortar cover without building up the expansive pressure and cracking. Although the pressure built-up and eventual cracking mechanisms (in the bulk cover material) are different in the steel-mortar and steel-concrete systems, the corrosion rate (an interface property) from steel-mortar systems can be used for estimating the corrosion propagation time in steel-concrete systems.

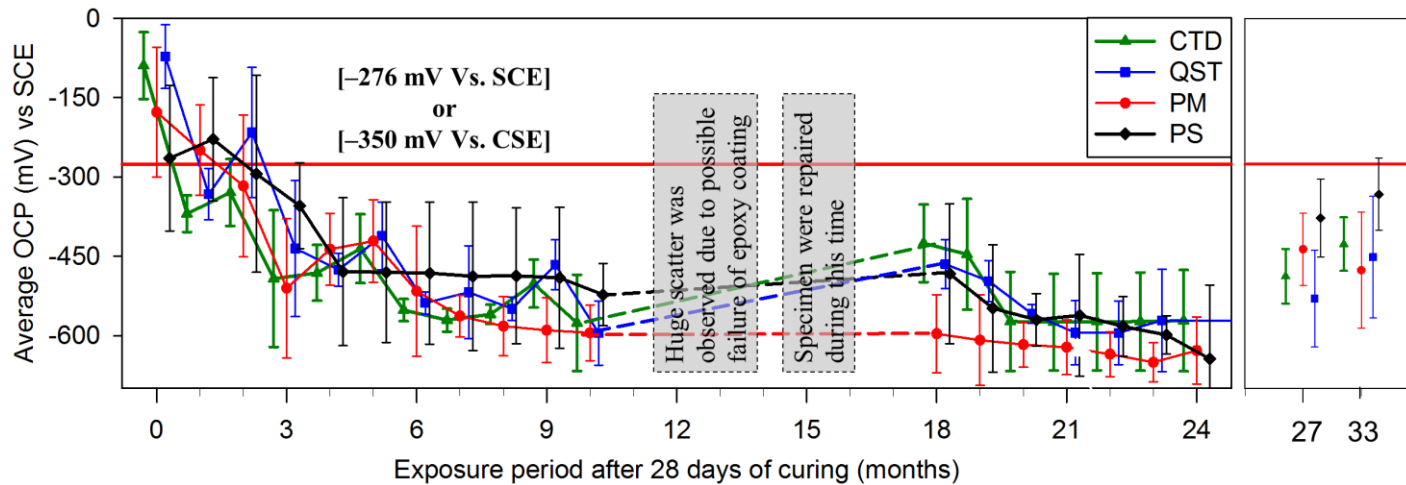


Figure 5.15 Average corrosion potential of PM, CTD, QST, and PS steel

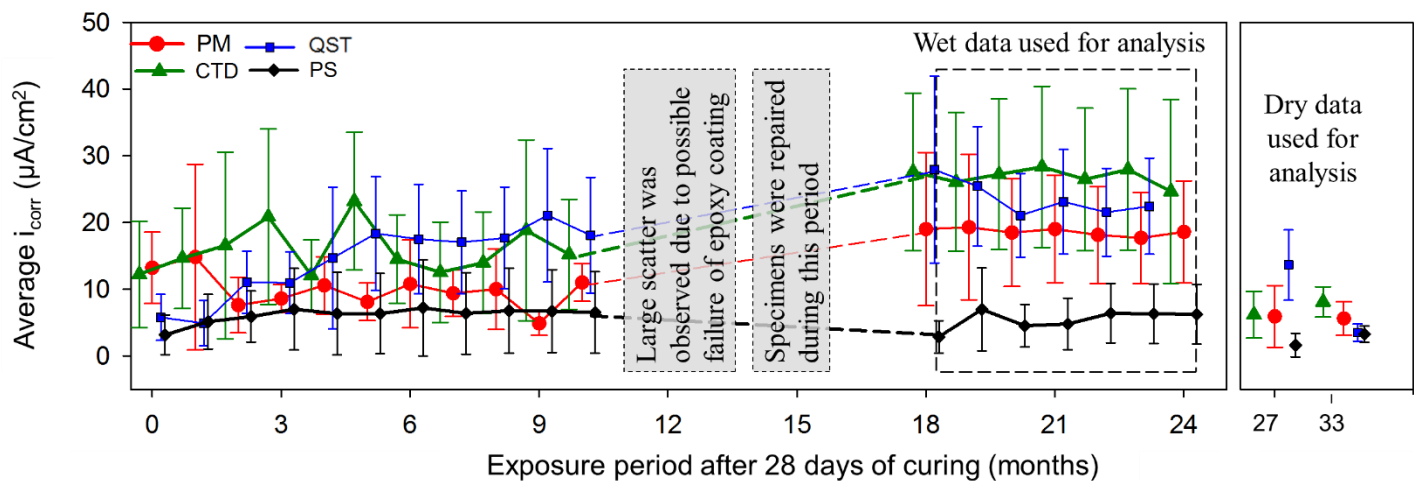
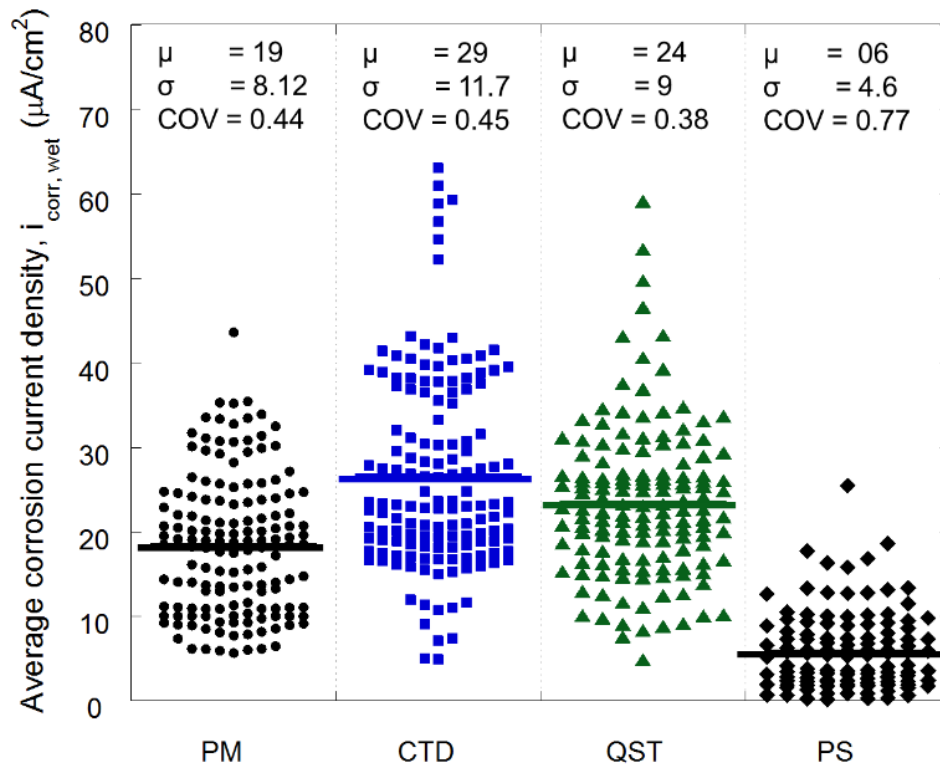


Figure 5.16 Average corrosion current density of PM, CTD, QST, and PS steel

### 5.5.1.1 $i_{corr, wet}$ measurements

Figure 5.17 shows the dot plot of the measured  $i_{corr, wet}$  of PM, CTD, QST, and PS steel reinforcement measured at the end of each wet period during cyclic wet-dry exposure from 19<sup>th</sup> to 24<sup>th</sup> month.



**Figure 5.17 Average  $i_{corr, wet}$  of various steels measured**

The average  $i_{corr, wet}$  of PM steel reinforcement is about 19  $\mu\text{A}/\text{cm}^2$  with a coefficient of variation (COV) of 0.44. The  $i_{corr, wet}$  data obtained for CTD steel reinforcement exhibited huge scatter with a mean of 29  $\mu\text{A}/\text{cm}^2$  and COV of 0.44. The  $i_{corr, wet}$  data obtained for QST steel reinforcement exhibited a mean value of 24  $\mu\text{A}/\text{cm}^2$  and COV of 0.38. Similarly, the PS steel reinforcement showed the average  $i_{corr, wet}$  of 6  $\mu\text{A}/\text{cm}^2$  and COV of 0.77. The results showed higher  $i_{corr, wet}$  values when compared to the value reported in the literature. However, the average  $i_{corr}$  in the real structure would be different from the instantaneous corrosion rate measured in the severe laboratory conditions. Thus, the weighted average annual corrosion rate

( $i_{\text{corr, annual}}$ ) is taken into consideration during the estimation of  $t_p$ , later in this thesis (See Section 5.5.2).

### 5.5.1.2 $i_{\text{corr, dry}}$ measurements

Figure 5.18 shows the dot plot of the measured  $i_{\text{corr, dry}}$  of PM, CTD, QST, and PS steel reinforcement. The average  $i_{\text{corr, dry}}$  of PM steel reinforcement is about  $5.8 \mu\text{A}/\text{cm}^2$  with a COV of 0.63. The  $i_{\text{corr, dry}}$  data obtained for CTD steel reinforcement exhibited huge scatter with a mean of  $7 \mu\text{A}/\text{cm}^2$  and COV of 0.4. The  $i_{\text{corr, dry}}$  data obtained for QST steel reinforcement exhibited a mean value of  $8.6 \mu\text{A}/\text{cm}^2$  and COV of 0.73. Similarly, the PS steel reinforcement showed the average  $i_{\text{corr, dry}}$  of  $2.5 \mu\text{A}/\text{cm}^2$  with COV of 0.7. In short, the  $i_{\text{corr, wet}}$  is  $\sim 2.5$  times higher than the average of  $i_{\text{corr, dry}}$  for QST and PS steel reinforcement. Similarly, the average  $i_{\text{corr, wet}}$  is  $\sim 3$  and 4 times higher than  $i_{\text{corr, dry}}$  for PM and CTD steel reinforcement, respectively.

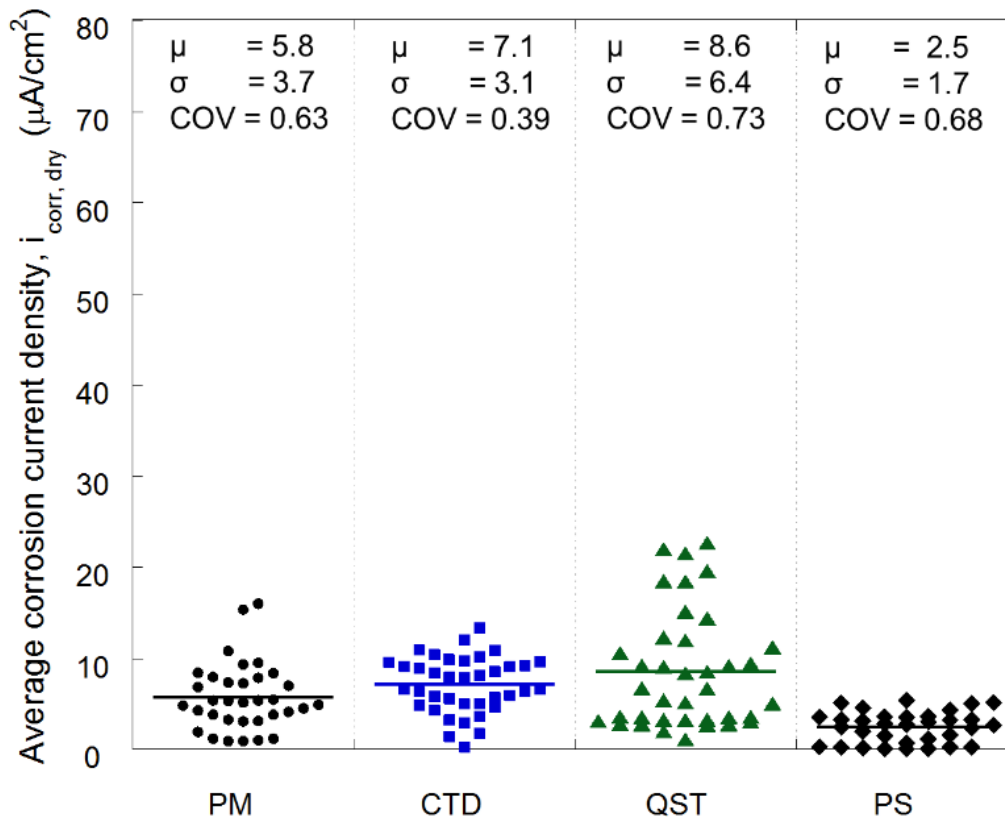


Figure 5.18 Average  $i_{\text{corr, dry}}$  of various steels measured

The CTD steel reinforcement experienced higher average corrosion rates than QST steel reinforcement. This may be because the CTD steel reinforcement is strain-hardened or cold-twisted during the manufacturing process to increase the yield strength. This process can lead to residual stresses and surface defects (at microstructure level), which can lead to corrosion when exposed to aggressive environments. The PM and PS steel reinforcement have smooth surfaces (i.e., without any ribs), and no residual stresses at the surface. Hence, they show less  $i_{\text{corr}}$  when compared to other steels. The difference in chemical composition may be another reason for the low corrosion rate.

### 5.5.2 Average annual corrosion rate in the field

In the current test program,  $i_{\text{corr}}$  data was measured at the end of each wet cycle followed by a dry period measurement. The  $i_{\text{corr}}$  at field conditions can vary as a function of the length of the annual rainy/sunny seasons (i.e., wet and dry periods). By considering the seasonal effects,  $i_{\text{corr, wet}}$ , and  $i_{\text{corr, dry}}$ , the weighted average of annual corrosion rate ( $i_{\text{corr, annual}}$ ) is calculated as given in Eq. 5.1 (IRC SP: 60-2002),

$$i_{\text{corr, annual}} = \alpha \times i_{\text{corr, wet}} + (1 - \alpha) \times i_{\text{corr, dry}} \quad \text{Eq. 5.1}$$

where,  $i_{\text{corr, annual}}$  = weighted average annual corrosion rate,  $i_{\text{corr, wet}}$  = corrosion rate in wet conditions,  $i_{\text{corr, dry}}$  = corrosion rate in dry conditions,  $\alpha$  = ratio of the duration of the rainy-to-summer season per year. The  $t_p$  estimated based on the  $i_{\text{corr, annual}}$  may better represent the corrosion propagation mechanism that occurs in field conditions.

### 5.5.3 Statistical distributions of corrosion rate of different steels

For simulation purpose,  $i_{\text{corr}}$  should be treated as a positive real number. Hence, choosing a normal distribution for the  $i_{\text{corr}}$  is mathematically incorrect. This is because the random data generated using a normal distribution might have negative numbers and can cause mathematical difficulties during simulation studies (Detwiler et al., 1999). Also, Shapiro-Wilkinson normality tests on the  $i_{\text{corr, wet}}$  and  $i_{\text{corr, dry}}$  data sets for PM, CTD, QST, and PS steel reinforcement concluded that the data sets do not follow a normal distribution. To find

appropriate statistical distributions, the software package EasyFit<sup>®</sup> was used. Based on the Kolmogorov-Smirnov (K-S) Goodness of Fit test (see Table 5.3), the data sets were ranked with different statistical distributions that are commonly used (e.g., Gaussian, Weibull, Gamma, Normal, and Lognormal).

**Table 5.3 Goodness of fit for  $i_{corr}$  of PM, CTD, QST, and PS steel reinforcement exposed from 19 to 24 month of wet data and 27<sup>th</sup> and 33<sup>rd</sup> month dry data**

	$i_{corr, wet}$				$i_{corr, dry}$			
	PM	CTD	QST	PS	PM	CTD	QST	PS
<b>Normal</b>	4	7	7	7	6	2	7	1
<b>Lognormal</b>	7	1	5	6	5	6	5	7
<b>Lognormal (3P)</b>	2	3	2	5	1	3	3	2
<b>Weibull</b>	1	6	4	3	3	7	4	3
<b>Weibull (3P)</b>	3	5	6	1	4	1	2	4
<b>Gamma</b>	5	2	1	2	2	5	6	5
<b>Gamma (3P)</b>	6	4	3	4	7	4	1	6

The measured  $i_{corr, wet}$  data for PM, CTD, QST, and PS steel reinforcement fit well with Weibull, Lognormal, Gamma, and Weibull 3P distributions, respectively. Similarly, for  $i_{corr, dry}$  data for PM, CTD, QST, and PS steel reinforcement fit well with Lognormal 3P, Weibull 3P, Gamma, and Normal distributions, respectively. Figure 5.19 (a) and (b) shows the histograms and the probability density functions (PDFs) for  $i_{corr, wet}$  and  $i_{corr, dry}$ , respectively of PM, CTD, QST, and PS steel reinforcement. Table 5.4 and Table 5.5 show the statistical parameters for  $i_{corr, wet}$  and  $i_{corr, dry}$  arrived for each steel type. A significant difference is observed between the  $i_{corr, wet}$ , and  $i_{corr, dry}$ . The variation in the type of distribution and the change in the statistical parameters clearly shows that the use of same corrosion rate and considering a normal distribution for all the steel types will lead to in erroneous estimation of  $t_p$ .

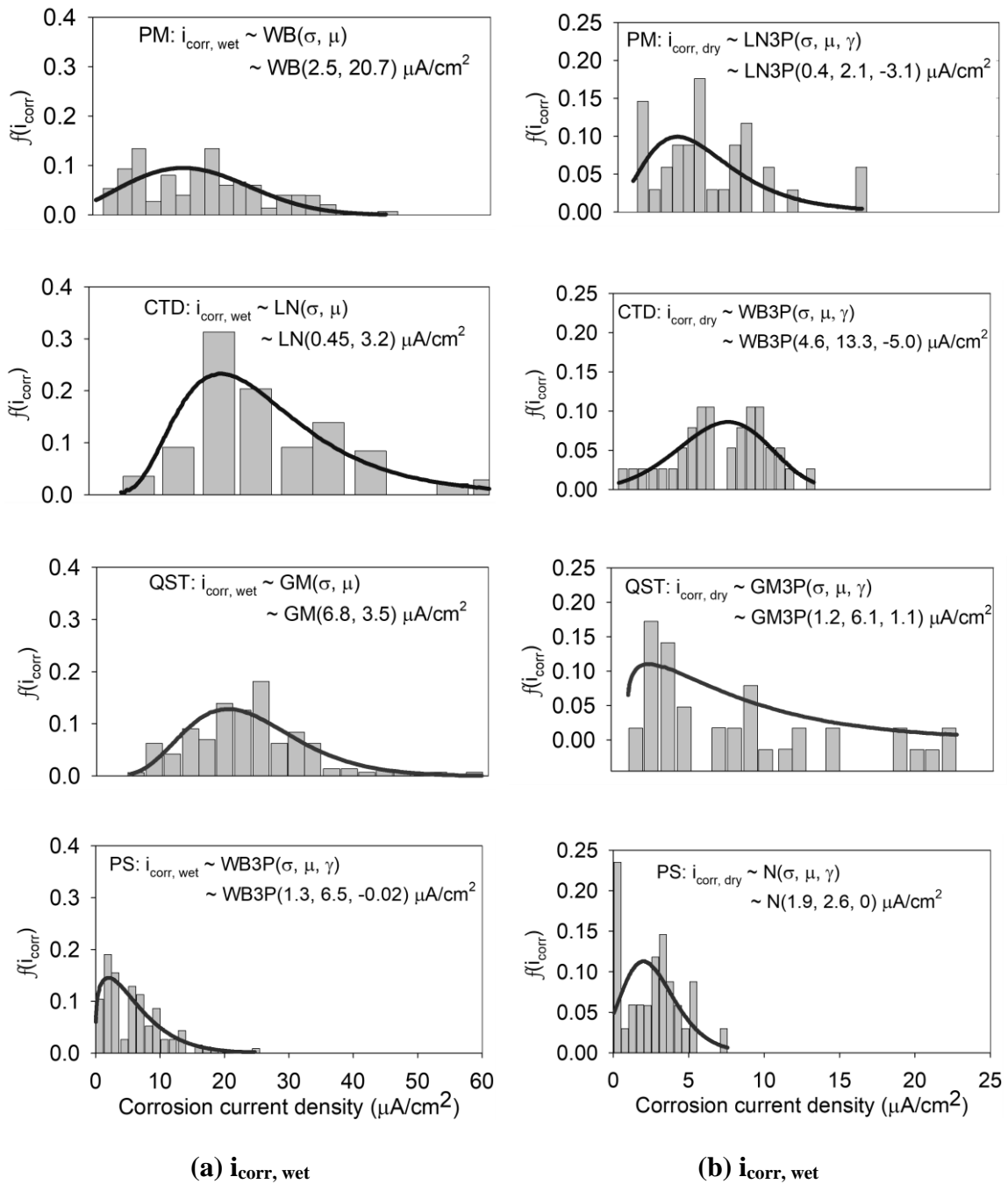


**Figure 5.19 Distributions for  $i_{\text{corr, wet}}$  and  $i_{\text{corr, dry}}$  of various steel reinforcement**

**Table 5.4 Summary of  $i_{\text{corr, wet}}$  distributions based on the corrosion rate of different steel reinforcement**

Steel type	Distribution type (D)	Parameter $\sim D (\sigma, \mu, \gamma)$ in $\mu\text{A}/\text{cm}^2$
PM	Weibull	$\sim\text{WB} (2.5, 20.7, 0)$
CTD	Lognormal	$\sim\text{LN} (0.45, 3.2, 0)$
QST	Gamma	$\sim\text{GM} (6.8, 3.5, 0)$
PS	Weibull (3P)	$\sim\text{WB3P} (1.3, 6.5, -0.02)$

**Table 5.5. Summary of  $i_{\text{corr, dry}}$  distributions based on the corrosion rate of different steel reinforcement**

Steel type	Distribution type (D)	Parameter $\sim D (\sigma, \mu, \gamma)$ in $\mu\text{A}/\text{cm}^2$
PM	Lognormal (3P)	$\sim\text{LN3P} (0.4, 2.1, -3.1)$
CTD	Weibull (3P)	$\sim\text{WB3P} (4.6, 13.3, -5)$
QST	Gamma (3P)	$\sim\text{GM3P} (1.2, 6.1, 1.1)$
PS	Normal	$\sim\text{N} (1.9, 2.6, 0)$

#### 5.5.4 Probabilistic estimation of $t_p$ to initiate crack in cover concrete

As mentioned earlier in Table 2.4, Wang and Zhao (1993) considered the  $i_{\text{corr, cover depth}} (C_v)$ , and compressive strength ( $f_{cu}$ ) of concrete as the major influencing parameters to estimate  $t_p$ . In this analysis, the statistical distributions of  $i_{\text{corr, annual}}$  for different steel was used which, was calculated from  $i_{\text{corr, wet}}$  and  $i_{\text{corr, dry}}$  using Eq. 5.1. The specimens did not exhibit crack during the exposure period of about 33 months. However, few rust stains are observed. The probable reason for this could be as follows. The overall/effective permeability of concrete can be less than that of mortar with similar paste quality; due to the presence of impermeable coarse aggregates occupying about 70% of volume. In the case of test specimens, the corrosion

products could easily permeate through the 12 mm thick mortar cover without building up the expansive pressure and cracking. Thus, for a parametric study, a concrete element was assumed and the input parameters required for Wang and Zhao (1993) model as listed in in Table 5.6. The  $t_p$  for concrete systems with different steel reinforcement was estimated using the model by Wang and Zhao (1993). A typical south Indian climate, in which one year can be divided into three months of wet season and nine months of dry season is considered for this parametric study. Figure 5.20 shows the probability density function (PDF) of  $t_p$  obtained for the systems with PM, CTD, QST, and PS steel reinforcement. The  $t_p$  for concrete systems with different steel reinforcement was estimated using the model by Wang and Zhao (1993).

**Table 5.6 Parameters considered for estimating  $t_i$  using Wang and Zhao (1993)**

<b>Parameters</b>	<b>Unit</b>	<b>Value</b>
Cover depth ( $C_v$ )	mm	50
Compressive strength of concrete ( $f_{cu}$ )	MPa	30
Initial steel diameter (D)	mm	16 for PM, CTD, QST 5.2 for PS
Equivalent weight of steel (W)	g	27.92
Faraday's constant (F)	Coulombs	96500
Density of steel ( $\rho_{st}$ )	gm/cm <sup>3</sup>	7.85
Crack expansion coefficient of concrete ( $\gamma$ )		3.02

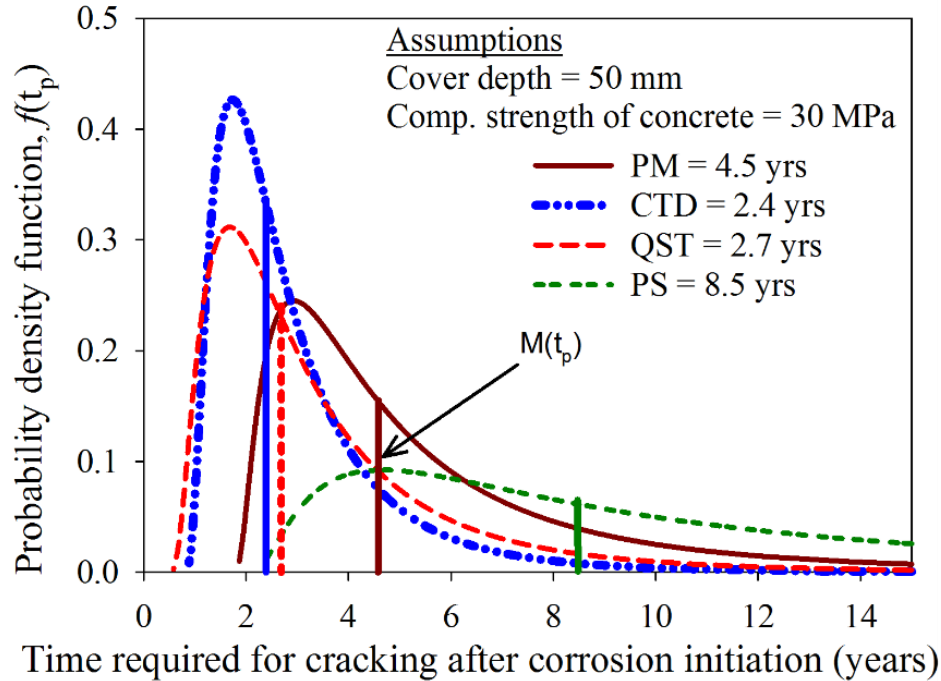


**Figure 5.20** Estimated crack initiation period based on  $i_{\text{corr, annual}}$

The annual monsoon is taken for a typical south Indian climatic conditions, in which one year can be divided into three months of wet season, and nine months of dry season. Note that these PDFs are skewed rightward. For skewed distributions, the *median* is a better statistic than the *mean or average* and the vertical lines within the PDF curves indicate the *median* values, which are herein denoted as  $M(t_p)$ . The model by Wang and Zhao (1993) estimates that the  $M(t_p)$  for concrete structures with PM, CTD, QST, and PS steel reinforcement are 4.5, 2.4, 2.7, and 8.5 years respectively.

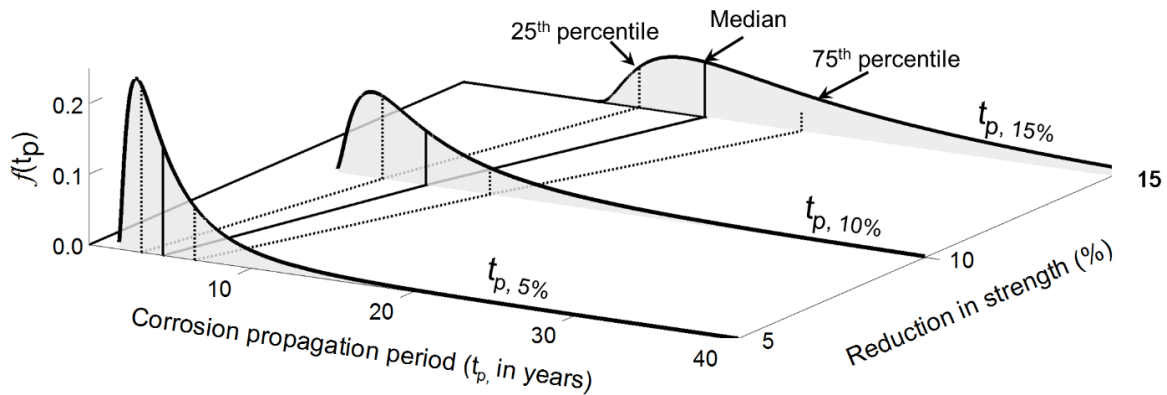
### 5.5.5 Probabilistic estimation of $t_p$ for varying reduction in cross-sectional area ( $t_p, \Delta\%$ )

In RC structures, when the loss in the cross-sectional area of steel reinforcement exceeds  $\approx 10\%$  of the nominal cross-sectional area, the structure may reach an unsafe level, and major repair/replacement of steel is exercised. That is, 10 % loss in cross-sectional area is approximately equal to 10 % reduction in tensile strength of steel rebars. When such a state is reached, repair/rehabilitation/retrofitting work is recommended because of the limited safety margins. Thus, the reduction in  $t_p$  with the corresponding percent reduction in the cross-

sectional area ( $\Delta\%$ ) of the rebar is studied and represented as  $t_{p, \Delta\%}$ . The study was conducted for  $\Delta\%$  of 5, 10, and 15 % and the PDF for the four steel were developed

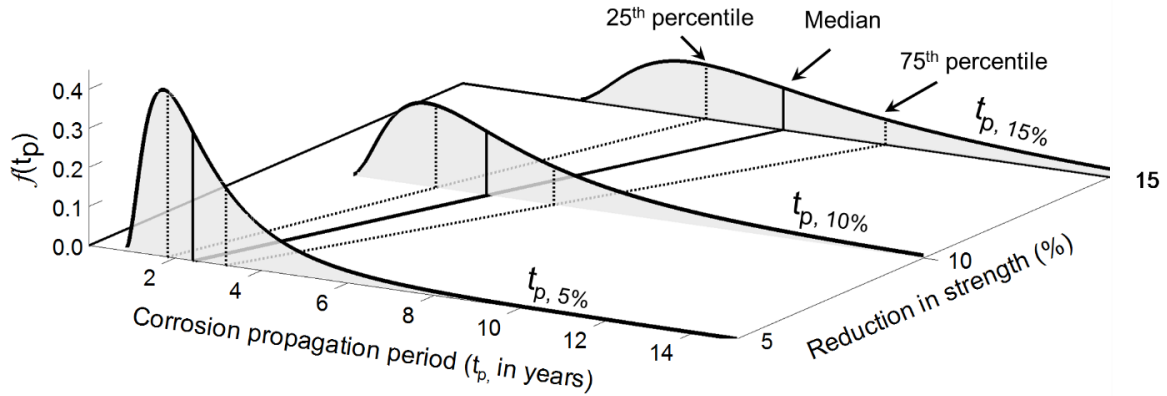
Once the crack is initiated, the rate of corrosion propagation may vary significantly, as the availability of moisture, oxygen is expected to be high. However, in this thesis, the  $t_{p, 5\%}$ ,  $t_{p, 10\%}$ , and  $t_{p, 15\%}$  was estimated using Eq. 2.12 (Andrade et al., 1989) by assuming a linear corrosion propagation mechanism and constant  $i_{\text{corr, annual}}$  determined from  $i_{\text{corr, wet}}$  and  $i_{\text{corr, dry}}$  using Eq.4. Figure 5.21 to Figure 5.24 shows the probability of  $M(t_{p, 5\%})$ ,  $M(t_{p, 10\%})$ , and  $M(t_{p, 15\%})$  for different steel reinforcement after the corrosion initiation. In the PDFs, the vertical solid line from the abscissa denotes the median (50<sup>th</sup> percentile), which is  $M(t_p)$  and the dotted vertical lines along the left and right side of the solid line denotes the 25<sup>th</sup> percentile and 75<sup>th</sup> percentile respectively of the estimated corrosion propagation period.

Figure 5.21 shows the probability of  $M(t_{p, 5\%})$ ,  $M(t_{p, 10\%})$ , and  $M(t_{p, 15\%})$  for PM steel reinforcement after the corrosion initiation. Based on the probabilistic estimation, the  $M(t_{p, 5\%})$ ,  $(t_{p, 10\%})$ , and  $M(t_{p, 15\%})$  for a concrete system with PM steel is about 4.5, 9, and 15 years, respectively.



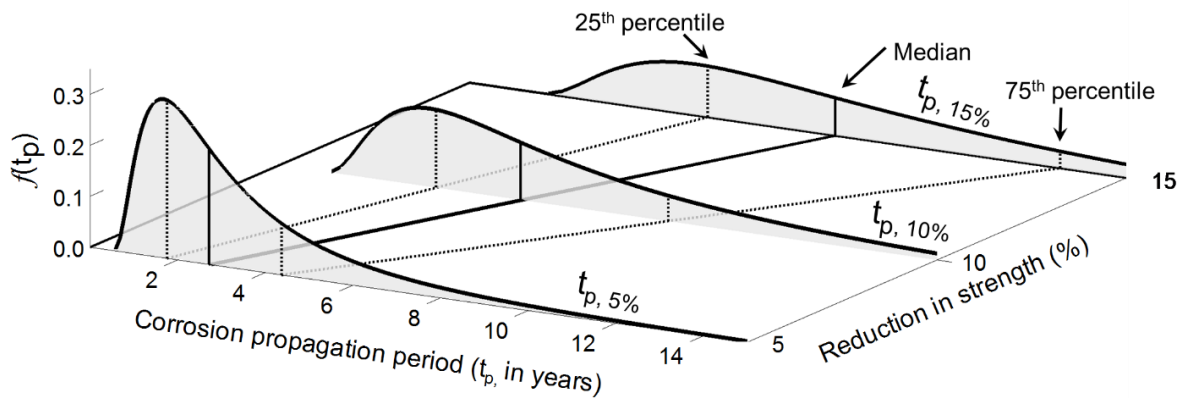
**Figure 5.21  $t_{p, 5\%}$ ,  $t_{p, 10\%}$ , and  $t_{p, 15\%}$  loss in PM steel rebar w.r.t. exposure period**

Figure 5.22 shows the probability of  $M(t_{p, 5\%})$ ,  $M(t_{p, 10\%})$ , and  $M(t_{p, 15\%})$  for CTD steel reinforcement after the corrosion initiation. The concrete system with CTD steel reinforcement may have  $M(t_{p, 5\%})$ ,  $M(t_{p, 10\%})$ , and  $M(t_{p, 15\%})$  as 2.5, 5, and 7.5 years respectively.



**Figure 5.22.  $t_{p, 5\%}$ ,  $t_{p, 10\%}$ , and  $t_{p, 15\%}$  loss in CTD steel rebar w.r.t. exposure period**

The concrete system with QST steel may have  $M(t_{p, 5\%})$ ,  $M(t_{p, 10\%})$ , and  $M(t_{p, 15\%})$  of 3, 5.5, and 9 years, respectively as shown in Figure 5.23.



**Figure 5.23  $t_{p, 5\%}$ ,  $t_{p, 10\%}$ , and  $t_{p, 15\%}$  loss in QST steel rebar w.r.t. exposure period**

As shown in Figure 5.24, the  $M(t_{p, 5\%})$ ,  $M(t_{p, 10\%})$ , and  $M(t_{p, 15\%})$  in the concrete system with PS steel reinforcement is around 8.5, 17, and 26 years, respectively.

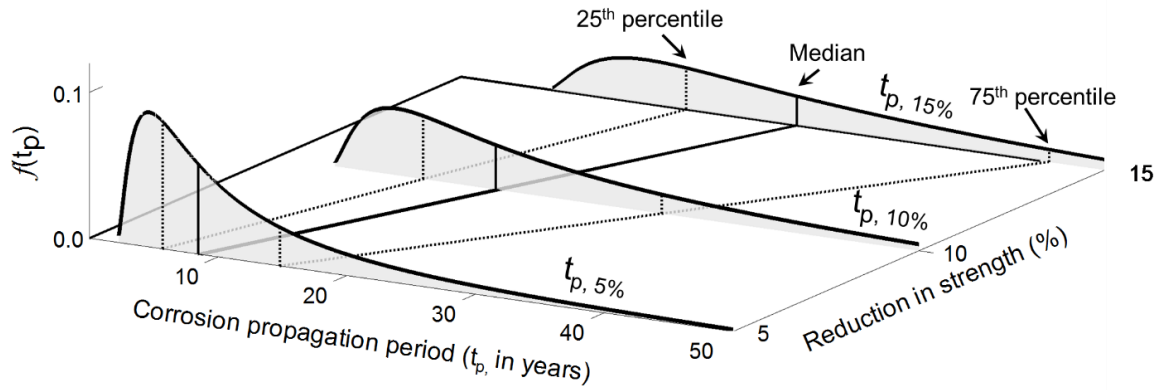


**Figure 5.24.  $t_{p, 5\%}$ ,  $t_{p, 10\%}$ , and  $t_{p, 15\%}$  loss in PS steel rebar w.r.t. exposure period**

Therefore, instead of assuming  $t_p$  as 6 years, it is recommended that the probabilistic distributions for  $i_{\text{corr, wet}}$  and  $i_{\text{corr, dry}}$  presented in this thesis and a suitable model may be used to estimate  $t_p$  for structures with different steel reinforcement.

### 5.5.6 Summary

Based on the experimental results and the corrosion propagation models discussed in this study, the following conclusions are drawn.

- When subjected to a wet cycle exposure to chloride environment, the corrosion rate,  $i_{\text{corr, wet}}$  of PM, CTD, QST and PS steel reinforcement can be statistically expressed as follows,
  1. PM: ~Weibull (2.5, 20.7, 0)  $\mu\text{A}/\text{cm}^2$
  2. CTD: ~Lognormal (0.45, 3.2, 0)  $\mu\text{A}/\text{cm}^2$
  3. QST: ~Gamma (6.8, 3.5, 0)  $\mu\text{A}/\text{cm}^2$
  4. PS: ~Weibull3P (1.3, 6.5, -0.02)  $\mu\text{A}/\text{cm}^2$
- When subjected to a dry exposure, the corrosion rate,  $i_{\text{corr, dry}}$  of PM, CTD, QST and PS steel reinforcement can be statistically expressed as follows,
  1. PM: ~Lognormal (0.4, 2.1, -3.1)  $\mu\text{A}/\text{cm}^2$
  2. CTD: ~Weibull3P (0.46, 13.3, -5)  $\mu\text{A}/\text{cm}^2$
  3. QST: ~Gamma3P (1.2, 6.1, 1.1)  $\mu\text{A}/\text{cm}^2$
  4. PS: ~Normal (1.9, 2.6, 0)  $\mu\text{A}/\text{cm}^2$
- Using the statistical distributions mentioned above and the Wang and Zhao (1993) model, the median of time required to crack the cover concrete  $M(t_p)$  is about 1.5 times higher in the case of PM and PS steel reinforcement than that in the case of CTD and QST steel reinforcement.
- Wang and Zhao (1993) model estimates 5 % reduction in cross-sectional area of steel rebar to initiate crack in the cover concrete (50 mm thick) with the compressive strength of 30 MPa
- The median of time required for 10 % reduction in tensile strength is around 1.2 times higher in PM and PS steel reinforcement than that of CTD and QST steel reinforcement embedded in the concrete structure.

The present study can help the engineers to schedule and strategize suitable repair activities to avoid severe damage and possible structural failures.



## 6 CONCLUSIONS AND FUTURE RECOMMENDATIONS

### 6.1 INTRODUCTION

The premature deterioration of reinforced concrete structures can lead to huge economical impact/burden to the society. Therefore, there is an increasing concern among the engineering community to truly enhance the service life of reinforced concrete systems. Special attention needs to be given to delay the initiation corrosion and to reduce the rate of corrosion propagation of steel reinforcement. Both these will in turn help in extending the overall service life of reinforced concrete structures. The two key parameters defining the corrosion initiation time ( $t_i$ ) and corrosion propagation period ( $t_p$ ) are chloride threshold ( $Cl_{th}$ ) and corrosion rate ( $i_{corr}$ ), respectively. Engineers are in need of the estimates of these parameters to perform material selection and schedule/estimate the maintenance operations. However, there is a lack of data base and short-term methodologies to estimate these parameters, especially for new materials systems (new types of steel reinforcement and corrosion inhibiting admixtures [CIAs]) that are being introduced into the construction market. This study has developed a test short-term test method (mACT test method) to estimate  $Cl_{th}$  for steel-cementitious systems with CIAs. This study has also developed statistical distributions for corrosion rates of various steels embedded in cementitious systems and exposed to chlorides.

For the estimation of  $Cl_{th}$ , many researchers have used external potential to reduce the test duration (by bypassing the time taken for chloride ingress) and assess the long-term performance of materials. This thesis has quantified the adverse effects of such potential application in the determination of  $Cl_{th}$ , especially for the systems with CIAs. Then, the thesis developed a more standardized, short-term test method to determine the  $Cl_{th}$  of steel embedded in cementitious systems with CIAs. This test method is named as ‘mACT’ test method. The mACT test method relies on chloride diffusion under saturated condition and uses the Linear Polarization Resistance (LPR) technique and a statistical method to detect the initiation of chloride-induced corrosion. The mACT test method takes about 3 to 4 months of testing period and can be used by engineers for determining the  $Cl_{th}$  of systems with new steels and CIAs and assess their effect on service life. This exercise can be done during the design stages and suitable materials systems can be selected on a scientific basis.

This thesis also developed statistical distributions for the rate of chloride-induced corrosion of the following steels that are used in the existing and new concrete structures.

- Plain Mild (PM)
- Cold-Twisted Deformed (CTD)
- Thermo-Mechanically Treated or Quenched & Self-Tempered (TMT/QST)
- Prestressing (PS)

These statistical distributions were developed using the corrosion rate data collected from a 33-month long chloride exposure test. The distributions for both wet and dry periods are developed, which can be used for estimating the corrosion propagation periods for structures experiencing different sunny/rainy seasons and chloride-induced corrosion. Such distributions and available corrosion propagation models can help the engineers to schedule and strategize suitable repair activities to avoid severe damage and possible structural failures.

## **6.2 CONCLUSIONS**

The specific conclusions from the present work are arranged in specific subsections

### **6.2.1 Effect of external potential on the migration of anions through mortar**

- a) The application of external potential can accelerate the movement of both chlorides and other anions in cementitious systems – leading to changes in the nitrite concentration at or near the steel-cementitious interface, which does not happen in real structures.
- b) The application of external potential for accelerating the movement of chlorides is not suitable for chloride threshold tests, especially while assessing steel-cementitious system with CIAs.

## 6.2.2 Development of mACT test method

- a) The mACT test method is developed for determining  $Cl_{th}$  of steel-cementitious systems with CIAs containing anions is developed. The time required to complete the mACT test is about 4 months. However, it should be noted that the better the inhibitors, the longer would be the test duration.
- b) The specimens without inhibitors exhibited an average  $Cl_{th}$  of about 1.12 %bwoc, which is like the range of the reported values in the literature (0.8 %bwoc). Considering the inherent variations in corrosion mechanisms and large scatter in measurements reported in the literature, it can be concluded that the mACT test method is a reasonably valid procedure.
- c) The  $Cl_{th}$  for TMT/QST steel in plain OPC cement concrete can be expressed as  $\sim N(1.12, 0.5)$  %bwoc

## 6.2.3 Chloride threshold of QST steel embedded in systems with CIAs

- a) The specimens with anodic and bipolar inhibitors exhibited an average  $Cl_{th}$  of 1.4 and 2 %bwoc, respectively.
- b) The  $Cl_{th}$  for TMT/QST steel in OPC cement concrete with calcium nitrite inhibitor (5.4 mg/l) can be statistically expressed as  $\sim N(1.4, 0.33)$  %bwoc
- c) The  $Cl_{th}$  for TMT/QST steel in OPC cement concrete with bipolar inhibitor (5 mg/l) can be statistically expressed as  $\sim N(2, 0.6)$  %bwoc
- d) For a case study with  $D_{cl}$  of  $23 \times 10^{-12} \text{ m}^2/\text{s}$ , cover depth of 50 mm, and compressive strength of 30 MPa, the use of anodic and bipolar CIAs could delay the corrosion initiation by about 1.5 and 2 times, respectively, when compared to that of steel embedded in the cementitious system without any corrosion inhibitor.
- e) Note that the results in this paper are for Portland cement mortar systems with a w/c ratio of 0.50. The times to corrosion initiation would be significantly increased for steel in concrete and for lower w/c ratios. Furthermore, the addition of supplementary cementitious materials could alter the pore solution composition and the chloride threshold, the influence of inhibitors and the time to initiate corrosion

#### 6.2.4 Corrosion rates of different steels

- a) Based on the average corrosion rate observed over a period of 24 months of cyclic wet-dry exposure using 3.5% NaCl solution, the four steels can be ranked (as per their corrosion rate) as follows:  
PS < PM < QST  $\approx$  CTD [Note: PS exhibited least corrosion rate]
- b) The specimens with similar configuration used in this study, when subjected to a wet cycle exposure to chloride environment, the corrosion rate,  $i_{\text{corr, wet}}$  of PM, CTD, QST and PS steel reinforcement can be statistically expressed as follows,
- PM:  $\sim$ Weibull (2.5, 20.7, 0)  $\mu\text{A}/\text{cm}^2$
  - CTD:  $\sim$ Lognormal (0.45, 3.2, 0)  $\mu\text{A}/\text{cm}^2$
  - QST:  $\sim$ Gamma (6.8, 3.5, 0)  $\mu\text{A}/\text{cm}^2$
  - PS:  $\sim$ Weibull3P (1.3, 6.5,  $-0.02$ )  $\mu\text{A}/\text{cm}^2$
- c) The specimens with similar configuration used in this study, when subjected to a dry exposure, the corrosion rate,  $i_{\text{corr, dry}}$  of PM, CTD, QST and PS steel reinforcement can be statistically expressed as follows,
- PM:  $\sim$ Lognormal (0.4, 2.1,  $-3.1$ )  $\mu\text{A}/\text{cm}^2$
  - CTD:  $\sim$ Weibull3P (0.46, 13.3,  $-5$ )  $\mu\text{A}/\text{cm}^2$
  - QST:  $\sim$ Gamma3P (1.2, 6.1, 1.1)  $\mu\text{A}/\text{cm}^2$
  - PS:  $\sim$ Normal (1.9, 2.6, 0)  $\mu\text{A}/\text{cm}^2$
- d) Using the statistical distributions mentioned above and the Wang and Zhao (1993) model, the median of time required to crack the cover concrete  $M(t_p)$  is about 1.5 times higher in the case of PM and PS steel reinforcement than that in the case of CTD and QST steel reinforcement.
- e) The median of time required for 10 % reduction in tensile strength is around 1.2 times higher in PM and PS steel reinforcement than that of structures with CTD and QST steel reinforcement.

The present study can help the engineers to estimate the probabilistic corrosion initiation and propagation periods (thereby overall service life), to select suitable steel and corrosion inhibitors and schedule/strategize suitable repair activities to avoid severe damage and possible structural failures.

### **6.3 RECOMMENDATIONS FOR FUTURE WORK**

- The mACT test method needs to be further simplified by modifying the specimen configuration and corrosion detection procedure.
- The effect of the dimension of steel specimen used as working electrode and the ratio of the surface areas of working electrode and counter electrode on the corrosion mechanism is necessary to study.
- Detailed investigation on the effect of ohmic drop due to the highly resistive mortar/concrete on the LPR measurements is required.
- In addition to laboratory-based corrosion testing, it is apparent that evaluation of field performance of the CIAs would be helpful for the practical applications.
- The present study is based on the submerged or continuous wetting to study the corrosion initiation behaviour. However, the corrosion initiation can happen at the interface where the wetting and drying is possible. Thus, the same experiments can be conducted on the specimens exposed to wet-dry cycles and real-time situations.
- A thorough study on the effect of corrosion inhibitor on the properties on fresh, hardened, and durability properties is required for more precise estimation of corrosion initiation period.
- The effect of the dosage of CIAs on  $Cl_{th}$  and transport properties needs to be studied.
- Effect of supplementary cementitious materials, water-binder ratio, different steel type, and other chemical admixtures on the chloride threshold need to be assessed.
- The corrosion rate in the cracked concrete needs to be studied.



## REFERENCES

- ACI 222R-01** (2010) Protection of metals in concrete against corrosion, ACI Publication, USA.
- Ahmad S.**, (2003) Reinforcement corrosion in concrete structures, its monitoring and service life prediction – A review. *Cement and Concrete Composites*, Vol. 25, pp. 459-471.
- Alexander M.G., Beushausen H., and Otieno M. B.**, (2012), “Corrosion of steel in reinforced concrete: Influence of binder type, water/binder ratio, cover and cracking”, Research monograph No.9, Concrete Materials and Structural Integrity Research Unit, Department of Civil Engineering, University of Cape Town. South Africa.
- Alonso, C., Andrade, C., Rodriguez, J., and Diez, J.M.** (1998) Factors controlling cracking of concrete affected by reinforcement corrosion. *Materials and Structures*, Vol. 31, pp., 435-441.
- Amey, S.L., Johnson, D.A., Miltenberger, M.A., and Farzam, H.** (1998) Prediction of service life of concrete marine structures: An environmental methodology. *ACI Structural Journal*, 95 (2), 205-214.
- Andrade C., Alonso C., and González J. A.** (1989) Approach to the calculation of the residual service life in corroding concrete reinforcements based on corrosion intensity values. *Proceedings of the 9<sup>th</sup> European Congress on Corrosion 89*, Utrecht, Netherlands.
- Andrade L., Alonso C., Nbova X.R., and Keddamt M.**, (1995), “The importance of geometrical considerations in the measurement of steel corrosion in concrete by means of AC Impedance”, *Corrosion Science*, vol. 37, pg. 2013-2023
- Andrade, C., Alonso, C., and Sarria, J.** (2002). Corrosion rate evolution in concrete structures exposed to the atmosphere. *Cement and Concrete Composites*, 24(1), 55-64.
- Andrade, C., and Alonso, C.** (1996) Corrosion Rate Monitoring in the Laboratory and on-site, *Construction and Building Materials*, V.10, No.5, 1996, pp.315-328.
- Andrade, C., and Rebolledo, N.** (2012). Accelerated evaluation of corrosion inhibition by means of the integral corrosion test (pp. 364–368). Cape Town.

**Andrade, C., Castelo, V., Alonso, C., and Gonzalez, J. A.** (1984). The determination of the corrosion rate of steel embedded in concrete by the polarization resistance and AC impedance methods. In Chaker, V., editor, Corrosion effect of stray currents and the techniques for evaluating corrosion of rebars in concrete, STP 906. ASTM International.

**Angst, U., Elsener, B., Larsen, C.K., and Vennesland, O,** (2009) Critical chloride threshold content in reinforced concrete – A review, *Cement and Concrete Research*, vol 39(12), pp. 1122-1138

**Ann K. Y. and Song H. W.** (2007), Chloride threshold level for corrosion of steel in concrete, *Corrosion Science*, 49 (11), 4113-4133.

**Ann K.Y., Jung H.S., Kim H.S., Kim S.S., and Moon H.Y.** (2006). Effect of calcium nitrite-based corrosion inhibitor in preventing corrosion of embedded steel in concrete, *Cement and Concrete Research* 36, pp.530 – 535.

**ASTM C192-16** (2016), Standard Practice for Making and Curing Concrete Test Specimens in the Laboratory. American Society of Testing and Materials, Conshohocken, PA, USA.

**ASTM C 876-15** (2015) Standard test method for Half-cell potentials of uncoated reinforcing steel in concrete., American Society of Testing and Materials, Conshohocken, PA, USA.

**ASTM C1202-12** (2012) Standard Test Method for Electrical Indication of Concrete's Ability to Resist Chloride Ion Penetration, American Society of Testing and Materials, 6

**ASTM C1556-16** (2016), Determining the Apparent Chloride Diffusion Coefficient of Cementitious Mixtures by Bulk Diffusion. American Society of Testing and Materials, Conshohocken, PA, USA.

**ASTM C204-16** (2016), Standard Test Methods for fineness of hydraulic Cement by air-permeability apparatus. American Society of Testing and Materials, Conshohocken, PA, USA.

**ASTM C876-15** (2015), Standard test method for corrosion potentials of uncoated reinforcing steel in concrete. American Society of Testing and Materials, Conshohocken, PA, USA.

**ASTM G109-16** (2016) Standard test method for determining effects of chemical admixtures on corrosion of embedded steel reinforcement in concrete exposed to chloride environments, American Society of Testing and Materials, Conshohocken, PA, USA.

**ASTM G1-11** (2011) Standard practice for preparing, cleaning and evaluating corrosion test specimens, American Society of Testing and Materials, Conshohocken, PA, USA.

**ASTM G59-14** (2014) Standard Test Method for Conducting Potentiodynamic Polarization Resistance Measurements, American standards for testing of Materials, 100 Barr Harbor Drive, West Conshohocken, PA 19428-2959, United States.

**Baweja D., Roper H., and Sirivivatnanon V.** (2003) Improved electrochemical determinations of chloride-induced steel corrosion in concrete, *ACI Materials Journal* Technical Paper, pg 547-584.

**Bazant, and Zdenik P.,** (1979), Physical Model for Steel Corrosion in Concrete Sea Structures-Theory, *Journal of the Structural Division* Vol. 105, no. ST6: 1137-1153.

**Bentur, A., Diamond, S., and Berke, S.** (1998) *Steel Corrosion in Concrete: Fundamentals and Civil Engineering Practice*, E and FN Spon,

**Berke N. S., Shen, D. F., and Sundberg K. M.** (1990) Comparison of the Polarization Resistance Technique to the Macrocell Corrosion Technique, *Corrosion Rates of Steel in Concrete*, ASTM STP 1065, N S Berke, V Chaker, and D Whiting, Eds, American Society for Testing and Materials, Philadelphia, pp. 38-51.

**Berke, N. S., and Hicks, M. C.** (2004). Predicting long-term durability of steel reinforced concrete with calcium nitrite corrosion inhibitor. *Cement and Concrete Composites*, 26(3), 191-198.

**Bouteiller, V., Cremona, C., Baroghel-Bouny, V., and Maloula, A.** (2012). Corrosion Initiation of reinforced concretes based on Portland or GGBS cement: Chloride contents and electrochemical characterizations versus time. *Cement and Concrete Research*, 42(11), 1456-1467.

**Broomfield J. P.,** (2007), *Corrosion of Steel in Concrete-Understanding, investigation, and repair*, Taylor and Francis, London.

**BS 8110** (1997) Structural use of concrete - Part 1: Code of practice for design and construction, British Standards Institution, London.

**Cady, Philip D.; R.E. and Weyers,** (1983) Chloride Penetration and the Deterioration of Concrete Bridge Decks, *Cement, Concrete, and Aggregates*, vol. 5, no. 2, pp. 81-87.

**Cao, Z., Hibino, M., and Goda, H.** (2012). Effect of nitrite concentration and pH on steel corrosion induced by chloride in simulated concrete pore environment. *SanYa*, 314-318.

**Carslaw, H. S., and Jaeger, J. C.** (1947). Conduction of heat in solids. Oxford University Press, London.

**CEB Design Guide** (1989), Bulletin d'Information N° 182, Durable Concrete Structures. 2<sup>nd</sup> Edition, Comité Euro-International du Béton, Lausanne, Switzerland, pp. 188-202.

**Cesiulis, H., Tsyntsaru, N., Ramanavicius, A., and Ragoisha, G.** (2016). The Study of Thin Films by Electrochemical Impedance Spectroscopy. In I. Tiginyanu, P. Topala, and V. Ursaki (Eds.), *Nanostructures and Thin Films for Multifunctional Applications: Technology, Properties and Devices* (pp. 3–42).

**Chernin, L. and Val, D.V.** (2011), Prediction of corrosion-induced cover cracking in reinforced concrete structures. *Construction and Building Materials*, Vol. 25, No. 4, pp. 1854-1869.

**Cigna, R., Proverbio, E. and Rocchini, G.** (1993). A study of reinforcement behavior in concrete structures using electrochemical techniques. *Corrosion Science*, 35(5-8), p.1579.

**Clear K. C.,** (1992) Measuring Rate of Corrosion of Steel in Field Concrete Structure, *Transportation Research Record*, No. 1211, pp. 28-38.

**Clear, K.C.** (1976), Time to corrosion of reinforcing steel in concrete slabs, FHWA-RD-76-70, (Washington, DC).

**COIN Project report 22,** (2010), Corrosion inhibitors – State of the art, SINTEF Building and Infrastructure.

**Detwiler R. J., Whiting D. A., and Lagergen, E. S.,** (1999). Statistical Approach to Ingress of Chloride Ions in Silica Fume Concrete for Bridge Decks, *ACI Materials Journal*, Vol. 96, No. 6, Nov.-Dec., pp. 670-675.

**Dong Bi-q, Qiu Qi-w, Xiang J, Huang C, Xing F, Han N, and Lu You,** (2014), Electrochemical impedance measurement and modeling analysis of the carbonation behavior for cementitious materials. *Construction and Building Materials*, 54: 558 -565.

**Duarte R.G, Castela A.S, Neves R, Freire L, and Montemor M.F,** (2014), Corrosion behavior of stainless steel rebars embedded in concrete: an electrochemical impedance spectroscopy study. *Electrochimica Acta*, 124: 218-224.

**EasyFit<sup>®</sup>,** MathWave Technologies, [www.mathwave.com](http://www.mathwave.com), 2014.

**El Maaddawy, T., and Soudki, K.** (2007). A model for prediction of time from corrosion initiation to corrosion cracking. *Cement and Concrete Composites*, 29(3), 168-175.

**El-Jazairi, B. and Berke, N. S.** (1990), The use of calcium nitrite as a corrosion inhibiting admixture to steel reinforcement in concrete, *Elsevier Applied Science*. 36 (7) 461-471.

**Elsener B., Andrade C., Gulikers J., Polder R., and Raupach M.** (2003), Half-cell potential measurements - Potential mapping on reinforced concrete structures, *Materials and Structures*, 36 (7) 461-471.

**Feliu, V., González, J. A., Andrade, C., and Feliu, S.** (1998). Equivalent circuit for modeling the steel-concrete interface. I. experimental evidence and theoretical predictions. *Corrosion Science*, 40(6), 975-993.

**Firodiya P., Sengupta A., and Pillai R. G.** (2015) Evaluation of Corrosion Rates of Reinforcing Bars for Probabilistic Assessment of Existing Road Bridge Girders, *Journal of Performance of Constructed Facilities*, Vol. 29(3).

**Frangopol, D.M, Lin, K.Y. and Estes, A.C.** (1997), Reliability of Reinforced Concrete Girders under Corrosion Attack, *Journal of Structural Engineering, American Society of Civil Engineers*, Vol. 123, No.3, pp. 286-297.

- Frederiksen, J. M.** (1996). In Chloride Penetration into Concrete, state of the art. Transport Processes, Corrosion Initiation, Tests Methods and Prediction Models, Copenhagen: The Road Directorate. Report No. 53
- Gaidis J. M.,** (2004), Chemistry of corrosion inhibitors, *Cement and Concrete Composites*, 26 (3), (2004), 181-189.
- Gaidis, J.M., and Rosenberg, A. M.,** (1987). The inhibition of chloride-induced corrosion in reinforced concrete by calcium nitrite. *Cement Concrete and Aggregates*, 9, 30-33.
- Goni, S., and Andrade, C.** (1990). Synthetic concrete pore solution chemistry and rebar corrosion rate in the presence of chlorides. *Cement and Concrete Research*, 20(4), p.525.
- González, J. A., E. Ramírez and A. Bautista** (1998). Protection of Steel Embedded in Chloride-Containing Concrete by means of Inhibitors. *Cement and Concrete Research* 28(4): 577-589.
- Hachani L. Carpio J., Fiaud C., Raharinaivo A., and Triki E.** (1992), Steel corrosion in concretes deteriorated by chlorides and sulphates: Electrochemical study using Impedance Spectrometry and “stepping down the current “method, cement and concrete research, Vol. 22, No.1.1, pp.56-66
- Hadley A. and Toumi, R.,** (2003) Assessing changes to the probability distribution of sulphur dioxide in the UK using a lognormal model, *Atmospheric Environment*, Vol. 37(11), pp.1461-1474.
- Hansson C. M., and Sorensen B.,** (1990) The Threshold Concentration of Chloride in Concrete for the Initiation of Reinforcement Corrosion, *Corrosion Rates of Steel in Concrete*, ASTM STP 1065, Berke N. S., Chaker V., and Whiting D., Eds, American Society for Testing and Materials, Philadelphia, pp. 3-16.
- Hansson, C. M.** (1984). Comments on electrochemical measurements of the rate of corrosion of steel in concrete. *Cement and Concrete Research*, 14(4), 574-584.
- Hansson, C.M., Mammoliti, L. and Hope, B.B.** (1998), Corrosion inhibitors in concrete - Part I: The Principles. *Cement and Concrete Research*, 28(12), pp.1775–1781.

**Hausmann, D. A.** (1967). Steel corrosion in concrete--how does it occur? *Materials Protection*, 6(11), p. 19.

**Hladky K., John D.G and Dawson J.L.**, Development in Rate of Corrosion Measurements for Reinforced Concrete Structures, *Proceedings of the conference on Corrosion 89*, 1989, NACE, Houston, TX, paper no. 169.

**Husain S., A1-Bahar. S., Abdul S. O., A1-Shamali**, (2004), “Accelerated AC impedance testing for prequalification of marine construction materials”, *Desalination*, vol 165, pg 377-384

**IRC SP: 60-2002**, An Approach Document for Assessment of Remaining Life of Concrete Bridges, Indian Roads Congress, New Delhi, India.

**IS 456:2000** (2005) Code of practice for Plain and Reinforced Concrete, Bureau of Indian Standards (BIS), New Delhi.

**IS:12269-2008**, Specification for 53 grade ordinary Portland cement, Bureau of Indian Standards (BIS), New Delhi, India.

**IS:1786-2008**, High strength deformed steel bars and wires for concrete reinforcement – specification, Bureau of Indian Standards (BIS), New Delhi, India.

**IS:2090-2014**, Specification for high tensile steel bars used in prestressed concrete, Bureau of Indian Standards (BIS), New Delhi, India.

**IS:383-1970 (2002)**, Specification for coarse and fine aggregates from natural sources for concrete, Bureau of Indian Standards (BIS), New Delhi, India.

**IS:4031-2008 (Part 1- 15)**, Methods of physical tests for hydraulic cement, Bureau of Indian Standards (BIS), New Delhi, India.

**IS:432-2004 (Part 1- 15)**, Specification for mild steel and medium tensile steel bars and hard-drawn steel wire for concrete reinforcement, Bureau of Indian Standards (BIS), New Delhi, India.

**Ismail M. and Ohtsu M.** (2006) Corrosion rate of ordinary and high-performance concrete subjected to chloride attack by AC impedance spectroscopy, *Construction and Building Materials*, vol. 20(7), pp. 458-469.

**ISO 8044** (2010) Corrosion of metals and alloys, basic terms and definitions, International Organization for Standardization, Geneva.

**Jaime P. V., Jordi C. F., and Pere L. M.** (2013). Bioelectronics for Amperometric Biosensors, State of the Art in Biosensors - General Aspects, Dr. Toonika Rincken (Ed.), InTech, DOI: 10.5772/52248.

**JIS A6205**, (2013), Corrosion inhibitor for reinforcing steel in concrete, Japan Industrial standard, 4-1-24, Akasaka, Minato-ku, Tokyo, 107-8440, Japan.

**John, D. G.** (1981). Use of AC impedance technique in studies on steel in concrete in immersed conditions. *British Corrosion Journal*, 16(2), p.102.

**Jones, and Denny A.** (1996). Principles and Prevention of Corrosion, Second Edition, Prentice Hall, Upper Saddle River, New Jersey, 572 pp.

**Jones, D. A., and Greene, N. D.** (1966). Electrochemical measurement of low corrosion rates, *Corrosion*, 12. P. 468.

**Karadakis, K.** (2010). Numerical investigation of the chemistry of the pore solution in the mill scale crevices of carbon steel rebar, MAsC Thesis, Carleton University, Ottawa.

**Karuppanasamy J., and Pillai R. G.,** (2014), Probabilistic Estimation of Corrosion Propagation Period for Prestressed Concrete Structures Exposed to Chlorides, 4th International Conference on Durability of Concrete Structures (ICDCS 2014), Purdue University, West Lafayette, Indiana, USA, 24–26 July 2014.

**Karuppanasamy J., and Pillai R. G.,** (2016a), Probabilistic corrosion rates of Cold-Twisted Deformed (CTD) and Thermo-Mechanically Treated or Quenched and Self-Tempered (TMT/QST) Steels in chloride-contaminated mortar, *Indian Concrete Journal*, Vol. 90, No.11, 45-55, 2016.

**Karuppanasamy J., and Pillai R. G.,** (2016b), Statistical distributions for corrosion rates of conventional and prestressing steel reinforcement embedded in chloride contaminated mortar, *NACE Corrosion Journal*. (Accepted for Publication).

**Karuppanasamy J., and Pillai R. G.,** (2016c), A short-term test method to determine the chloride threshold of steel-cementitious systems with corrosion inhibiting

admixtures, *RILEM Journal of Materials and Structures*, Springer, (Submitted; Under Review).

**Li L. and Sagues A. A.**, (2001) Chloride corrosion threshold of reinforcing steel in alkaline solution - open-circuit immersion tests, *Corrosion*, 57 (1) 19-28.

**Life-365™** v2.2.1, Life-365 Consortium III, Silica Fume Association, Lovettsville, www.life-365.org, 2014.

**Liu Y.**, (1996), Modeling the Time-to-Corrosion Cracking of the Cover Concrete in Chloride Contaminated Reinforced Concrete Structures, Doctoral Thesis, Virginia Polytechnic Institute, and State University, Blacksburg, Virginia.

**Liu, Y. and Weyers, R.** (1998), Modeling the time-to-corrosion cracking in chloride contaminated reinforced concrete structures. *ACI Materials Journal*, Vol. 95, No. 6, pp. 675-681.

**Lu, C., Jin, W., and Liu, R.** (2011). Reinforcement corrosion-induced cover cracking and its time prediction for reinforced concrete structures. *Corrosion Science*, 53(4), 1337-1347.

**Mackechnie, J. R., Alexander, M. G., Heiyantuduwa, R. and Rylands, T.** (2004) The effectiveness of organic corrosion inhibitors for reinforced concrete', Research monograph No. 7, Department of Civil Engineering, University of Cape Town, S.A., 2004.

**Mammoliti, L., Hansson, C. M., and Hope, B. B.** (1999). Corrosion inhibitors in concrete Part II Effect on chloride threshold values for corrosion of steel in synthetic pore solutions. *Cement and Concrete Research*, 29, 1583-1589.

**Richardson M. G.**, (2002). *Fundamentals of Durable Reinforced Concrete*" Taylor and Francis, 2002. pp.:101-132.

**Monfore, G. E.** (1968). The electrical resistivity of concrete. *Journal of the PCA Research and Development Laboratories*, p. 35.

**Montes, P., Bremner, T.W., and Lister, D.** (2004), Influence of calcium nitrite inhibitor and crack width on corrosion of steel in high performance concrete subjected

to a simulated marine environment, *Cement and Concrete Composites*, Vol.26, pp.243-253.

**Morinaga, S.**, (1990). Prediction of service lives of reinforced concrete buildings based on the corrosion rate of reinforcing steel. Proceedings of Building Materials and Components, Brighton, UK. 7–9, November 5–16.

**Morris W., and Vazquez M.**, (2002) Migrating corrosion inhibitor evaluated in concrete containing various contents of admixed chlorides, *Cement and Concrete Research*, vol. 32, pp. 259–267.

**Neville A. M.** (1996) Properties of concrete, Addison Wesley Longman Ltd

**Nmai C. K.** (2004). Multi-functional organic corrosion inhibitor. *Cement and Concrete Composites*, 26(3), 199-207.

**Nmai C. K., Farrington S. A., and Gregory S.** (1992). Organic-Based Corrosion-Inhibiting Admixture for Reinforced Concrete, *Concrete International*, Vol. 14, No. 4, Apr., pp. 45-51.

**Nöggerath J. and Böhni H.**, (1992) "Macro Cell Corrosion of Steel in Chloride Containing Concrete", *Materials Science Forum*, Vols. 111-112, pp. 659-676.

**Ormellese M., Berra M., Bolzoni F., Pastore T.**, (2006), "Corrosion inhibitors for chlorides induced corrosion in reinforced concrete structures", *Cement and Concrete Research*, vol 36, pg 536 – 547

**Oslakovic, I. S., Bjegovic, D., and Mikulic, D.**, (2010). Evaluation of service life design models on concrete structures exposed to marine environment. *Materials and structures*, 43(10), 1397–1412.

**Page C. L.**, (2009), Initiation of chloride-induced corrosion of steel in concrete: role of the interfacial zone, *Materials and Corrosion* 60 (8) 586-592.

**Page, C. L., Treadaway, K. W. J., and Bamforth, P. B.**, (1990) The use of calcium nitrite as a corrosion inhibiting admixture to steel reinforcement in concrete, *Cement and Concrete Composites*, p. 571-585.

- Pillai, R.G. and Annapareddy, A.,** (2013), Service life models for chloride-laden concrete structures: A review and nomographs, *International Journal of 3Rs (Repair, Restoration, and Renewal of Built Environment)*, 4 (2): 563-580.
- Poupard O., Abdel., Ait-Mokhtar., Paul D.,** (2004), “corrosion by chlorides in reinforced concrete: determination of chloride concentration by impedance spectroscopy”, *cement concrete research*, vol 34, pg 991-1000.
- Pour-Ghaz, M., Isgor, O.B., Ghods, P.,** (2008), The effect of temperature on the corrosion of steel in concrete. Part 1: Simulated polarization resistance tests and model development., *Corrosion Science*, 51 (2), pp. 415-425.
- Poursaee, A., and Hansson, C. M.** (2007). Reinforcing steel passivation in mortar and pore solution. *Cement and Concrete Research*, 37(7), 1127-1133.
- Pradhan B.,** (2007), Performance of TMT and CTD steel bars, OPC and blended cements against chloride induced corrosion in concrete, *Doctor of Philosophy thesis*, Department of Civil Engineering, IIT Delhi, India
- Pradhan B. and Bhattacharjee B.,** (2009) Performance evaluation of rebar in chloride-contaminated concrete by corrosion rate, *Construction and Building Materials*, Vol. 23(6), pp.2346-2356.
- Princeton applied research,** 2000, Basics of electrochemical impedance spectroscopy, Application Note AC-1.
- Qian, S., Cusson, D., Chagnon, N., and Baldock, B.** (2008). Corrosion-Inhibiting systems for durable concrete bridges. II: Accelerated laboratory investigation. *Journal of Materials in Civil Engineering*, 20(1), 29–36.
- Rakanta, E., Zafeiropoulou, T., and Batis, G.** (2013). Corrosion protection of steel with DMEA-based organic inhibitor. *Construction and Building Materials*, 44, 507-513.
- Ramachandran, V. S.** (1984) *Concrete Admixtures Handbook: Properties, Science, and Technology*. Park Ridge, NJ: Noyes Publications.

**Ranjith A., Balaji Rao K., and Manjunath K.** (2016), Evaluating the effect of corrosion on service life prediction of RC structures – A parametric study, *International Journal of Sustainable Built Environment*, Volume 5, Issue 2, Pages 587-60.

**Reale, T. and O'Connor, A.** (2012), A review and comparative analysis of corrosion-induced time to first crack models. *Construction and Building Materials*, Vol. 36, pp. 475-483.

**RILEM TC 235-CTC** (2014), Technical committee Corrosion initiating chloride threshold concentrations in concrete, [www.rilem.org](http://www.rilem.org), activity started in 2009.

**Rincon T. O., Perez O., Paredes E., Caldera Y., Urdaneta C., and Sandoval I.,** (2002), Long-term performance of ZnO as a rebar corrosion inhibitor, *Cement and Concrete Composites*, 24 (1), 79-87.

**Saricimen, H., Mohammad, M., Quddus, A., Shameem, M., and Barry, M. S.** (2002). Effectiveness of concrete inhibitors in retarding rebar corrosion. *Cement and Concrete Composites*, 24(1), 89–100.

**Schiessl P.** (1987) Influence of the composition of concrete on the corrosion protection of the reinforcement. pp. 1633-1645. In Scanlon, J.M., (ed.), *Concrete durability*, ACI SP 100, American Concrete Institute, Detroit.

**SHRP-330** (1993), Standard Test Method for Chloride Content in Concrete Using the Specific Ion Probe, In *Condition Evaluation of Concrete Bridges Relative to Reinforcement Corrosion-Volume 8: Procedure Manual*, SHRP-S/FR-92-110, Strategic Highway Research Program, Washington, DC, USA, pp. 85-105.

**Silva N., Boubitsas D., Luping T, and Lindqvist J.E.** (2012) Critical conditions for depassivation of steel in concrete: Interface chloride profiles and steel surface condition, *Concrete Research*, 45, 111-123

**Soeda, K., and Ichimura, T.** (2003). Present state of corrosion inhibitors in Japan. *Cement and Concrete Composites*, 25(1), 117-122.

**Song, H. W, Lee, C. H., and Ann, K. Y.** (2008), Factors Influencing Chloride Transport in Concrete Structures Exposed to Marine Environments, *Cement and Concrete Composites*, Elsevier Sciences Ltd. Vol. 30, pp. 113-121.

- Soylev T. A. and Richardson M.G.**, (2008), “Corrosion inhibitors for steel in concrete: State-of-the-art report”, *Construction and Building Materials*, 22(4), 609-622.
- Spellman D. L. and Stratfull R. F.**, (1968) Chlorides and Bridge Deck Deterioration, State of California Department of Public Works, Division of Highways, Materials and Research Department, Committee on Effect of Ice Control, 49th Annual Meeting.
- Stern, M. and Geary, A. L.** (1957) Electrochemical polarization I: theoretical analysis of shape of polarization curves, *Journal of Electrochemistry Society*, (104), pp. 56-63
- Stratfull. R. F.** (1957). The Corrosion of Steel in a Reinforced Concrete Bridge, *Corrosion* 13, p. 173.
- Tait. W. S.**, (1994), An introduction to electrochemical corrosion testing for practicing engineers, Pairodox publishers.
- Tang, L.** (2008). Engineering expression of the ClinConc model for prediction of free and total chloride ingress in submerged marine concrete. *Cement and Concrete Research*, 38(8), 1092–1097.
- Taylor P. C., Mohammad A. N., and David A. W.** (1999), Threshold Chloride Content for Corrosion of Steel in Concrete: A Literature Review, Portland Cement Association, Serial No. 2169.
- Torres-Acosta, A. and SagüØs, A.A.**, (2004) Concrete Cracking by Localized Steel Corrosion-Geometric Effects, *ACI Materials Journal*, Vol. 101, No. 6.
- Trejo D. and Miller D.**, (2002). System and Method for Determining the Chloride Corrosion Threshold Level for Uncoated Steel Reinforcement Embedded in Cementitious Material, *US Patent Application, Serial No. 60/288,210*.
- Trejo, D. and Pillai R. G.**, (2003) Accelerated chloride threshold testing - Part II: Corrosion-resistant reinforcement. *ACI Materials Journal*, 101(1): 57-64.
- Tutti K.**, (1982) *Corrosion of Steel in Concrete*, Report No. 4, Swedish Cement and Concrete Research Institute, Stockholm, Sweden.

- Vaysburd A. M. and Emmons P. H.** (2004), “Corrosion inhibitors and other protective systems in concrete repair: concepts or misconcepts”, *Cement & Concrete Composites*, 26, pp 255-263.
- Venu, K., Balakrishnan, K., and Rajagopalan, K. S.** (1965). A potentiokinetic polarization study of the behaviour of steel in NaOH-NaCl system. *Corrosion Science*, 5, p. 59.
- Verbeck, G.J.,** (1987). Mechanism of Corrosion of steel in Concrete. *Corrosion of Metals in Concrete, Special Publication 49*, American Concrete Institute, Detroit, Michigan, pp. 21-38.
- Virmani, Yash P., and Clemena G.** (1998). Corrosion Protection-Concrete Bridges, Report No. FHWA-RD-98-088, Federal Highway Administration, Washington, D.C.
- Vu, K., Stewart, M.G., and Mullard, J.,** (2005), Corrosion-Induced Cracking: Experimental Data and Predictive Models, *ACI Structural Journal*, Vol. 102, No. 5.
- Wang X. M., and Zhao H.Y.,** (1993) The residual service life prediction of RC structures, In: Nagataki S., eds. *Proceedings of the 6<sup>th</sup> International Conference on Durability of building materials and components*, Omiya, Japan.
- Wu-Man, Z., and Heng J. B.** (2011). Accelerated life test of concrete in chloride environment. *Journal of Materials in Civil Engineering*, 23(3), 330-334.
- Xu J., Jiang, L., Wang W., and Jang Y.,** (2011), Influence of CaCl<sub>2</sub> and NaCl from different sources on chloride threshold value for the corrosion of steel reinforcement in concrete, *Construction and Building Materials*, 25 (2), 663-669.
- Yonezawa T., Ashworth V., and Procter R.P.M.,** (1988), Pore solution composition and chloride effects on the corrosion of steel in concrete, *Corrosion*, 44 (7) 489-499.
- Yoon S. C., Kim, J. G., and Lee, K. M.,** (2006). Corrosion behavior of steel bar embedded in fly ash concrete. *Corrosion Science*, 48(7), 1733–1745.
- Zhang, Q., Sun, W., and Shi, J.,** (2010), Influence of mineral admixtures on chloride threshold level for corrosion of steel in mortar. *Kuei Suan Jen Hsueh Pao/Journal of the Chinese Ceramic Society*, 38(4), 633–637.

# APPENDIX A – mACT PROCEDURE TO DETERMINE THE CHLORIDE THRESHOLD OF STEEL EMBEDDED IN CEMENTITIOUS SYSTEMS

## 1. Introduction

This method is proposed to determine the critical chloride threshold ( $Cl_{th}$ ) of steel reinforcement embedded in mortar with corrosion inhibiting admixtures. The chlorides in the ponded solution are moved towards the steel surface by diffusion to initiate steel corrosion. Open circuit potential (OCP), Linear polarization resistance (LPR) and Electrical impedance spectroscopy (EIS) tests are performed at defined intervals to detect the corrosion initiation in the steel specimen. When it is detected as corrosion initiated, the concentration of chloride and nitrite from the mortar adjacent to the steel interface. The procedure to determine the concentration of chloride and nitrite is given in Appendix B and Appendix C respectively. The chloride concentration is defined as the  $Cl_{th}$  of the steel used. The  $Cl_{th}$  can be used as a comparative parameter for evaluating the new or existing steel, CIAs, and cementitious system. Figure A.1 shows the procedure in the form of the flow chart.

To evaluate the performance of the steel, the cementitious system surrounding the steel specimen should be similar and homogenous. This section will describe the design of mACT specimen, procedure for casting, curing and testing the specimen to determine the  $Cl_{th}$ .

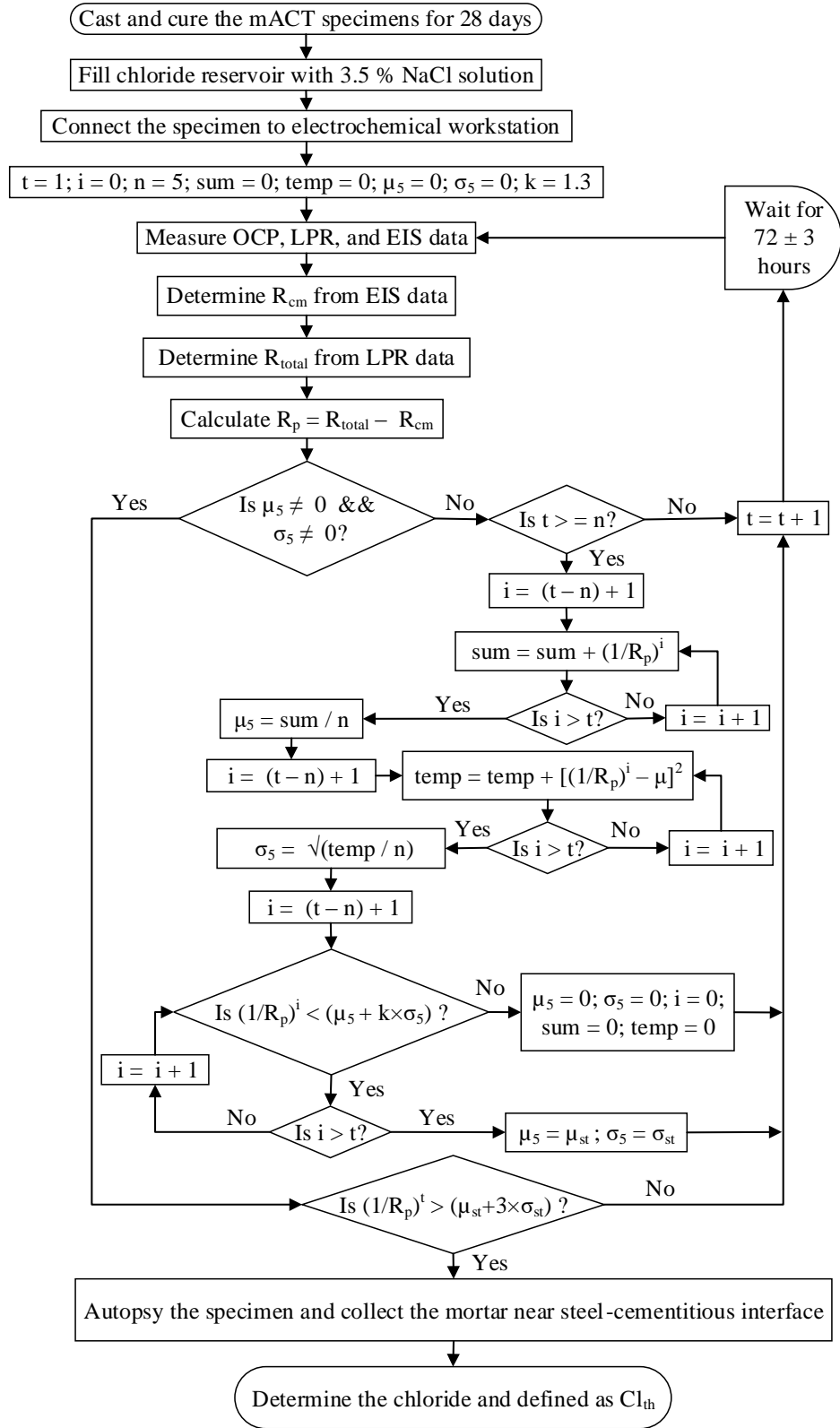


**Figure A.1 Flow chart of mACT procedure**

## 2. Apparatus

The test procedure requires the following apparatus.

1. Potentiostat coupled with an impedance analyzer (Solartron SI 1287 and SI 1260) was used for this study. However, any potentiostat with sufficient compliance voltage can be satisfactory to conduct the corrosion tests.
2. A computer containing CorrWare, ZPlot software to measure  $R_{total}$  and  $R_{cm}$ . CorrView, and ZView software to analyze the measured data.

## 3. Materials and reagents

1. *Steel rebar (working electrode)*: Any steel reinforcing bar type can be used as a working electrode in this test. Figure A.2 in Appendix A shows a typical working electrode used for this test. In this study, 16 mm diameter QST steel piece of length 20 mm was used.

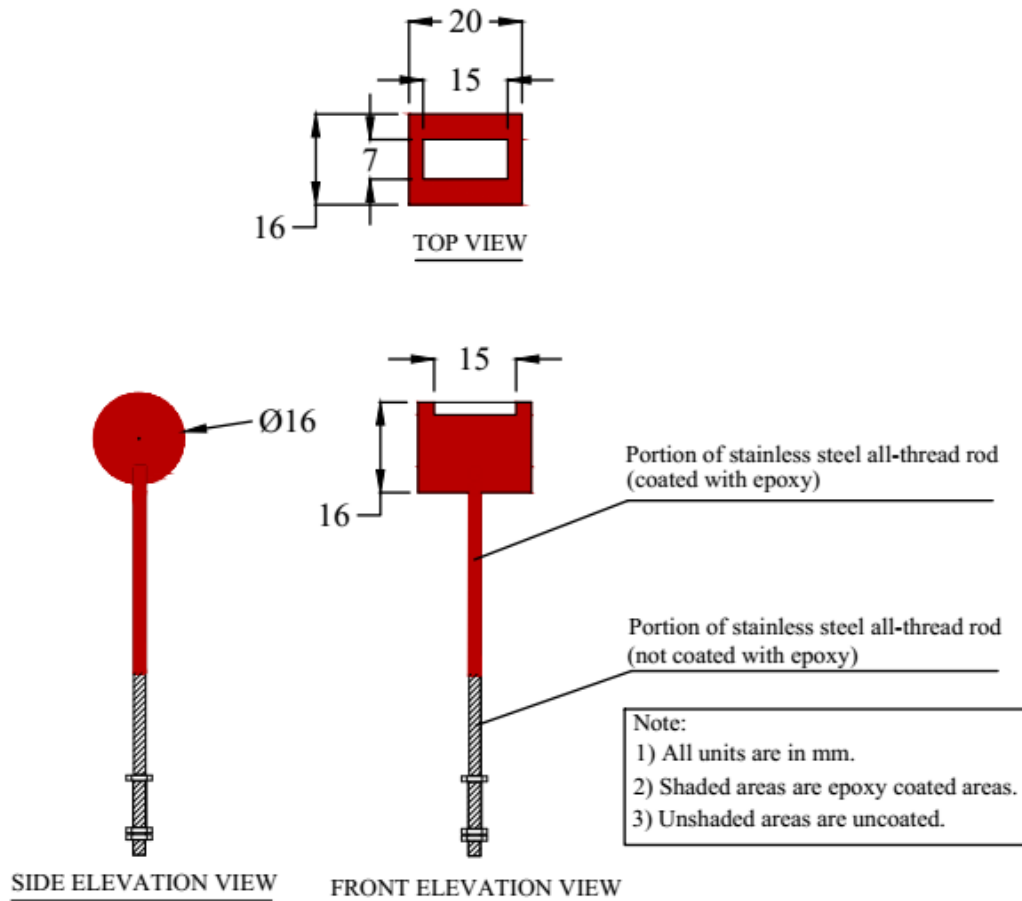


**Figure A.2 Fabrication of working electrode for ACT testing**



**Figure A.3 A typical working electrode used for ACT testing**

2. *Nichrome mesh (counter electrode)*: The counter electrode is a  $25 \times 25$  mm square Nichrome mesh. The counter electrode mesh is soldered with two copper wires (3 mm diameter) such that electrical lead wires can be connected. These copper wires also function as a supporting system for the counter electrode. After epoxy coating at the Nichrome-copper wire junction, the effective surface area of the counter electrode is approximately  $3.42 \text{ cm}^2$
3. *Mortar*: Cement and clean sand mixed with a constant water-cement ratio (w/c) shall be used. The weight ratio of the constituent materials shall be same for each sample in the similar set of test specimens. For the preliminary testing, a w/c of  $0.45 \pm 0.05$  was used, and weight ratios of the materials were 0.45:1:2.25 (water: cement:sand). OPC cement and standard sand can be used for standardized testing.
4. *Test cylinders*: Prefabricated Poly Vinyl Chloride (PVC) cylinders of 70 mm diameter and 115 mm height shall be used as the mould to contain the steel-cementitious system with 3-electrode corrosion cell setup embedded in it.

5. *Reservoir system for chloride solution:* A 50 mm diameter plastic cylinder, open on both ends, will be used to confine the chloride solution on the top of the mortar sample. This reservoir cylinder will be inserted directly into the top of the mACT specimen during casting. The embedment depth of the reservoir cylinder shall not exceed 6 mm into the mortar. Care shall be taken to ensure that the retaining reservoir is centrally embedded on the top of the specimen.
6. *Stainless steel threaded rod:* The stainless steel threaded rod of 4 mm shall be clean and able to support the steel sample without considerable deflection and shall be protected from galvanic corrosion with an epoxy coating.
7. *Threading tools:* Threading tools shall be 4 mm taps and 3 mm dies for use on the PVC mould and copper rod, respectively. It is necessary to the position of the electrode while assembling the accessories of the mould before casting.
8. *Haber-luggin probes:* A glass tube with a probe to be used to function as a container for filling the Luggin probe electrolyte, which functions as a conductive bridge between the area near the steel surface and the tip of the reference electrode. See Figure 4.12.
9. *Luggin probe electrolyte:* Saturated potassium chloride (KCl) solution to be placed in Luggin probe. This provides a Luggin probe electrolyte that matches with the solution in Saturated Calomel Electrode (SCE) used.
10. *Chloride ponding solution:* Mix 35 grams of crystalline NaCl in 1000 mL of distilled water for the solution to be placed in the reservoir. This provides a 3.5 % NaCl solution.

#### **PROCEDURE FOR CASTING SPECIMENS**

1. Make sure that the working electrode, the counter electrode, and other parts are properly (i.e.; proper dimensional settings) fastened or installed.
2. Measure precisely the exposed area of the steel specimen.
3. Draw a vertical guide-line on the outside of the mould which will help in aligning different parts of the mACT cylinder while casting.
4. Label the mACT cylinder properly.

5. Fill the Luggin probe with Luggin probe electrolyte (Sat. KCl solution) as shown in Figure 4.12. Make sure that no air is trapped inside the probe (1.5 mm inner diameter).
6. Batch all materials required for making control mortar mixture. Make water content corrections as required for fine aggregate moisture level and the solid content of the admixtures.
7. Mix sand, cement, and water as required by following the procedure given in ASTM C192 (2016).
8. Place the lower portion of mACT cylinder (Part A in Figure A.10) on a flat surface and ensure that the working electrode is secured in place. The top surface of the working electrode should be even with the level of PVC cylinder.
9. Place mortar in the cylinder and around the working electrode. The mortar shall be placed in three equal lifts. The side or top of the cylinder shall be tapped 10 times (using a rubber or wooden mallet) to allow entrapped air to escape to the free surface and to ensure proper consolidation.
10. Place Part B over Part A, ensuring that the semi-circular cut-outs from both parts are aligned. Part B should fit tightly on top of Part A. If found difficult to place or fit, hammer vertically with a wooden mallet. Care shall be taken, as explained in the previous section, to ensure that no visible air voids are trapped below the working electrode.
11. Recheck if the Luggin probe is properly filled with the Luggin probe electrolyte.
12. Cover the top mouth of the Luggin probe with a cap such that contamination of Luggin probe electrolyte with external materials and moisture in the curing room is avoided.
13. Insert Luggin probe tip into the hole drilled into the edge of Part B. Place the Luggin probe such that the probe tip is resting on the exposed area of the steel working electrode. The Luggin probe is designed such that the Luggin probe tip will lie at the centre of the exposed surface of the working electrode.

14. After the tip has been properly inserted, tape the Luggin probe to the outside edge of Parts A and/or B to secure the Luggin probe to the sample. Care shall be taken as to not break the Luggin probe tip. After the mortar has set (preferably after one day), apply silicone sealant to the Luggin probe-cylinder interface to prevent the probe from breaking during testing.
15. Place approximately 10 cm<sup>3</sup> of mortar on top of the steel specimen-Luggin probe tip region. This extra mortar should come through the counter electrode mesh disk while placing it as explained next. This will also ensure that no visible air is trapped at the interface between the bottom face of the counter electrode and the mortar. Care shall be taken to ensure that no visible air voids are trapped below the counter electrode.
16. Fill the remaining volume above the counter electrode with mortar. Carefully tap the sides of Part B to ensure proper consolidation of the mortar and removal of big air voids. Strike the surface of the mortar such that it is in level with the top of Part B.
17. Centrally place chloride solution reservoir (40 mm diameter plastic pipe) on top of mortar surface. Twist the reservoir sample or pipe while pushing into the mortar to a depth of approximately 6 mm. Carefully and gently tap the sides of Part B to reconsolidate the mortar around the reservoir. Hard hitting may cause further settlement of the reservoir pipe.
18. Cover sample(s) with moist clothes and plastic sheathing until the cementitious material is hardened. Care should be taken that the clothes or other forms of coverings are not touching the mACT samples until the cementitious material is hardened.
19. Cure samples as required. Curing during the initial test program included curing the samples in a 25 ± 2°C and 100 % relative humidity environment for 28 days.

## PROCEDURE FOR TESTING SPECIMENS

After curing the samples for the required period, the samples shall be placed on a flat surface near the potentiostat and impedance analyzer.

1. Place the 3.5 % sodium chloride solution in the reservoir on top of the specimen. The reservoir should be approximately 75 % filled. The new solution shall be placed after every 20 days and shall not be allowed to dry. Also, if the sodium chlorides tend to precipitate on the inside of the reservoir, new solution shall be placed after cleaning the reservoir.
2. Fasten all the electrical lead wires to the mACT specimen.
3. Connect the three-electrode system as required by the potentiostat specifications.
4. Determine the open circuit potential (OCP) of the working electrode until stable for 1 minute.
5. Immediately following the determination of the OCP, hold the sample potentiostatically for another 30 seconds at -0.015 V vs OCP.
6. Immediately following the potentiostatic experiment, scan the sample from - 0.015 to + 0.015 Volts (or minimum allowable range possible) versus the OCP to obtain the polarization resistance ( $R_{total}$ ). The scan rate shall be 0.1667 mV/sec.
7. Immediately after the completion of the OCP, potentiostatic holding, and  $R_{total}$  scans the data must be downloaded and evaluated. Determine the polarization resistance as follow:

$$R_{total} = \left( \frac{\Delta E}{\Delta i} \right)_{E \rightarrow E_{corr}} \quad (\text{Eq. A.5})$$

where  $E$  is the instantaneous overvoltage applied, and  $i$  is the instantaneous corrosion current density is measured.

8. At last, electrical impedance spectroscopy (EIS) with a stable AC potential of 10 mV and swept from  $1 \times 10^6$  Hz to  $1 \times 10^{-1}$  Hz was conducted to determine the bulk resistivity of the steel-cementitious interface.
9. The resistivity of concrete was deducted from the total polarization resistance value determined using the LPR method as given in Eq. 4.1.

$$R_p = R_{total} - R_{cm}$$

Eq. A 6

10. Perform statistical analysis with inverse polarization resistance ( $1/R_p$ ) data to determine if corrosion level is stabilized and corrosion has initiated using the flowchart given in Figure A.1. If there is no activation detected, go to step 4, else go to step 10.
11. When a sixth reading that falls below 1.3 times the standard deviation ( $\sigma_5$ ) of the preceding five data (i.e.,  $\mu_5 + 1.3 \sigma_5$ ) then the specimen will be considered having stable electrochemical performance, and those five readings will be considered as stable data. That is the mean ( $\mu_5$ ) and standard deviation ( $\sigma_5$ ) of stable data is considered as  $\mu_{st}$  and  $\sigma_{st}$  respectively.
12. The test will be continued, and the specimen will be considered as corrosion initiated, if the forthcoming three consecutive  $1/R_p$  value exceeds the  $\mu_{st} + 3\sigma_{st}$  of the stable data.
13. The step 5 to 13 will be repeated until the specimen was considered as corrosion initiated.
14. After it has been determined that the working electrode (steel reinforcing sample) is in an active state, the sample shall be disconnected from the potentiostat. Separate the luggin probe and all electrical from the sample. Cut the plastic chloride reservoir from the top of the sample. Break the sample as shown in Figure A.4.



**Figure A.4 Bottom portion of the mACT specimen showing the corroded steel piece**

15. Obtain ground samples in 2 mm depths for analysis of chloride and nitrite profile. Figure A.5 shows the broken mACT sample with the center area near the steel reinforcement ground for 2 mm depth.

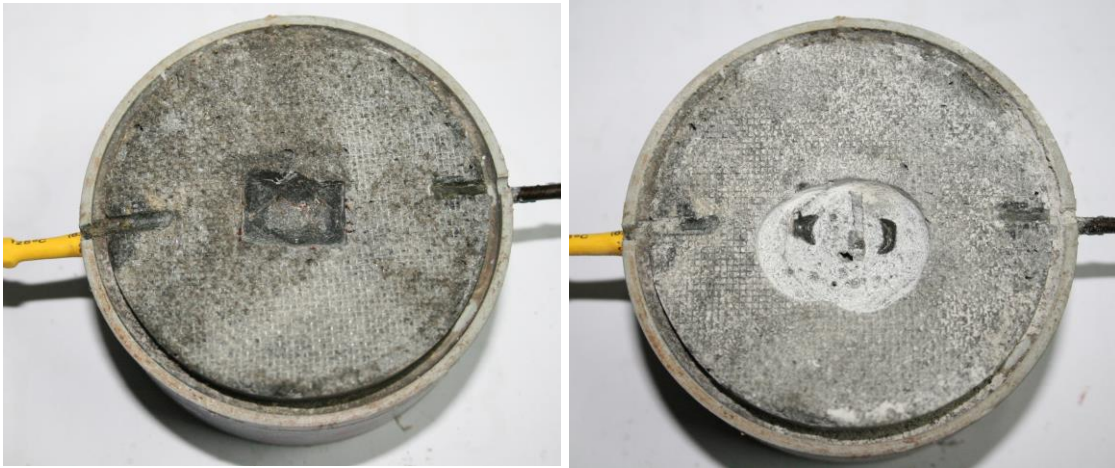


**Figure A.5 Top portion of the specimen broken and ground into mortar powder**

16. Perform chloride testing following standard total chloride test procedures (acid soluble). A modified version of the *Standard test method for Total Chloride Content in Concrete Using the Specific Ion Probe* [SHRP-S/FR-92-110 1993] has been provided in Appendix B. This modified test procedure is recommended for the chloride analysis of mACT specimens. The chloride level at a depth of the steel reinforcement is considered the critical chloride threshold value. Perform nitrite testing following the test procedure (UV-Visible spectrometer) provided in Appendix C.

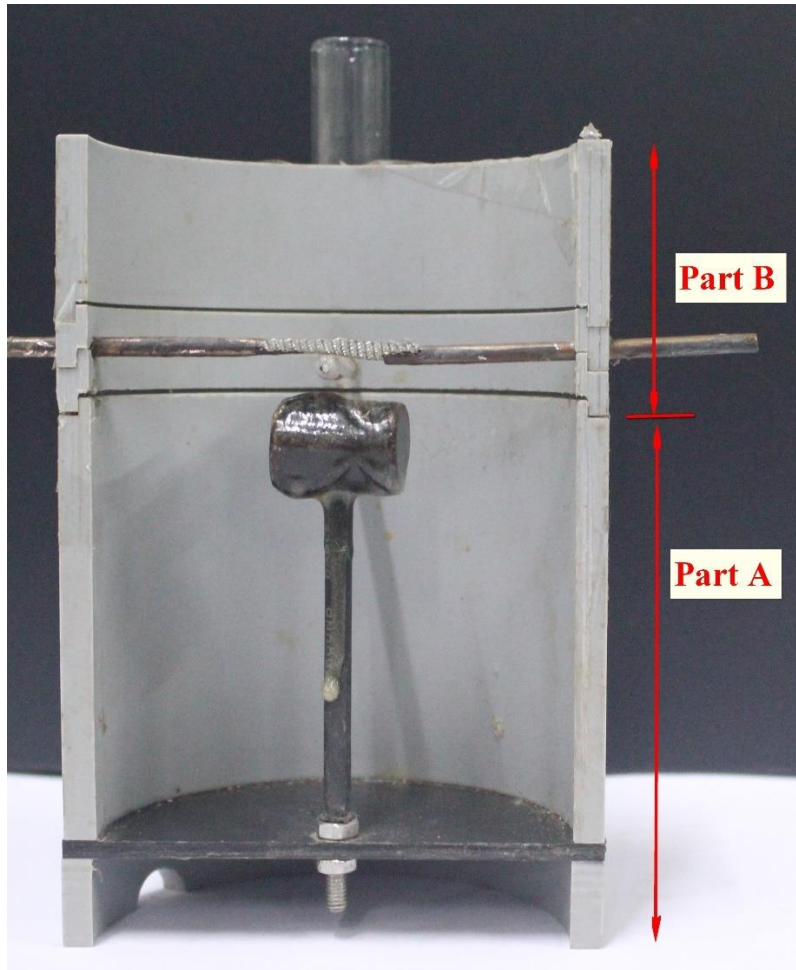


**Figure A. 6 Cross section of mACT test specimen PVC mould**

- |                                      |                                       |
|--------------------------------------|---------------------------------------|
| 1. Reference electrode (SCE)         | 5. Working electrode (steel specimen) |
| 2. Chloride solution reservoir       | 6. Haber-lugin probe                  |
| 3. 15% Sodium chloride solution      | 7. Cement mortar                      |
| 4. Counter electrode (Nichrome mesh) | 8. PVC cylinder mould                 |

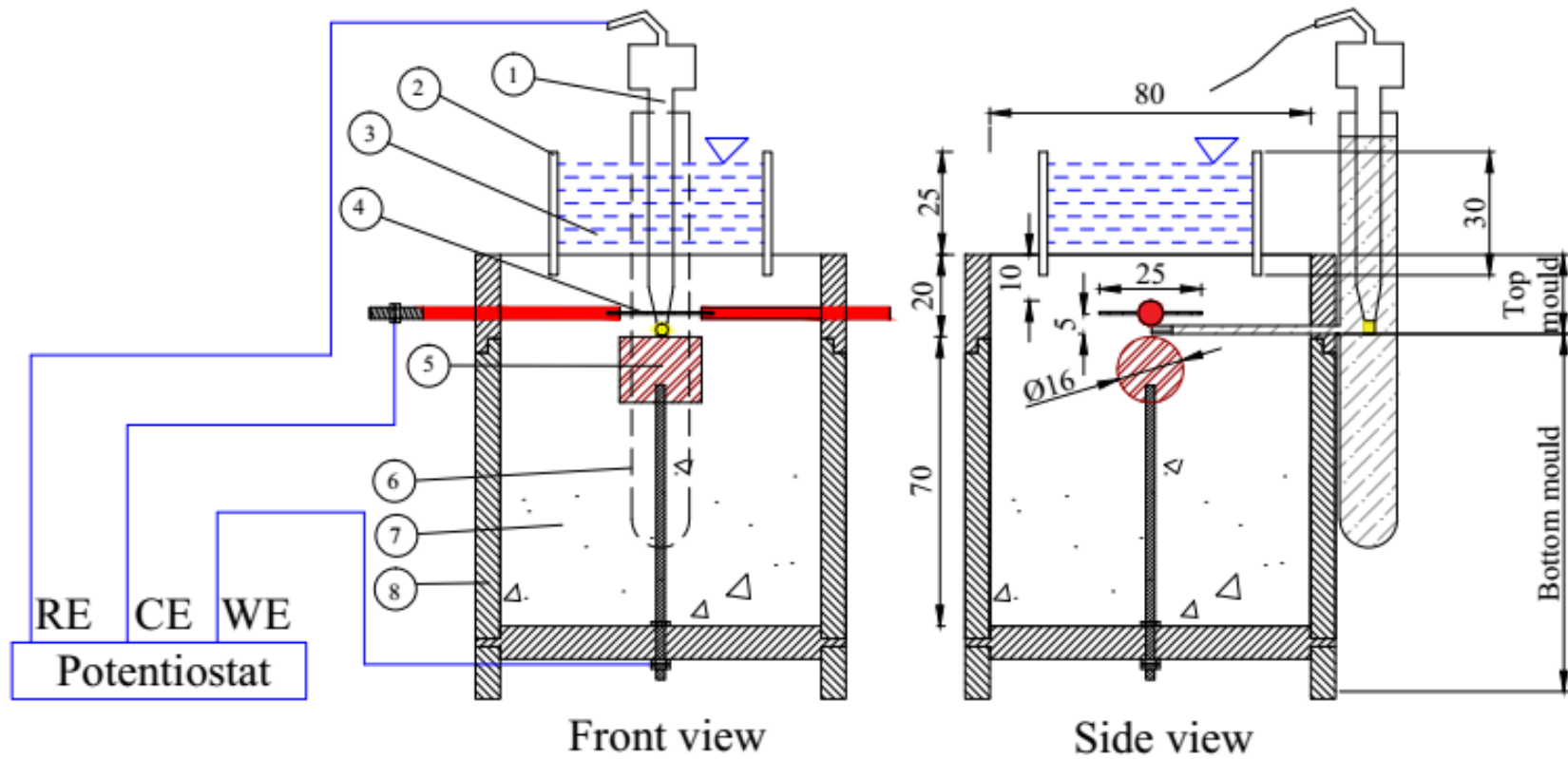
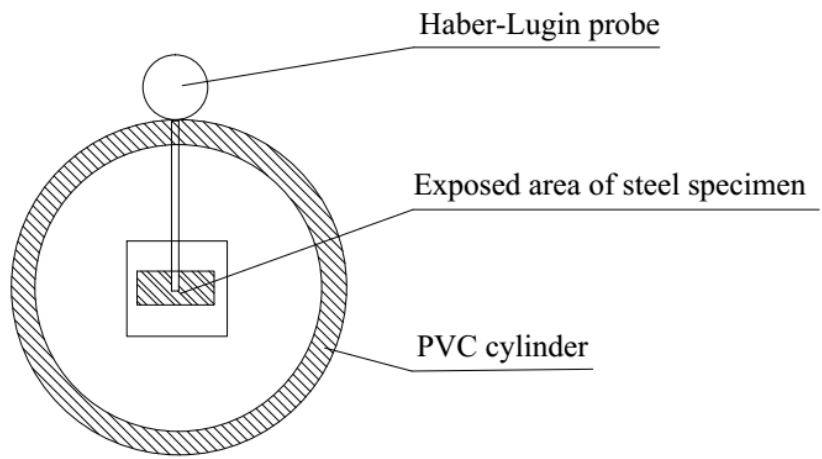
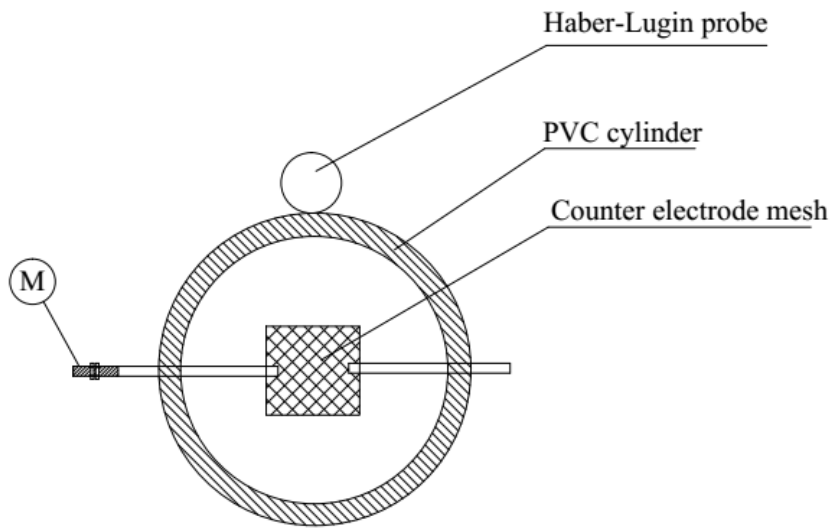


Figure A.7 Elevation views of mACT specimen



**Figure A.8 Top view of bottom portion of mACT specimen**



**Figure A.9 Top view of top portion of mACT specimen**



# **APPENDIX B - STANDARD TEST METHOD TO DETERMINE TOTAL CHLORIDE CONTENT IN MORTAR OR CONCRETE USING THE SPECIFIC ION PROBE**

## **INTRODUCTION**

This method is based on a chloride test method developed under the Strategic Highway Research Program and reported in SHRP-S-330, Condition Evaluation of Concrete Bridges Relative to Reinforcement Corrosion, Volume 8: Procedure Manual, 1993. Some modifications have been made such that the test applies to testing mortar for chloride threshold levels. Also, the description of the equipment development in the SHRP test method is not included in test method because the commercially available equipment is now available. Corrections to the test method have been made where necessary.

## **SCOPE**

This method covers the determination of the total chloride content in cement mortar samples using the prescribed procedure with a chloride-specific ion probe.

This standard may involve hazardous materials, operations, and equipment. This standard does not purport to address all of the safety problems associated with its use. It is the responsibility of the user of this standard to consult and establish appropriate safety and health practices and determine the applicability of regulatory limitations prior to use.

## **SUMMARY OF TEST METHOD**

A 1.5-gram ground mortar (or concrete) powder sample is digested in 10 ml of digestion solution and stabilized by the addition of 40 ml of stabilizing the solution. Millivolt readings taken for the final solution using a chloride-specific ion probe are converted mathematically into equivalent total percent chloride content or chloride content in kilogram per cubic meter or chloride content in pounds per cubic yard of mortar (or concrete).

## SIGNIFICANCE AND USE

Total chloride content in mortar (or concrete) is used to evaluate the degree of chloride contamination and indicates the probability of reinforcement corrosion.

## INTERFERENCES

This test procedure is unsuitable for determining the chloride contents of mortars (or concretes) containing mineral aggregates having significant quantities of pyrite. The operational response of the specific ion electrode is interfered with by the presence of  $[OH]^-$ ,  $S^-$ ,  $B^-$ ,  $I^-$ , and  $[CN]^-$  in the measured solution and is based on the electrode manufacturer's allowable chloride interference ratio.

## APPARATUS

1. Grinder - A Profile Grinder is used for obtaining ground mortar (or concrete) from the surface adjacent to the steel reinforcement. This equipment grinds mortar (or concrete) into dust from the surface adjacent to the steel reinforcement for chloride analysis over a depth increment of 0.25 mm by using an 18 mm diameter diamond grinding bit positioned in a grinding machine held against the surface by a grinding plate. The grinding takes place by working the surface over in successive rotations with the grinding bit. The grinding takes dust from a section 1 mm deep and 35 mm in diameter to produce the required dust for chloride testing.
2. After each sample collection, the grinding arrangement is thoroughly cleaned to prevent contamination of future test samples.
3. Air-tight plastic bags – Air-tight plastic bags are required to collect and store the mortar dust after grinding.
4. Weighing Papers - 75 x 75 mm size of treated papers are needed for weighing the powdered mortar (or concrete) samples.
5. Marking Pens - Permanent markers are required for labeling the plastic bags, bottles, etc.

6. Balances - An electronic balance sensitive to 0.1 gram is needed to weigh the mortar dust. An electronic balance sensitive to 0.0001 gram is needed to weigh sodium chloride for preparing the calibration and stabilizing solutions.
7. Specific Chloride Ion Electrode - The specific ion electrode used to measure the concentration of chlorides present in solution must conform to the following specifications:
8. Concentration range: 1 to  $5 \times 10^{-5}$  M, or 500 to 2 ppm.
9. pH shall range from 2 to 12
10. The electrode resistance shall be less than 1 m $\Omega$ .
11. Reproducibility shall be  $\pm 2$  %.
12. A minimum of 3 mL sample solution is required.

NOTE 1 - A suitable specific ion electrode has been found to be the Cole-Parmer combination chloride ion selective electrode Model 27504-08 with chamber filling solution kit no. 27502-63 (for use with chloride solution concentrations up to 500 ppm).

13. Multimeter - The multimeter used in the procedure must conform to the following specifications:
14. Maximum common mode voltage shall be 1500 V DC or peak AC.
15. Resolution at minimal range shall be 100  $\mu$ V.
16. Accuracy shall be  $+(0.25\%$  of the reading  $+1$  digit).
17. Operating temperature range shall be 0 to 50oC (32 to 122°F).
18. Input impedance shall be greater than 2 M $\Omega$ .

NOTE 2 -The Cyber Scan 510 pH can be a suitable meter which have a BNC connector to connect the chloride ion probe.

19. Spatula - The spatula used to measure the powdered mortar samples shall be designed to extract material from the storage contained in small quantities.
20. Digestion Solution - 10 ml is needed for each measurement.

21. Stabilizing Solution - 40 ml of stabilizing solution is needed for each test.
22. Calibration Solution - Five calibration solutions with 0.01, 0.03, 0.3, 0.6, and 1.25 % Cl<sup>-</sup> concentrations based on 3 grams powdered mortar (or concrete) specimen are needed to calibrate the instrument.

NOTE 3 - 1 ml of Ionic Strength Adjuster (ISA) solution is required for every 50 ml of the test solution while using the Cole-Parmer Combination Chloride Electrode Model 27504-08 with chamber filling solution kit no. 27502-63

## **MATERIALS**

1. Sodium Chloride - Certified biological grade having an iodide concentration no greater than 0.0004 %.
2. Acetic Acid - Glacial acetic acid having the following properties
  - Specific gravity: 1.05.
  - Chloride content: less than or equal to 0.4 ppm.
  - Normality: 17.4.
3. Isopropyl Alcohol - Standard grade having the following properties:
  - Density at 25°C: 0.781 to 0.783.
  - Boiling point: 82.3 ° ± 0.1 °C.
4. Distilled Water - Common distilled water produced in a laboratory still.
5. Mortar (or Concrete) Sample - The mortar (or concrete) sample to be analyzed shall be in powdered form, 99% passing the 75 µm sieve, as taken from the grinding extraction procedure.
6. Nalgene<sup>®</sup> Containers - Two sizes of wide-mouth Nalgene<sup>®</sup> containers (bottles) are needed:
  - For test solutions: one, 80 ml.
  - For calibration solutions: five, 80 ml.
  - For stabilizing solution: one, 1000 ml.
  - For digestion solution: one, 1000 ml.

## REAGENTS

1. Digestion Solution - The digestion solution is produced by combining acetic acid, isopropyl alcohol, and distilled water. Measure 940 grams of distilled water in a 1 litre container. Add 60 grams of glacial acetic acid and 50 grams of isopropyl alcohol to the distilled water. Thoroughly stir the solution. Dispense the solution into 8 ml Nalgene® bottles in 20 ml volumes.
2. Calibration Solutions - The calibration solutions are made by dissolving sodium chloride in distilled water. The concentration levels are 1.25, 0.6, 0.3, 0.03, and 0.01 % by weight Cl<sup>-</sup> based on 3 grams of mortar sample. To achieve the respective concentration levels, mix the following quantities of sodium chloride with 1 liter of distilled water: 0.6169 grams, 0.2961 grams, 0.1481 grams, 0.0148 grams, and 0.0049 grams. (This will result in solutions having chloride concentrations of 374, 180, 90, 9, and 3 ppm, respectively, which in turn correspond to the previously listed percentages by weight of concrete). Dispense 20 ml into the 40 ml Nalgene® bottles and label each appropriately.
3. Stabilizing Solution - The stabilizing solution is a dilution, standard chloride addition solution. It is prepared as follows: Place 0.1545 grams of sodium chloride into 1 litre of distilled water. Add 40 ml of this solution to 960 ml of distilled water. This produces a 3.75 ppm chloride solution.
4. Temperature - The temperature of the solution during testing significantly affects the determined chloride concentration. To minimize errors caused by temperature variations, ensure that the calibration, digestion and stabilizing solutions are maintained at  $24 \pm 3^{\circ}\text{C}$ .

## SAMPLE PREPARATION

1. Obtain a sample of the ground mortar (or concrete) sample using the grinder.
2. Collect at least 1.5 grams of powdered mortar (or concrete) in the filter. A 1 mm deep and 35 mm diameter hole will yield approximately 1.5 grams of a powdered mortar (or concrete) sample.
3. Place the contents of the filter containing the sample in the 30 ml sample container.

## CALIBRATION OF THE SPECIFIC ION ELECTRODE

The measurement of the calibration solutions determines the response characteristics of the specific ion electrode in combination with the multi-meter. Mathematical regression of the responses produces a representative equation for the combination used to determine the chloride contents of powdered concrete samples. The minimum of five calibration solution concentrations is needed to adequately calibrate the equipment and the electrode. Any alterations to equipment combinations shall require the formulation of a new calibration equation.

The calibration equation is determined as follows:

1. Calculate the  $\log_{10}$  of the chloride concentrations (ppm) of the calibration solutions, e.g.,  
 $\log_{10}(374 \text{ ppm Cl}^-) = 2.573$ .
2. Perform a linear regression of the millivolt readings (abscissa) versus the  $\log_{10}$  of the chloride concentrations (ordinate) of the respective calibration solutions, producing an equation in the following format:

$$\log_{10}(\text{ppm Cl}^-) = \text{intercept} + (\text{slope} \times M) \quad (\text{Eq. B.1})$$

NOTE 4 - The intercept and slope will vary with varying equipment combinations. However, the intercept is numerically characterized by  $+Y.XXXX$  and the slope is numerically characterized by  $-0.0XXXX$ , where  $Y$  represents a non-zero digit and  $X$  represents any digits from 0 through 9. The term  $M$  in Equation B.1 represents millivolt readings of the calibration solutions. The slope should be between 54 and 60 millivolts/decade at 25°C. If not, then consult the troubleshooting section of the manual for the electrode or the manufacturer. Figure B.1 shows a typical electrode calibration plot.

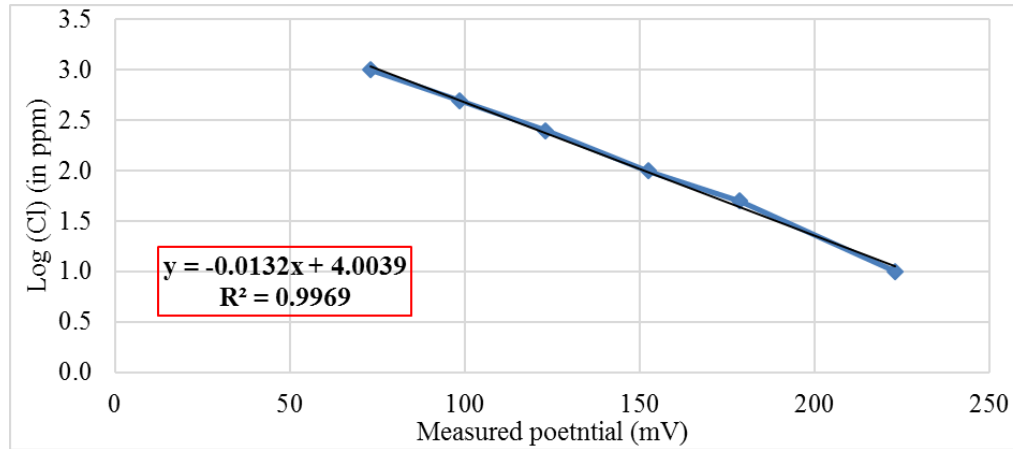


**Figure B.1 Typical electrode calibration plot for the chloride analysis.**

- The percent chloride is determined from the logarithmic inverse of the regression equation (Equation 1) minus the chloride added by the stabilizing solution, converted to percent chloride by weight of concrete, as follows:

$$R_p = R_{total} - R_{cm} \quad \text{Eq. B.2}$$

$$\%Cl^- = (10^{[y.xxx+(-0.0xxx) \times M] - 3}) \times 0.00333 \quad \text{Eq. B.3}$$

NOTE 5 - The term M in the Equation B.1 and B.2 are the millivolt readings obtained from the calibration solutions and sample test solutions, respectively.

Although unnecessary for calibration, daily measurements of the calibration solutions are recommended as a check on the operational integrity of the instrument combination. A deviation in the millivolt readings of calibration solutions indicates a problem involving one or more of the following:

- Contamination of calibration solutions.
- Contamination of the internal filling solution of the specific ion electrode.
- Defective specific ion electrode.
- Defective multi-meter.

The percent chlorides are based on a 1.5 grams powdered mortar (or concrete) sample, and the ppm of chloride is the resulting concentration of a 100 ml solution. The allowable deviations of the specific ion electrode are presented below:

<b>Concentration</b> $\%Cl^-$ ( $ppmCl^-$ )	<b>Allowable Deviation</b> <b>(millivolts)</b>
1.25 (374)	1.5
0.60 (180)	1.5
0.30 (90)	1.5
0.03 (9)	1.5
0.01 (3)	4.5

The calibration equation shall be based on the data from ten calibration runs, each consisting of measurements of the five calibration solutions. The potentiometer shall be switched off between each of the ten runs.

#### **PROCEDURE**

1. Place 10 ml of the digestion solution in a clean, dry 80 ml plastic bottle.
2. Remove the powdered mortar (or concrete) sample from the filter and place it in the 30 ml plastic storage bag. Shake and stir the powdered concrete sample to provide a uniform sample.
3. Weigh  $1.5 \pm 0.1$  grams of mortar or concrete sample on a weighing paper.
4. Place the concrete sample in the bottle containing the 10 ml digestion solution, place the cap on the bottle, and shake vigorously to suspend the powder in the solution. Let the powder digest for 3 minutes. The bottle may be opened after shaking to relieve pressure from effervescence due to the reaction, and then closed immediately.
5. Carefully remove the bottle cap and add 40 ml of the stabilizing solution (a 3.75 ppm chloride solution).
6. Replace the cap and shake vigorously for 1 minute.

7. Add 1 ml ISA solution if the expected concentration of chloride is less than 3 ppm.
8. Remove the bottle cap and place the electrode to a depth of mid-height in the extraction solution.
9. Wait 3 minutes or more minutes and record the stable millivolt reading. The millivolt reading is defined to be stable when it oscillates by less than  $\pm 0.5$  millivolts.
10. After each millivolt measurement, the electrode shall be rinsed clean with distilled water.

### CALCULATIONS

Calculate the predicted percent chloride content in the sample as follows:

$$\log_{10}(\text{ppm } Cl^{-}) = (C + D + M) \quad \text{Eq. B.4}$$

where,  $C$  and  $D$  are the characteristic constants of the electrode calibration curve ( $y=C+Dx$ ); typical values are 3.0352 and -0.018487, respectively. The term  $M$  is the potentiometer reading of the sample test solution in millivolts. Figure B.1 shows a typical electrode calibration plot. The % chlorides can be determined using:

$$\%Cl^{-} = (10^{(C+D+M)} - 3) \times 0.00333 \quad \text{Eq. B.5}$$

or

$$Cl^{-}(\text{lb}/\text{yd}^3) = (10^{(C+D+M)} - 3) \times 0.00333 \times W \times 10^{-2} \quad \text{Eq. B.6}$$

or

$$Cl^{-}(\text{kg}/\text{m}^3) = 0.5937 \times (10^{(C+D+M)} - 3) \times 0.00333 \times W \times 10^{-2} \quad \text{Eq. B.7}$$

where  $W$  is the unit weight of concrete or mortar in  $\text{kg}/\text{m}^3$  or  $\text{lb}/\text{yd}^3$  or % by weight of cement.



## **APPENDIX C - PROCEDURE TO DETERMINE THE NITRITE CONCENTRATION FROM HARDENED CEMENTITIOUS SYSTEM USING UV SPECTROMETER**

### **PREPARATION OF STANDARD CALIBRATION CURVES FOR NITRITE ION.**

1. Prepare the nitrite solution with known concentration, say, 500, 250, 100, 50, 25, 10, 5, and 1 ppm.
2. Take 10 mL of solution in a 25 ml container and add a sachet of Potassium disulfate, Iron (II) Sulfate Heptahydrate), (Nitrite high range reagent by Hanna Instruments, Product ID: HI93708) to the solution and shake gently.
3. Allow the solution to stand for 10 minutes by which it develops colour.
4. Add the solution to the cuvette provided with a UV-Visible spectrometer and place it in the sample holder.
5. Measure the absorbance of the solution using the spectrometer at a wavelength between 200 and 800 nm.
6. Follow the step 2 to step 5 for each solution concentrations.
7. Plot graph showing wavelength Vs absorbance from data logged from software provided to acquired data from UV-spectrometer and find the absorbance value at 450 nm (peak value of the absorbance) for each solution as shown in Figure C.1
8. Plot the graph of the known concentration (in ppm) Vs its corresponding absorbance value at 450 nm (peak value of the absorbance) as given in Figure C.2 and fit the linear regression equation for the plot.

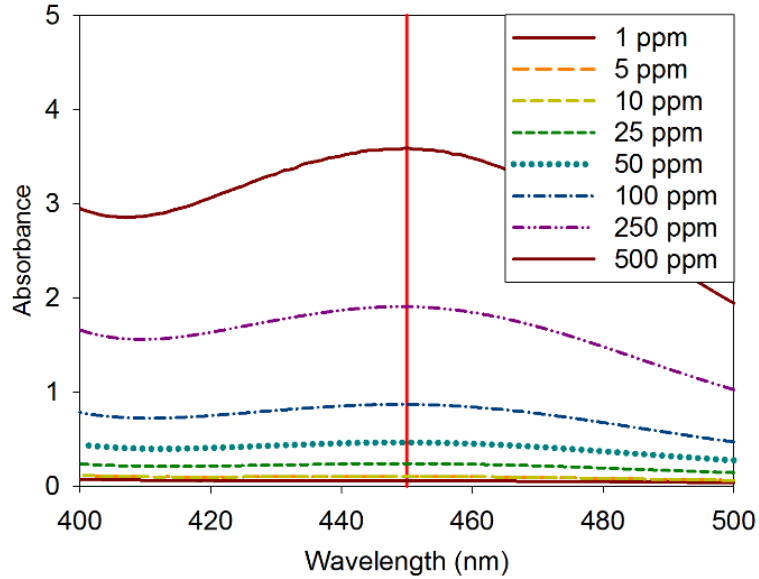


**Figure C.1 Absorbance for different nitrite concentration**

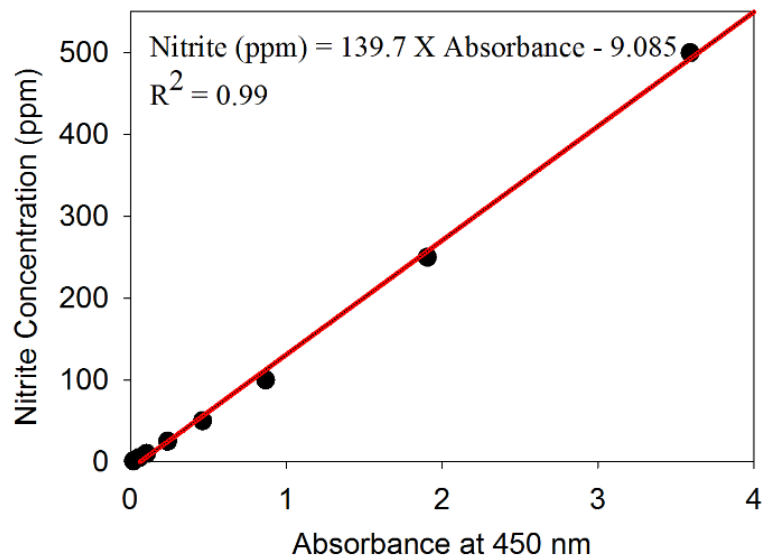


**Figure C.2 Calibration curve for nitrite ions**

**SAMPLE EXTRACTION AND NITRITE DETERMINATION FROM CEMENTITIOUS POWDER.**

1. Take 100 ml of deionized water (micro pore water filtered with 0.2  $\mu\text{m}$  nylon filter) in a 125 ml glass bottle.
2. Add 2 grams of ground concrete or mortar powder passing through 600  $\mu\text{m}$  sieve.
3. Stir the solution using the magnetic stirrer at 500 rpm for 30 minutes.

4. Add a pinch of Zinc powder (0.003 grams) to the extracted solution (a solution that has ions extracted from cementitious powder) and shake well for a minute.
5. After 15 minutes of the rest period, filter the solution using filter paper that retain particles size greater than 3  $\mu\text{m}$  (Whatman Grade No.44).
6. Take 10 mL of the filtered solution in a 25 ml container.
7. Add a sachet of Potassium disulfate, Iron (II) Sulfate Heptahydrate), (Nitrite high range reagent by Hanna Instruments, Product ID: HI93708) to the solution and shake gently.
8. Allow the solution to stand for 10 minutes by which it develops colour.
9. Add the solution to the cuvette provided with a UV-Visible spectrometer and place it in the sample holder.
10. Measure the absorbance of the sample on the spectrometer at a wavelength of 450 nm.
11. Calculate nitrite content (in ppm) using linear equation obtained from the standard calibration curve.
12. As per the requirement, report the concentration of nitrite in terms of percent by weight of cement (% bwoc) or quantity per unit volume of concrete. ( $\text{kg}/\text{m}^3$  of concrete).



## APPENDIX D - CORROSION PROPAGATION MODELS FROM LITERATURE

The following table shows the empirical models that are commonly used by many researchers to estimate the corrosion propagation period ( $t_p$ ). The input parameters required for each model where compared and the model that requires parameters that are easily available for practicing engineer is used for this study.

**Table D.1: Andrade *et al.* (1998)**

Model	Parameters
$W_t = 0.05 + \mu (P_x - P_{x0})$ $P_{x0} = 83.8 + 7.4 d/\phi - 22.3 f_{c,sp}$	$W_t$ = Crack width, $P_x$ = Corrosion penetration (after reduction in diameter) $\mu$ = Constant = 0.01 $P_{x0}$ = Initiation penetration of corrosion at crack initiation. $d/\phi$ = Ratio of cover depth to the diameter of rebar $f_{c,sp}$ = Split tensile strength of concrete

**Table D.2: Stratfall Model (1997)**

Model	Parameters
$t_{cr} = \frac{129d^{1.22}}{[Cl]^{0.42}(w/c)}$	$t_{cr}$ = time required to initiate crack in cover concrete $D$ = cover depth $Cl$ = chloride content of water in contact with concrete $w/c$ = water to cement ratio

**Table D.3: Clear (1976)**

$$t_{cr} = \left[ (0.052 d^{1.22} t^{0.21}) / (C_{S,Cl}^{0.24} (w/c)) \right]^{0.83}$$

D = cover depth

Cl = chloride content of water in contact with concrete

W/c - water to cement ratio

T = time of exposure

$C_{S,Cl}$  = chloride content in concrete surface

**Table D.4: Andrade et al., (1998)**

$$x = 0.0116 i_{corr} t$$

$$x_0 = a + b \frac{C_V}{\phi}$$

x = Depth of corrosion penetration (mm)

$i_{corr}$  = Corrosion current density ( $\mu\text{A}/\text{cm}^2$ )

t = Time (years)

$x_0$  = Depth of corrosion penetration ( $\mu\text{m}$ )

a = Corrosion constant = 7.53

b = Corrosion constant = 9.32

$C_V$  = Cover depth

$\phi$  = Diameter of the reinforcement

**Table D.5: Liu et al. (1998)**

$$W_{rust} = \left( s \int_0^t 0.098 \frac{1}{\alpha_r} \pi D \cdot i_{corr} \cdot dt \right)^{1/2}$$

$W_{rust}$  is related to corrosion rate

corrosion current density  $i_{corr}$  in  $\mu\text{A}/\text{cm}^2$

$\alpha_r$  is a coefficient related to the type of rust products

**Table D.6: Vu et al. (2005)**

$$t_{sp} \approx t_{1st} + k_R 0.0114 i_{corr} \left[ A \left( \frac{C}{wc} \right)^B \right]$$

$$k_R \approx 0.95 \left[ \exp \left( - \frac{0.3 i_{corr(exp)}}{i_{corr(real)}} \right) - \frac{i_{corr(exp)}}{2500 i_{corr(real)}} + 0.3 \right]$$

$t_{sp}$  = Time to excessive cracking for reinforced concrete structures (years)

$t_{1st}$  = Time to crack initiation

$k_R$  = Rate of loading correction factor

$i_{corr}$  = Corrosion current density ( $\mu A/cm^2$ )

A, B = Constants based upon the crack width limit state selected

C = Cover depth (mm)

wc = Water to cement ratio

A and B are related to the limit crack width

$i_{corr(exp)}$  = The applied corrosion rate used during the experiment ( $\mu A/cm^2$ )

$i_{corr(real)}$  = The corrosion rate observed in the structure being analyzed

**Table D.7: Torres-Acosta and Sagues (2004)**

$x_{crit} \approx 0.011 \left( \frac{C}{\phi} \right) \left( \frac{C}{L} + 1 \right)^2$	$x_{crit}$ = Critical corrosion penetration (mm) C = Cover depth (mm) $\phi$ = Reinforcing bar diameter (mm) L = Length of the anodic region (mm)
---	--

**Table D.8: Tepfers 1979, Martín-Pérez et al., 1999**

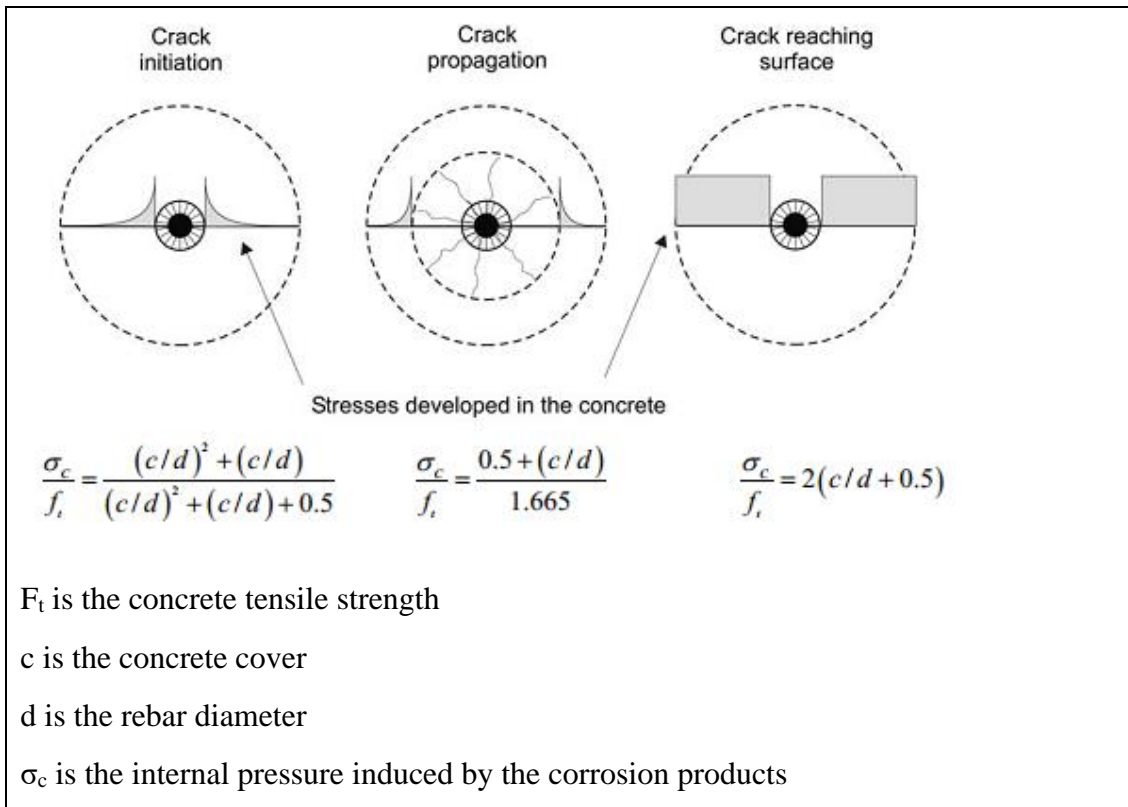


**Table D.9: Cady-Weyers' Deterioration Model (1983)**

$A_t = A_c + \left[1 - \frac{A_c}{100}\right] A_d$	<p>At = percent of the deck area having rebars in critical chloride contaminated concrete at time t.</p> <p>Ac = percent of the deck area having subsidence cracking</p> <p>Ad = percent of the deck area having bars in critical chloride contaminated concrete at time t resulting from diffusion.</p>
--	--

**Table D.10: Liu and Weyer (1998)**

$t_{cr} = \frac{W_{crit}^2}{2k_p}$ $W_{crit} = \rho_{rust} \left( \pi(d_s + d_0)D + \frac{W_{st}}{\rho_{st}} \right)$ $k_p = 2.59 \times 10^{-6} \left( \frac{1}{\alpha} \right) \pi D i_{corr}$	<p><math>\alpha</math> is related to types of rust products as constant</p> <p><math>D</math> is the steel diameter (in.)</p> <p><math>i_{corr}</math> is the annual mean corrosion rate (mA/ft<sup>2</sup>)</p> <p><math>\rho_{rust}</math> is the density of corrosion products</p> <p><math>\rho_{st}</math> is the density of steel</p> <p><math>d_0</math> thickness of pore band around the steel/concrete interface</p> <p><math>d_s</math> thickness of corrosion products to generate the tensile stresses</p> <p><math>W_{st}</math> is the mass of corroded steel</p> <p><math>W_{crit}</math> is the critical amount of corrosion products</p>
--	--

**Table D.11: Morinaga model (1990)**

Model	Nomenclature
$t_{cor} = \frac{Q_{cr}}{J_r}$ $J_r = \left(\frac{W}{F}\right) I_{corr}$ $Q_{cr} = 0.602 \times D \left(1 + \frac{2C_v}{D}\right)^{0.85}$	<p><math>t_{cor}</math> is time required for steady state corrosion cracking (Years)</p> <p><math>D</math> is initial diameter of the wire (mm)</p> <p><math>p</math> is perimeter of the wire (mm)</p> <p><math>j_r</math> is instantaneous corrosion rate (gm/cm<sup>2</sup>/s)</p> <p><math>W</math> is the equivalent weight of steel=27.93 g</p> <p><math>F</math> is the Faraday's constant = 96487 Coulombs</p> <p><math>Q_{cr}</math> is amount of corrosion when concrete cracks (x10<sup>-4</sup> gm/cm<sup>2</sup>)</p> <p><math>C_v</math> is the thickness of concrete cover (mm)</p> <p><math>i_{corr}</math> is corrosion current density (μA/cm<sup>2</sup>)</p>

**Table D.12: El Maaddawy, and Soudki (2007)**

$$T_{cr} = \left[ \frac{7.117.5(d+2\delta_0)(1+\gamma+\psi)}{iE_{cf}} \right] \left[ \frac{2C_v f_{ct}}{d} + \frac{2\delta_0 E_{cf}}{(1+\gamma+\Psi)(d+2\delta_0)} \right]$$

$T_{cr}$  = corrosion initiation time to cracking

$d$  = Diameter of the rebar

$C_v$  = Cover thickness

$i$  = Corrosion current density,  $\mu A/cm^2$

$E_{cf}$  = Effective elastic modulus of concrete =  $\frac{E_c}{(1+\phi_{cr})}$

$E_c$  = Elastic modulus of concrete,  $E_c = 5000\sqrt{f_{ck}}$  (IS 456:2000)

$\Phi_{cr}$  = Concrete creep coefficient assumed as 2.35 as per CSA standard (A23.3- 1994)

$\gamma$  = Poisson's ratio of concrete assumed as 0.18

$\delta_0$  = Porous layer assumed as 10  $\mu m$  thickness

$f_{ct}$  = Tensile strength of concrete,  $f_{ct} = 0.7\sqrt{f_{ck}}$  (IS 456:2000)

$f_{ck}$  = Compressive strength of concrete at the end of 365 days.

$\Psi = \frac{D'^2}{2C_v(C_v+D')}$  where  $D' = d + 2\delta_0$

**Table D.13: Bazant model (1979)**

Service life models to estimate corrosion induced damage	Nomenclature
$t_{cor} = \rho_{cor} \frac{D \times \Delta D}{p j_r}$ $\rho_{cor} = \left[ \left( \frac{1}{\rho_r} \right) - \left( \frac{0.583}{\rho_{st}} \right) \right]^{-1} \frac{\pi}{2}$ $P_r = \left( \frac{W}{F \rho_{st}} \right) I_{corr}$ $J_r = \left( \frac{W}{F} \right) I_{corr}$ $\Delta D = \delta_{app} P_r$ $\delta_{app} = \frac{(1 + \gamma) D}{E_{ef}}$ $E_{ef} = \frac{E}{(1 + \varphi_{cr})}$	<p><math>t_{cor}</math> is time required for steady state corrosion cracking (Years)</p> <p><math>\rho_{cor}</math> is combined density factor for steel and rust (g/cm<sup>2</sup>)</p> <p><math>D</math> is initial diameter of the wire (mm)</p> <p><math>p</math> is perimeter of the wire (mm)</p> <p><math>j_r</math> is instantaneous corrosion rate (gm/cm<sup>2</sup>/s)</p> <p><math>P_r</math> is the penetration rate (cm/s)</p> <p><math>\delta_{app}</math> is the bar hole flexibility</p> <p><math>\gamma</math> is the Poisson ratio of concrete (<math>\approx 0.18</math>)</p> <p><math>E_{ef}</math> is the effective elastic modulus of concrete</p> <p><math>E</math> is the elastic modulus of concrete</p> <p><math>\varphi_{cr}</math> is the creep coefficient (<math>\approx 2</math>)</p> <p><math>\Delta D</math> is increase in diameter of wire due to rust formation (mm)</p> <p><math>W</math> is the equivalent weight of steel=27.93 g</p> <p><math>F</math> is the Faraday's constant = 96487 Coulombs</p> <p><math>\rho_{st}</math> is the density of steel (7.85 gm/cm<sup>3</sup>)</p> <p><math>i_{corr}</math> is corrosion current density (<math>\mu A/cm^2</math>)</p>

**Table D.14: Wang and Zhao model (1993):**

<b>Service life models to estimate corrosion induced damage</b>	<b>Nomenclature</b>
$t_{cor} = \frac{H}{P_r}$ $P_r = \left( \frac{W}{F \rho_{st}} \right) I_{corr}$ $\frac{\Delta}{H} = \gamma = 0.33 \left( \frac{D}{C_v} \right)^{0.565} f_{cu}^{1.436}$	<p><math>t_{cor}</math> is time required for steady state corrosion cracking (Years)</p> <p><math>D</math> is initial diameter of the wire (mm)</p> <p><math>P_r</math> is the penetration rate (cm/s)</p> <p><math>W</math> is the equivalent weight of steel=27.93 g</p> <p><math>F</math> is the Faraday's constant = 96487 Coulombs</p> <p><math>C_v</math> is the thickness of concrete cover (mm)</p> <p><math>\gamma</math> is the crack expansion coefficient of concrete</p> <p><math>f_{cu}</math> is the cube strength of concrete (MPa)</p> <p><math>\rho_{st}</math> is the density of steel (7.85 gm/cm<sup>3</sup>)</p> <p><math>\Delta</math> is the thickness of corrosion product (obtained from FEM)</p> <p><math>H</math> is the depth of rebar penetration (mm)</p> <p><math>i_{corr}</math> is corrosion current density (<math>\mu\text{A}/\text{cm}^2</math>)</p>

In addition to these models, there are many other empirical and probabilistic models available in the literature. However, Wang and Zhao (1993) was chosen for this study.



## APPENDIX E – CHLORIDE DIFFUSION MODELS FROM LITERATURE

The following tables shows the empirical models that are commonly used by many researchers to estimate the diffusion of chloride in the cementitious system.

**Table E.1: Closed–form solutions [Carslaw and Jaeger 1947]**

<p>Case (i): For constant chloride concentrations at the concrete surface, the surface buildup rate, <math>\Phi(t) = C_0</math>,</p> $C(x,t) = C_i + (C_s - C_i) \cdot \operatorname{erfc}\left(\frac{x}{\sqrt{4Dt}}\right)$ <p>Case (ii): For cases where chloride concentration at the concrete surface varies linearly with the time of exposure, i.e., <math>\Phi(t) = kt</math>, then;</p> $C(x,t) = kt \left\{ \left(1 + \frac{x^2}{2Dt}\right) \cdot \operatorname{erfc}\left(\frac{x}{\sqrt{4Dt}}\right) - \frac{x}{\sqrt{\pi Dt}} \cdot \exp\left(-\frac{x^2}{4Dt}\right) \right\}$ <p>Case (iii): For cases where chloride concentrations at the concrete surface varies as a <i>the</i> function of the square root of time of exposure, i.e. <math>\Phi(t) = k\sqrt{t}</math>, then,</p> $C(x,t) = k\sqrt{t} \left\{ \exp\left(-\frac{x^2}{4Dt}\right) - \frac{x\sqrt{\pi}}{\sqrt{4Dt}} \cdot \operatorname{erfc}\left(\frac{x}{\sqrt{4Dt}}\right) \right\}$
<p><math>C(x,t)</math> is the chloride concentration at depth, <math>x</math>, at exposure time, <math>t</math></p> <p><math>C_i</math> is the initial chloride concentration at depth <math>x</math> (<math>t = 0</math>)</p> <p><math>C_s</math> is the surface chloride concentration (<math>t \geq 0</math>)</p> <p><math>\operatorname{erfc}</math> is the complementary error function has limit from 0 to <math>\frac{x}{\sqrt{4Dt}}</math></p> <p><math>k</math> is a proportionality constant.</p>

**Table E.2: Life-365™ [Life-365 2012]**

$D(t, T) = D_{ref} \left( \frac{t_{ref}}{t} \right)^m e^{\frac{U}{R} \left( \frac{1}{T_{ref}} - \frac{1}{T} \right)}$ <p>where <math>m = 0.2 + 0.4 \left( \frac{\%FA}{50} + \frac{\%SG}{70} \right) \leq 0.6</math></p> $D_{ref} = 10^{-12.06 + 2.4(w/c)} \cdot e^{-0.165 \cdot SF} ; FA \leq 50\%; SG \leq 70\%; SF \leq 15\%$
<p>D(t,T) is diffusion coefficient at time t and temperature T;</p> <p>m is diffusion decay or age factor, <math>m = 0.2 + 0.4 \left( \frac{\%FA}{50} + \frac{\%SG}{70} \right)</math>, whose value is limited to 0.6); %FA and %SG are percentages of fly ash (<math>\leq 50\%</math>) and slag (<math>\leq 70\%</math>) in the cement, respectively</p> <p><math>D_{ref}</math> (= <math>D_{28}</math>) is the apparent chloride diffusion coefficient at time <math>t_{ref}</math> (= 28 days)</p> <p><math>T_{ref}</math> = Temperature (= 293 K);</p> <p>U is activation energy of the chloride diffusion process (<math>35000 \text{ J} \cdot \text{mol}^{-1}</math>);</p> <p>R is universal gas constant (<math>8.31 \text{ J} \cdot \text{mol}^{-1} \text{K}^{-1}</math>),</p>

**Table E.3: CHLODIF [Oslaković et al. 2010]**

$C(x, t) = \left\{ [C_o + k(t-1)] \cdot \text{erfc} \left( \frac{x}{2\sqrt{\tau}} \right) \right\} + k \left\{ \left( 1 + \frac{x^2}{2\tau} \right) \cdot \text{erfc} \left( \frac{x}{2\sqrt{\tau}} \right) - \frac{x}{\sqrt{\pi\tau}} e^{-\frac{x^2}{4\tau}} \right\}$ <p>where</p> $d\tau = D(t) dt ; \tau = \int_0^t D(s) ds ; D(t) = \text{Constant} \times t^{-m}$
<p><math>C_o</math> is the initial surface chloride concentration</p> <p>k is the coefficient of linear increase in <math>C_o</math></p> <p>t is the time</p> <p>erfc is the complimentary error function</p> <p>x is the clear cover depth</p> <p><math>\tau</math> is a factor that accounts for the temporal variation of the apparent chloride diffusion coefficient (D)</p>

**Table E.4: ClinConc [Tang 2008]**

$$\frac{c - c_i}{c_s - c_i} = \operatorname{erfc} \left( \frac{x}{2 \sqrt{\frac{k_D D_0}{1-n} \left[ \left(1 + \frac{t'_{ex}}{t}\right)^{1-n} - \left(\frac{t'_{ex}}{t}\right)^{1-n} \right] \cdot \left(\frac{t'_{6m}}{t}\right)^n \cdot t}} \right)$$

$$D_o = \frac{(0.8a_t^2 - 2a_t + 2.5)(1 + 0.59K_{b6m}) \cdot k_{TD}}{1 + k_{OH6m} \cdot K_{b6m} \cdot k_{Tb} \cdot f_b \cdot \beta_b \left(\frac{c_s}{35.45}\right)^{\beta_b - 1}} \cdot D_{6m}$$

$$n = -0.45a_t^2 + 0.66a_t + 0.02$$

$D_o$  is the initial apparent diffusion coefficient

$t'_{6m}$  is the age of concrete at the start of exposure

$t$  is the duration of the exposure;  $n$  is the age factor to account for the decrease in the diffusivity with time;

$a_t$  is the time-dependent factor for chloride binding

$D_{6m}$  is the diffusion coefficient from laboratory tests at the start of exposure ( $t'_{6m}$ )

$K_b$  is the binding factor

$k_{TD}$  and  $k_{Tb}$  are the temperature factors for diffusion coefficient and chloride binding

$k_{OH}$  is the factor describing the effect of alkalinity

$f_b$  and  $\beta_b$  are chloride binding constants;

$c$ ,  $c_s$  and  $c_i$  are the free chloride concentrations in the concrete pore solution at depth  $x$ , in seawater (or surrounding environment) and initially in concrete at  $x$

**Table E.5: DuraCrete [DuraCrete 2000]**

$$g = C_{cr}^d - C^d(x, t) = C_{cr}^d - C_{s,cl}^d \cdot \operatorname{erfc} \left( \frac{x^d}{2 \sqrt{R_{cl}^d(t) t}} \right)$$

$$P_f(T) = 1 - P\{g(x, t) > 0 \text{ for all } t \in [0, T]\} \text{ and } \beta = -\Phi^{-1}(P_f)$$

$C_{cr}^d$  and  $C_{s,cl}^d$  are design chloride concentration in concrete and at the surface,

$x^d$  is design cover thickness

$R_{cl}^d$  is design chloride resistance (year/mm<sup>2</sup>, inverse of chloride diffusion coefficient)

$t$  is the time (year)

## **LIST OF PUBLICATIONS BASED ON THIS THESIS**

### **REFEREED JOURNALS**

1. Jayachandran Karuppanasamy and Radhakrishna G. Pillai, "Probabilistic corrosion rates of Cold-Twisted Deformed (CTD) and Thermo-Mechanically Treated or Quenched and Self-Tempered (TMT/QST) Steels in chloride-contaminated mortar", Indian Concrete Journal, Vol. 90, No.11, 45-55, 2016.
2. Jayachandran Karuppanasamy and Radhakrishna G. Pillai, "Statistical distributions for corrosion rates of conventional and prestressing steel reinforcement embedded in chloride contaminated mortar", NACE Corrosion Journal (Accepted for publication).
3. Jayachandran Karuppanasamy and Radhakrishna G. Pillai, "A short-term test method to determine the chloride threshold of steel-cementitious systems with corrosion inhibiting admixtures", Journal of Materials and Structures (under 2<sup>nd</sup> peer-review).

### **INTERNATIONAL CONFERENCE PAPERS**

\* Indicates presenter

1. Jayachandran Karuppanasamy\* and Radhakrishna G. Pillai, "Service life estimation of concrete structures with different steel types exposed to chloride environment", NACE Concrete Service Life Extension Conference, Orlando, Florida, USA, May 23-25, 2016.
2. Jayachandran Karuppanasamy\* and Radhakrishna G. Pillai, "A test method to determine the effect of corrosion inhibitors on chloride threshold of steel-cementitious systems", International Conference and Expo on Corrosion (CORCON), Chennai, India, November 19-21, 2015.
3. Jayachandran Karuppanasamy\* and Radhakrishna G. Pillai, "Issues with the application of potential gradient in evaluating the performance of corrosion inhibitors in steel-cementitious systems", International Conference on Ecstasy in Concrete (ACECON 2015), Kolkata, India, October 08-10, 2015.

4. Jayachandran Karuppanasamy and Radhakrishna G. Pillai\*, 2014, “Probabilistic Estimation of Corrosion Propagation Period for Prestressed Concrete Structures Exposed to Chlorides”, 4<sup>th</sup> International Conference on Durability of Concrete Structures (ICDCS 2014), Purdue University, West Lafayette, Indiana, USA, 24–26 July 2014.
5. Jayachandran Karuppanasamy, Vibha Venkataramu, and Radhakrishna G. Pillai\*, 2013, “Effect of corrosion inhibitors on the chloride threshold of TMT steel”, International Conference on Sustainable Construction Materials & Technologies at Kyoto, Japan, August 18-21, 2013.
6. Vibha Venkataramu, Jayachandran Karuppanasamy\*, and Radhakrishna G. Pillai, 2013, “Effect of calcium nitrite corrosion inhibitor on the chloride threshold of TMT steel”, International Conference on Innovations in Concrete Constructions at NIT Jalandhar, India, March 5-8, 2013. (ISBN:978-93-82880-06-6).

### **PRESENTATION**

\* Indicates presenter

1. Radhakrishna G. Pillai\*, Jayachandran Karuppanasamy, Dhanya B. S., Sooraj A.O. Nair, Manu Santhanam, and Ravindra Gettu, "Enhancing the corrosion resistance of reinforced concrete structures - Indian Scenario and challenges ahead", Invited Lecture, International Conference and Expo on Corrosion (CORCON), Chennai, India, November 19-21, 2015.

## **DOCTORAL COMMITTEE**

### **CHAIRPERSON**

Dr. K. Ramamurthy  
Professor and Head  
Department of Civil Engineering

### **GUIDE**

Dr. Radhakrishna G. Pillai  
Assistant Professor  
Department of Civil Engineering

### **MEMBERS**

Dr. Manu Santhanam  
Professor  
Department of Civil Engineering

Dr. Amlan Kumar Sengupta  
Professor  
Department of Civil Engineering

Dr. S. Ganesh Sundara Raman  
Professor  
Metallurgical and Materials Engineering

Dr. M.S. Sivakumar  
Professor  
Department of Applied Mechanics



## CURRICULUM VITAE

**Name** : Jayachandran Karuppanasamy

**Date of birth** : October 21, 1985

### **Educational qualifications**

**2008** **Bachelor of Engineering (B.E.)**

**Institution** : K. S. Rangasamy College of Technology,  
Affiliated to Anna University Chennai  
Tiruchengodu, India

**Specialization** : Civil Engineering

**2010** **Master of Engineering (M.E.)**

**Institution** : College of Engineering Guindy  
Anna University Chennai  
Chennai, India

**Specialization** : Construction Engineering and Management

**2017** **Doctor of Philosophy (Ph.D.)**

**Institution** : Indian Institute of Technology Madras  
Chennai, India

**Specialization** : Durability of Reinforced Concrete Systems  
Civil Engineering